STUDIES ON REGENERATED NON-MULBERRY SILK FIBROIN AND ITS BLENDS

Thesis

Submitted to

DELHI TECHNOLOGICAL UNIVERSITY

for the partial fulfillment of the requirements for the degree of

DOCTOR OF PHILOSOPHY

in

Applied Chemistry

by

Radhika Batra

(2K17/PhD/AC/06)

Under the supervision of

Prof. Roli Purwar

Department of Applied Chemistry
Delhi Technological University
Delhi-110042

December 2021

Dedicated to the love and hope
of my family and friends that
has guided me throughout

DELHI TECHNOLOGICAL UNIVERSITY

Formerly Delhi College of Engineering

(Under Delhi Act 6 of 2009, Govt. of NCT Delhi)

Shahabad Daulatpur, Main Bawana Road, Delhi- 110042

CERTIFICATE

This is to certify that the work, embodied in the thesis entitled **"Studies on Regenerated Non-mulberry Silk Fibroin and its Blends"** done by **Radhika Batra,** roll no. **2K17/PhD/AC/06**, as a full time Ph.D. scholar in the Department of Applied Chemistry, Delhi Technological University, Delhi is an authentic and bona fide work carried out by her.

This work is based on original research and the matter embodied in this thesis has not been submitted earlier for the award of any degree or diploma to the best of our knowledge and belief.

Dr. Roli Purwar

Professor
Department of Applied Chemistry
Delhi Technological University
Delhi- 110042

DELHI TECHNOLOGICAL UNIVERSITY

Formerly Delhi College of Engineering

(Under Delhi Act 6 of 2009, Govt. of NCT Delhi)

Shahabad Daulatpur, Main Bawana Road, Delhi- 110042

DECLARATION

This is to certify that the work presented in this thesis entitled **"Studies on Regenerated Non-mulberry Silk Fibroin and its Blends"** has been carried out by me for the degree of **Doctor of Philosophy** under the supervision of Dr. Roli Purwar, Professor, Department of Applied Chemistry. This thesis is a contribution of my original research work. Wherever research contributions of others are involved, every effort has been made to clearly indicate the same. To the best of my knowledge, this research work has not been submitted in part or full for the award of any degree or diploma of Delhi Technological University or any other University/Institutions.

Radhika Batra

Research Scholar

(Reg. No. 2K17/Ph.D./AC/06)

Date:

Time:

Acknowledgements

carry out the cell studies and for their periodic technical guidance. I am thankful to **Mr. Aman Verma**, Indian Institute of Technology, Patna for helping with the XRD studies.

I am obliged for the help of all the non-teaching as well as technical staff of numerous departments in DTU which made my PhD journey as easy as possible. Throughout the pursuance of my degree, I was blessed with the nurturing research environment that my seniors, lab mates and fellow scholars provided. I'd specially like to mention **Dr. Chandra Mohan Srivastava**, **Dr. Priti Gupta**, **Priya Bansal**, **Reetu Yadav**, **Radha Sachan**, **Dr. Aman Prasad** and **Mr. Rajat Bajaj** who took the load off my shoulders as & when needed. Their presence and availability during the stressful times made me inexhaustibly sail through this PhD journey. Some friendly support is all you need during the times of failures and to cherish the little victories during the course of life. I'd like to especially present my gratitude to the saviour friends **Ms. Priya Rathi**, **Ms. Sukrati Sharma** and **Ms. Awantika Chadha** for always being there and keeping me sane during the troublesome times of this Ph.D. journey .

Radhika Batra
2K17/PhD/AC/06

List of Figures with Page Number

iv

List of Tables with Page Number

List of Contents

Abstract

Antheraea mylitta (Tasar) silk fibroin, possessing exceptional properties, is one of the major materials of interest amongst the existing different varieties of silk. In the past few years, inclination of researchers towards exploring the potentiality of tasar silk fibroin has increased in the fields of tissue engineering and regenerative medicine. However, its slow biodegradation rate and reduced mechanical strength (brittleness) upon regeneration are the issues of concern for researchers. One of the possible ways to tackle these problems is through blending. The tasar silk fibroin can be blended with other polymers which can enhance the overall flexibility and tune the biodegradability of new blend material generated. In this research work, two such polymers, polyvinyl alcohol (PVA) and gelatin have been explored to blend with tasar silk fibroin with the intention to impart flexibility and alter their biodegradability. The properties of prepared blends have been studied in solutions, films and nanofibrous forms. Various blend ratios of the polymers have been prepared and analysed to fine tune the physiochemical properties of blend materials. Montmorillonite nanoclay has been modified with cetyl trimethyl ammonium bromide (CTAB) as a model drug and this modified clay in further doped into blend solutions to prepare nanowebs via electrospinning. The prepared blend films and nanofibers comprising tuneable properties have shown their potential utility in the biomedical field.

Thesis Overview

The entire research work is divided into 7 chapters of this thesis. Chapter 1 introduces the research area and highlights the motivation behind this research. The objectives of the research work have also been outlined in this chapter. Chapter 2 provides the detailed literature survey of non-mulberry silk fibroin based blends reported till date. Chapter 3 describes the preparation, characterization and rheological studies of tasar silk fibroin and PVA blend solutions for their steady and dynamic shear analysis. The preparation and characterization of flexible tasar silk fibroin-PVA blend films are discussed in chapter 4, the films showed potential for their utility in biomedical field. The chapter 5 discusses the modification of montmorillonite nanoclay with cetyl trimethyl ammonium bromide (CTAB) and its characterization and details the preparation of 3D nanowebs from tasar silk fibroin PVA blend solutions with and without incorporation of modified nanoclay through electrospinning. The properties of developed nanowebs are discussed in details through different characterization methods. In chapter 6, another biopolymer gelatin has been explored to blend with tasar silk fibroin. Two different preparation routes followed and the obtained their properties analysed through various characterization techniques are presented in detail. The chapter 7 concludes and briefly summarizes the entire research study and sheds light on the future prospects of this particular work. The end of the thesis features all the literature that has been referred to conduct this research work.

Chapter 1

General Introduction

This chapter is intended to introduce silk fibroin, its different varieties and extraction sources. Polymer blending along with already explored and potential polymers which have the capacity to be blended with silk fibroin are concisely reported. The silk fibroin-based polymer nanocomposites are touched upon with their versatile applications. The current status of these materials is briefly discussed along with the existing research gap in this area. The motivation to carry out this study and the objectives of research work are stated at the end of the chapter.

1.1 Introduction

Advances in the field of materials research over the past century has led to the development of silk fibroin based materials for numerous diverse applications from textile to wound healing to tissue engineering [1]. A variety of sources (e.g. spiders, silkworms, mites, scorpions and flies) are available, from which silk can be extracted. Silk obtained from silkworm is considered to be a good source of development of material of biomedical interest [2]. There are different types of silkworms which produce silk fiber, and are broadly classified into two varieties, mulberry and non-mulberry. The silk produced by Bombycidae family (*Bombyx mori*) is known as mulberry and the one produced by Saturniidae family (*Antheraea mylitta, Antheraea assamensis, Philosamia ricini* etc.) is known as non-mulberry [3].

Natural silk fiber extracted from silkworm glands or cocoons comprises of two major proteins, fibroin (structural component) and Sericin (water soluble gummy protein).

Silk fibroin of B. mori is composed of a heavy chain containing Gly-X (X being Ala, Ser, Thr, Val) repeats, and a hydrophilic light chain linked together by a disulfide bond [4]. These chains are non-covalently linked by a glycoprotein P25 [5]. Non-mulberry silks lack light (L) chain and P25 [6,7]. Instead, they contain heavy (H) chain homo-dimers with a molecular weight of ~330 kDa formed by individual proteins (~160 kDa) [8]. They also exhibit a higher Ala/Gly ratio and poly-alanine blocks, which form β-sheets [9]. There is presence of RGD sequence which is known to be responsible for cell adherence and proliferation. As a consequence of such distinctions, the non-mulberry silk fibroin shows significant difference in its properties from the mulberry variety and has gained interest of researchers worldwide [10].

Silk fibroin (SF) is being used as medical sutures and in textile field since a long time. In the past few decades' utilization of SF in biomedical field as biomaterial has gotten wings due to its low cost, good mechanical properties, biocompatibility, exceptional biodegradability, nontoxicity, good oxygen and water vapor permeability and easy availability. Lately, plentiful research studies have been reported using non-mulberry SF extracted from silkworm gland in various forms such as films [11], cryogels [12], nanofibers and several scaffolds [13–15]. Kasoju *et al*. have prepared silk fibroin films by extracting protein from glands of *Antheraea assama* silkworm [16]. Kar *et al*. have reported the preparation of muga gland extracted silk fibroin 2D films and have found them to be compatible with MG-63 human osteoblast cells [17]. It is pertinent to note that despite such fascinating features, the use of non-mulberry SF is limited due to its poor solubility in conventional solvents which are used to dissolve mulberry SF, its less hydrophilicity and poor rate of mass loss. Recently few research studies have been reported utilizing ionic liquid as solvent for dissolution of cocoon extracted non

mulberry silk fibroin which has introduced the all-new prospective avenues of exploring this material for wide range of applications. Goujan *et al*. have prepared *Antheraea assama* silkworm cocoon extracted silk fibroin films by dissolving in 1-butyl-3-methylimidazolium chloride, BMIMCI or 1-butyl-3-methylimidazolium acetate, BMIMAC ionic liquids. Electrospun nanofibrous mats of muga silk fibroin-ionic liquid (BMIMAC) solution have been prepared for skin tissue engineering applications [18]. Srivastava *et al*. have reported the preparation of flexible muga, tasar cocoon extracted silk fibroin films by dissolving in BMIMAC ionic liquid and have modified by adding dextrose for wound dressing application [19].

Polymer blending is a powerful tool which can generate new improved class of materials with enhanced physico-chemical properties by assembling the advantages of each individual component [20]. There is a plethora of literature available in which mulberry silk fibroin blended with other polymers such as gelatin [21–23], chitosan [24–28], PVA [29–32], polyethylene oxide [33–35], cellulose [36–40] etc. have been reported to improve the properties of SF. A few studies have also been reported on non-mulberry silk fibroin blends but the source of extraction of SF in majority of work is from silk worm gland [12,41–44].

Polyvinyl alcohol (PVA) is one of the most widely used, water soluble biodegradable polymer [45]. It has excellent barrier properties, odor lessness and non-toxicity, making it suitable for a range of applications in the field of packaging as well as healthcare [46,47]. Silk and PVA both having excellent properties been explored by researchers to create materials in different forms like films, hydrogels, 3D scaffolds and nanofibers etc. [11,31,48,49]. The regenerated silk fibroin being brittle is often blended with PVA to provide it with the flexibility and to create advanced materials. The materials prepared using neat PVA have limited scope in biomedical applications as they are unstable in the

physiological environment and dissolve readily in water. Researchers have crosslinked PVA with different chemical agents like glutaraldehyde, glyoxal's etc. to address this concern [50,51]. It is pertinent to note that amongst the limited studies available in literature on silk fibroin and PVA blends, most of them utilize either mulberry variety of silk fibroin or extract non mulberry silk from silkworm glands [52,53]. Non-mulberry silk fibroin blended with PVA can work synergistically to overcome the limitations associated with them in pure state without using any additives.

Another useful polymer which can be considered to blend with silk fibroin is gelatin. It is a natural polymer, derived from collagen found in animal tissues such as skin, muscle, and bone. It is an inexpensive, biocompatible, non-immunogenic, biodegradable and water-soluble protein having arginine-glycine-aspartate (RGD) sequences providing it with cell attachment sites. Gelatin due to its interesting properties has been extensively employed as biomaterial in several biomedical applications [54,55]. Yet, biomaterials obtained from gelatin have limited applicability because of their high degradation rate and weak mechanical strength. On the other hand SF has good mechanical strength but has a disadvantage of slow degradation rate [56]. Therefore gelatin can be a good candidate for blending with SF to tailor the physicochemical properties of biomaterials derived from it for specific applications [57,58]. Moreover, advanced polymer blend materials with greater electrical, mechanical, thermal and biological responses can be generated in the form of nanocomposites. A number of fillers like bioactive ceramics and metal oxide nanoparticles are being explored by research groups for versatile applications.

Nanoclays are one of the widely employed class of fillers that are used to prepare biomedical constructs for extensive range of applications like wound healing, tissue

engineering, drug delivery etc. to name a few. Montmorillonite (MT), a smectite family layered silicate clay, is broadly being investigated as an active ingredient in polymer nanocomposite biomaterials for applications in tissue engineering and regenerative medicine. The exceptional properties of MT like high aspect ratio, surface area, biocompatibility, and charged layer structure provides it with a variety of possible interactions with polymers and other organic molecules like drugs [59]. In literature, wide-ranging research has been reported on pure and modified clay incorporating polymer biomaterials with the motive to study its implication not only as a filler to improve the mechanical strength of polymers but also as a drug carrier for sustained release of drugs [60–62]. Moreover, inclusion of MT has been reported to improve the cell- scaffold interaction and proliferation of cells for a variety of scaffolds prepared from natural polymers like gelatin, chitosan and silk etc. [63]. Therefore, exploration of modified clay loaded non-mulberry silk fibroin blend based biomedical constructs with tailorable properties is an innovative and fascinating area of research.

In order to develop polymeric blend materials with tailorable properties, it is advantageous to check the behaviour of prepared solutions beforehand to get an essence of their miscibility and process parameters to be used while production. Rheology studies are used to evaluate the behaviour of blend solutions like effect of blend ratios on viscosity, their miscibility and viscoelasticity etc. In literature, number of studies have been reported with the motivation to explore the rheological behaviour of pure silk fibroin and its blend solutions, however, they are limited to the mulberry variety of silk fibroin leaving non-mulberry silk fibroin-based blend solutions unexplored [64–66].

1.2   Research gap

- Very limited literature available on studies of non-mulberry silk fibroin despite its immense potential.

- Only a few studies have been carried out on cocoon extracted tasar silk fibroin blend materials.

- Almost Negligible work has been reported for structural property analysis of tasar silk fibroin blends.

- No work available in literature on the rheological analysis of tasar silk fibroin blends.

1.3   Motivation of Research

India is rich source of non-mulberry silk i.e., *Antheraea mylitta*, an under explored potential biomaterial, both in case of pure as well as its blends, that too extracted from silkworm cocoon. Most of the latest studies on non-mulberry silk fibroin and its blends are confined to development of material through extraction of silk fibroin from silkworm gland which is commercially not feasible. So, the need of the hour is to emphasize on the feasible source of non-mulberry silk fibroin extraction, its regeneration and further improvement in the properties of materials developed through it, by blending with other biopolymers, in order to achieve tailor-made materials for specific applications.

1.4   Objectives

The broad objective of this work was to design and develop regenerated non-mulberry silk fibroin blend materials in different forms like films and 3D nanofibrous constructs.

1.4.1 Specific Objectives

To achieve the above broad objective, the specific objectives were as follows:

- Rheological analysis of regenerated *Antheraea Mylitta* (Tasar) silk fibroin/PVA blend solutions

- Preparation and characterization of regenerated *Antheraea Mylitta* (Tasar) silk fibroin/PVA blend films.

- Fabrication and characterization of drug/clay loaded regenerated *Antheraea Mylitta* (Tasar) silk fibroin/PVA nanofibers using electrospinning.

- Creation and characterization of regenerated *Antheraea Mylitta* (Tasar) silk fibroin/gelatin blend films.

Chapter 2
Literature Review

2.0   Overview

This chapter is designed to provide an extensive literature review of the non-mulberry silk fibroin-based blend solutions and materials in different forms. The comprehensive detail of various extraction sources, processing conditions and final developed forms of material along with their intended applications are specified. Further, a discussion about the current status of this research area throughout the world is written in detail.

Silk fibroin regeneration is a powerful tool to engineer silk in useful forms like films, fibers, scaffolds etc for suitable applications in several biomedical fields (e.g. wound dressing, tissue engineering, surgical sutures, biosensors etc.). Silk extracted from silk worm cocoon cannot be used directly as such, to obtain silk fibroin from the silk filaments, it needs to be first degummed. Degumming is a process of removal of silk sericin (boiling the chopped silk cocoons in 0.02M sodium carbonate solution for ~40 mins or boiling cocoons for 1 hr at 130°C) which has been known to affect the solubility of fibroin in several solvents [67]. Degumming is followed by dissolution of silk fibroin in suitable solvents to obtain silk solution. After that silk solution is processed in different forms of films, foams, hydrogels, fibers etc. Degumming, dissolution and processing are collectively called regeneration. The structure and properties of silk fibroin proteins can be controlled by surface modification, allowing it to blend with other polymers or by incorporating several biological materials in it.

2.1 Preparation of silk fibroin solution for blends

There are wide range of protic and non protic solvents available in which mulberry silk fibroin can be dissolved but most of these solvents fail or only partially dissolve cocoon extracted non mulberry silk fibroin in them. Lately, a few studies have been reported, utilizing ionic liquids for non-mulberry silk fibroin regeneration. Goujan *et al* have reported the dissolution of *A. asamanese* in 1-butyl-3-methylimidazolium chloride, BMIMCI or 1-butyl-3-methylimidazolium acetate, BMIMAC ionic liquids [68]. Our own research group has also reported several papers on dissolution and processing of muga and tasar SF using ionic liquid. Regenerated muga and tasar fibroin flexible films have been prepared by dissolving cocoon extracted silk in ionic liquid for wound dressing applications [19]. Srivastava *et al* has reported the fabrication of electrospun nanofibrous mat using dope solution prepared by dissolving *Antheraea assama* silk fibroin in ionic liquid for skin tissue engineering [18].

2.3 Regenerated non-mulberry silk fibroin blends

A few polymers like PVA, PCL, Chitosan, P(LLA-CL) and agarose have been explored in order to make blends with non-mulberry silk fibroin in the form of films [69–71], scaffolds [12,72], hydrogels [42] and nanofibers [41,43,44,73–77] for biomedical and several tissue engineering applications, as summarized in Table 2. In most of the studies silk fibroin has been extracted from the gland of non-mulberry silk worm for the blend preparation [12,41–44,73]. *A. mylitta* SF extracted from silkworm glands has been blended with poly(e-caprolactone) [43,73] and PVA [41] for bone tissue engineering applications.

PVA has been chosen as one of the blend materials for blending with non-mulberry SF due to its properties like hydrophilicity, semi crystallinity, non-toxicity and

biocompatibility which are suitable for biomedical applications. Moreover, presence of ample number of hydroxyl groups in PVA enables it to self-crosslink with fibroin.

PCL is a hydrophobic polymer having suitable mechanical properties, ease in fabrication, biodegradability and cytocompatibility but lacks recognition sites so cannot provide optimal environment for cell attachment and growth so is being blended with bioactive proteins chitosan, collagen, gelatin and silk fibroin.

Tussah SF extracted from silkworm cocoon have been blended with poly (L-lactic-co-glycolic acid) [76] and *B. mori* SF [77] in order to generate nanofibers by electrospinning for tissue engineering applications.

Poly(L-lactic-co-caprolactone), a copolymer of L-lactic acid and caprolactone, is a synthetic biodegradable material with unique mechanical properties but has limited use in tissue engineering scaffolds because of its poor hydrophilicity and unavailable cell recognition sites. It has been blended with *A. pernyi* SF which possesses poor mechanical properties but has bioactive sites in order to generate improved tissue engineering materials with enhanced mechanical properties and biocompatibility [75].

Agarose is a transparent polysaccharide, having neutral charge and thermo reversibility, has been explored as biomaterial for in vitro tissue engineering of cartilage. But, the applicability of agarose based materials in animal models has been restricted due to its non-customizable mechanical properties and significantly low cell adhesion and proliferation. In order to overcome its valid drawbacks, it has been blended with other polymers like chitosan, gelatin and silk. Non mulberry silk being superior choice for blending due to its excellent biocompatibility and tuneable mechanical properties [42]. Gelatin has not been explored as a blend material for non-mulberry SF yet.

Table 2.1: Non-mulberry silk fibroin blend materials and their applications

S. No.	Type of Silk	Blend Material	Morphology	Processing technique	Application	Reference
1	*A. Pernyi* (cocoon)	Poly (L-lactic acid-co-caprolactone)	Nanofibrous scaffolds	Electrospinning	peripheral nerve tissue regeneration	[75]
2	Tussah (cocoon)	poly (L-lactic-co-glycolic acid)	Nanofibers	Electrospinning	Bone tissue engineering	[76]
3	*Antheraea pernyi*	chitosan	Scaffolds	Freeze drying	Bone tissue engineering	[72]
4	i) *B. Mori* (Cocoon) ii) *A. assama* (gland) iii) *P. ricini* (gland)	poly(vinyl alcohol)	Nanofibrous Mats	Electrospinning	Accelerated wound healing	[44]
5	*B. Mori* (Cocoon)	i) *A. Mylitta* (Tasar) ii) *A. assama* (Muga) iii)*Philosamia ricini* (Eri) iv) Thai mulberry	Films	Casting	-	[70]
6	A. mylitta (gland)	poly($\mathcal{E}$-caprolactone)	Nanofibrous scaffolds	Electrospinning	bone tissue engineering	[43,73]
7	*Antheraea pernyi*	*Bombyx mori*	films	Casting	-	[69]
8	*Antheraea pernyi*	chitosan	films	Casting	-	[71]
9	Tussah (cocoon)	*Bombyx mori*	Nanofibers	Electrospinning	tissue engineering	[77]
11	Philosamia ricini (Eri) (cocoon)	*Antheraea* Mylitta (Tasar) (cocoon)	Nanofibrous scaffolds	Electrospinning	bone tissue grafts	[74]
12	B. Mori (Cocoon) *Antheraea* Mylitta (gland)	Chitosan	scaffolds	Freeze drying	Cartilage repair	[12]
13	B. Mori (Cocoon) *Antheraea assama* (gland)	Agarose	hydrogels	Freeze drying	cartilage repair	[42]
14	*Antheraea Mylitta* (gland)	poly(vinyl alcohol)	Nanofibers	Electrospinning	Bone scaffolding material	[41]

11

2.3.1   Techniques for developing non-mulberry silk fibroin blends

In order to process non-mulberry silk fibroin blends in the form of films, fibers or scaffolds, techniques like casting, freeze-drying and electrospinning have been adopted by researchers.

2.3.1.1 Non mulberry silk fibroin blends by casting

Silk fibroin blend films can be prepared by casting the blend solution in polystyrene plates. After drying, the casted films are treated with organic solvents like methanol, ethanol or water in order to improve the β-sheet crystallinity. Xue *et* al studied the thermal and structural properties of cast films prepared by blending *B. mori* silk fibroin with Tussah, Muga, Eri, and Thai silks in different ratios [70]. The blending of non-mulberry silk fibroin into mulberry showed significant improvement in the thermal properties of the blend material. In another study *B. mori*/ *Antheraea pernyi* SF blend films were prepared by casting and their physical properties along with thermal behavior was investigated. The two protein components were suggested to show poor compatibility with clear phase separation. Kweon *et* al have reported the preparation of cast blend films by mixing the aqueous *Antheraea pernyi* SF and chitosan acetic acid solutions. Structural and thermal analysis of these blend films was carried out and was reported to show phase separation but presence of some intermolecular interactions between the two polymers [71].

2.3.1.2 Silk fibroin blend fibrous scaffolds

Electrospinning is a fiber fabrication technique broadly utilized for the formation of polymer fibers of nano to sub-micron range. The electrospun nanofibers have extremely high surface to volume ratio, tuneable porosity, malleability to conform to

wide variety of sizes and shapes and ability to control the nanofiber composition in order to achieve desired results from its properties and functionality, which makes them applicable for a wide range of applications like filtration, wound dressing materials [44], biological scaffolds [12,75], tissue engineering scaffolds [72,76,77].

A typical electrospinning set up consists of three components; a high voltage supplier, a capillary needle or pipette and a ground collector. The electrospinning technique involves the generation of strong electric field between a polymer solution contained in a reservoir like a syringe with a capillary tip or needle, and a metallic collection plate or drum. At a critical voltage the electric force from the applied field becomes higher than the surface tension of the droplet, the charge overcomes the surface tension of the deformed drop of suspended polymer solution formed on the needle, a charged get of solution is formed and ejected in the direction of the applied field. Under electro-hydrodynamic forces the diameter of electrically charged jet decreases and this jet undergoes a series of several electrically induced bending instabilities during passage to the collection plate, which result in extensive stretching [78]. During stretching process rapid evaporation of the solvent takes place, which results in the reduction in the diameter of the jet. After stretching and drying, these fibers collected randomly or in an aligned manner on the surface of collecting plate. The diameter of electrospun nanofiber can be controlled by changing the processing parameters such as concentration of solution, viscosity and electric field, type of solvent employed, distance from tip to collector plate, flow rate [79], diameter and angle of spinneret [80].

Recently, few researchers have reported the preparation of non-mulberry silk fibroin nanofibers through electrospinning [18,44,70,74]. *Antheraea pernyi* silk fibroin-blended

P(LLA-CL) nanofibrous scaffolds have been fabricated and have reported to show superior hydrophilicity and mechanical properties than the pure SF [75]. These nanofibrous scaffolds significantly promoted the cell growth and are considered to be a potential peripheral nerve tissue regeneration material. In another study electrospun nanofibrous scaffolds have been prepared by blending tussah silk fibroin with poly (L-lactic-co-glycolic acid) for bone tissue regeneration [76]. These scaffolds were also bio mineralized with hydroxyapatite, the resulting material showed excellent mechanical properties, osteoinductivity and cytocompatibility. Bhattacharjee et al have carried out a comparative study of gland extracted *A. mylitta* SF/poly(e caprolactone) nanofibrous scaffolds with *A. mylitta* SF grafted aminolyzed electrospun nanofibrous PCL scaffolds [43]. They reported, the inclusion of *A. mylitta* SF into PCL in both the cases improved the osteoinductivity and mechanical properties of scaffolds but grafted SF showed better cell adhesion, growth, and formation of ECM as compared to blended SF/PCL scaffolds. These nanofibrous blend scaffolds were further investigated for in vivo studies by implanting the scaffolds into white New Zealand rabbits with bone defects and were reported to comprehend early bone formation, implant infiltration and strong bonding at bone-implant interface with slight immune reaction at initial stage but was normal within 4 weeks of implantation [73].

Zang *et* al have prepared *Bombyx mori* SF/Tussah SF blend nanofibers using hexafluoroisopropanol (HFIP) as solvent by electrospinning and further treated them with ethanol for recrystallization [77]. The nanofibers obtained were found to have poor compatibility with each other but showed improvement in thermal degradation and hydrophilicity, the cell adhesion and biocompatibility was enhanced due to blending.

In another study Eri/Tasar SF blend nanofibers were prepared and were compared to *B. mori* and Gelatin scaffolds as control [74]. It was found that eri-tasar blend scaffold had better hydrophilicity and mechanical strength as compared to the control samples. Also, the blend scaffolds exhibited superior bioactivity with enhanced cell adhesion and higher metabolic activity of cells grown over them. Another blend was obtained from gland extracted tasar SF and PVA. Electrospun nanofibrous matrices were fabricated by blending aqueous SF and PVA solutions. The nanofibers exhibited, mechanical strength similar to that of naïve bone tissue, higher cell attachment, growth and extra cellular matrix formation as compared to pure PVA (control) samples showing osteoinductivity.

2.3.1.3 Silk fibroin blends through freeze drying

Freeze drying is a low temperature water removal technique in which the material is first frozen at low pressure followed by removal of ice by sublimation process. This is also called lyophilisation. A few non mulberry silk fibroin blends have been prepared via this technique. Bissoyi *et. al* have prepared freeze dried *A. pernyi* SF/chitosan blended polyelectrolyte complex scaffolds for bone tissue engineering applications. In another study, silk worm gland extracted *A. mylitta* SF/chitosan blended porous 3D scaffolds have been prepared utilizing freeze drying technique for cartilage tissue repair applications [12]. Singh and co-workers [42] have prepared A. *assama* SF/agarose hydrogels by freeze drying the blend solution for cartilage repair applications.

2.4   Properties of non-mulberry silk fibroin blends

Native silk fibroin proteins are known to possess β-sheet conformations, which on dissolution in solvents gets converted to random coil. These regenerated random coil

samples have poor mechanical stability and get easily dissolved in aqueous atmosphere; so, they are coagulated in some organic solvents like methanol, ethanol, in order to induce β-sheet crystallinity. To determine the structural properties of proteins, their conformations are analysed via spectroscopic tools like FTIR, XRD, CD and tools like TGA, DSC, DMA and UTM are used to study their thermal and mechanical properties respectively. The biodegradation of the blend materials is analysed in phosphate buffer saline (PBS) solution and enzymatic degradation of materials is often studied.

2.4.1 Structural Properties

Protein materials are known to have certain specific conformations like α-helix, β-sheet, random coil and their conformations are determined in terms of structural properties. Any processing of these materials leads to change in their conformation, as a result altering the properties. These changes in protein conformations can be analysed by techniques like FTIR, CD, XRD.

Fourier transform infrared (FTIR) spectroscopy is one of the many techniques that have been applied to investigate specific molecular bonding interactions in polymer blends. When two polymers are in separate and distinct phases (complete immiscible systems), it can be assumed that the two components do not interact in IR spectral terms (except perhaps at the interface of the two phases). In that case, the spectrum of the blend reflects the appropriate addition of the IR spectrum of the two individual components. In the case of miscible or partially miscible polymer blends, the IR spectrum may show the formation of new bands as the results of miscibility; and disappearance of some component bands. Shifts in the specific bands would give

information on the switches from component specific bonds to the bonds between components [81]. In FTIR studies, the infrared region between 1700-1600, 1600-1500 and 1300-1200 cm^{-1}, corresponding to the amide I (indicative of C=O stretching along the SF backbone), amide II (representative of N–H deformation in the SF amide groups), and amide III (the vibration of O–C–O and N–H groups) respectively, are used for study of secondary structure of fibroin proteins. The β-sheet and random coil conformation of silk fibroin proteins are characterized by absorption bands at 1,650 cm^{-1} and 1,630 cm^{-1} for amide-I, 1,540 cm^{-1}, and 1,520 cm^{-1} for amide-II, 1,230 cm^{-1} and 1,270 cm^{-1} for amide-III, respectively [19,82].

Blending of SF with other polymers has shown to influence its structural properties. In the FTIR studies of tasar SF/ PVA blend nanofibers Bhattacharya et al have reported the presence of absorption peaks along with β-sheet corresponding to both the components without any major alterations, indicating structural stability of blends [41]. Moreover, the fibers on blending had slightly collapsed with reduction in diameter (~50 nm), which as a result enhanced cell migration. Poly(e-caprolactone) has been effectively blended with tasar gland SF as indicated by smooth and uniform appearance of scaffolds without bead formation [43]. The FTIR spectra also indicated peaks of SF as well as PCL without deviation showing blending of both the components. The reduction in fiber diameter upon blending from ~498 (pure PCL) to ~170 nm improved its bioactivity. Bissoyi *et* al have shown, the amide groups of SF have been altered, and the C=O and NH$_2$ functional groups peaks of Chitosan are missing in the FTIR spectra of *A. pernyi* SF/ chitosan blend composite indicating their involvement in specified interactions. *A. pernyi* SF blended with 40% chitosan have been reported to show phase separation, as indicated by its SEM images [71]. Studies

reported on *A. perneyi* SF/ P(LLA-CL) blends have shown the blending of two components without involvement of any chemical bond reaction [75]. SF/PVA blends prepared by chouhan and co-workers have shown homogeneous blending with smooth, beadless, and randomly oriented, porous networks [44]. Electrospun *B.mori*/tasar SF blends have shown heterogeneous microstructures with coexistence of α-helix and β-sheets (in presence of 40% tasar SF content) with weak or no molecular interactions between the two components, indicated by FTIR [77]. Phase separation was observed in the blend films of *A. pernyi*/*B. mori* SF [69]. Xue *et al* have obtained completely miscible (in micrometres scale) blend films by mixing B. mori SF with tussah, muga and eri SF respectively [70]. The blending of muga SF with agarose resulted in transparent hydrogels (in hydrated state) with no significant phase separation and presence of intermolecular interaction between the two components indicated by shift in amide I and amide II peaks in the FTIR spectra [41]. Also, the pore size of blend material has increased quite significantly due to incorporation of SF resulting in higher extracellular matrix production.

2.4.2 Thermal properties

The thermal properties of non-mulberry silk fibroin materials have been shown to be affected by blending with other polymers and can be examined by techniques like TGA, DSC, DMTA. The effectiveness of blending, blend miscibility or phase separation, thermal degradation behaviour %crystallinity and blend composition are certain properties of blend materials which can be analysed through thermal analysis. Blending of *A. pernyi* with chitosan has been reported to effectively enhance the decomposition temperature of chitosan component in the blend by 14° [71]. The DSC thermogram showed mixed form of two components indicating incomplete miscibility

of blends. A number of studies have been reported on blending the B. mori SF with the non-mulberry varieties in order to generate different morphologies like films and nanofibers and the influence of blending on the thermal properties of blends have been studied [69,70,77]. In general, it was observed that, incorporation of non-mulberry SF fraction (Tasar, muga) has increased the thermal decomposition temperature of blend due to more compact crystalline structure of non-mulberry SF, improving their thermal stability. Also the different blend ratios altered the thermal properties differently showing varied functional performance in case of A. pernyi/*B. mori* blends [69]. The films with higher *A. pernyi* showed more stability and stiffness while the ones with higher *B. mori* were found to be soft as indicated by their thermal expansion and contraction properties in TMA.

2.4.3 Mechanical properties

Blending has been reported to enhance the mechanical properties of blend materials having one of the components as non-mulberry silk fibroin. Nanofibrous matrices of Tasar SF/PVA blend with 2%SF have shown higher tensile strength (4.87±0.3 MPa) as compared to naïve trabecular bones (1.2 MPa), as well as pure PVA nanofibers due to the formation of inter fiber bonds attributable to blending [41]. The tensile strength of PCL nanofibers was slightly improved from 2.3 ±0.44 to 4.89 ± 0.68 MPa upon blending with tasar silk fibroin as a result of formation of inter fiber bonds [43]. On blending chitosan with *A. pernyi* SF, its compressive strength has been improved quite significantly [72]. Also, the equilibrium moduli of blended scaffolds were found to be higher than the pure components, making them more suitable for bone tissue engineering. The stability and stiffness of Agarose/Muga SF were enhanced as a consequence of blending [42].

2.4.4   Biodegradability

Biodegradability is an important feature of biomaterials for use in tissue engineering. The degradation should be optimum neither too fast resulting in collapse of material nor too slow. The degradability of materials has been shown to be altered by blending. The addition of tasar SF into PVA in the blend films has increased its degradation rate making it more suitable as tissue engineering biomaterial [41]. Tasar/ agarose hydrogels have been reported to show improved degradation process with 35% reduction in mass due to incorporation of SF into the blend as compared to no mass loss shown by pure agarose hydrogels, after 28 days incubation in enzymatic solution [42].

2.5   Applications of non-mulberry silk fibroin blends

Non mulberry silk fibroin having very high toughness and load bearing ability along with exceptional biocompatibility, superior bioactivity and controllable degradation has gained the interest of most of researchers as an excellent candidate in the field of tissue engineering and drug delivery applications. Utilization of non-mulberry silk fibroin as one of the components for producing blend materials is relatively new and is being focused upon for majorly tissue engineering and biomedical applications.

2.5.1   Tissue engineering Applications

- **Bone Tissue Engineering**: Bone scaffolding materials have been prepared by utilizing gland extracted tasar silk fibroin and blending it with PCL and PVA respectively [41,43]. Incorporation of non-mulberry silk fibroin, having the cell recognition RGD sequence sites, into the blends results in significant increased surface roughness, promoting cell adhesion which as a result improved the organization and production of extracellular matrix. The process of osteogenesis in

scaffolds was followed by mineralization resulting in osteoinductive nanofibrous blended scaffolds for bone regeneration. Inclusion of tussah SF into P(LLA-GA) post mineralization has significantly improved the blend scaffold properties in terms of cell adhesion, proliferation and mesenchymal stem cell (MSC) differentiation towards osteoblasts, making them versatile cytocompatible scaffolds for bone tissue engineering applications [76]. *A. pernyi/*chitosan blend polyelectrolyte complex have shown improved cell adhesion and osteogenic differentiation capability of MSC to be utilized for promising biomaterial for possible biomedical applications and bone tissue engineering [72]. Tasar SF blended with eri SF nanofibrous scaffolds also showed similar properties with respect to cytocompatibility and bioactivity, so can be used as potential bone tissue grafts [75].

- **Peripheral nerve tissue regeneration:** Blended nanofibrous scaffolds of *A. pernyi*/P(LLA-CL) have been prepared as a potential candidate for application in peripheral nerve tissue engineering [75]. These scaffolds have shown better growth and proliferation of Schwann cells (which play vital role in peripheral nerve regeneration) seeded on them as compared to pure P(LLA-CL) scaffolds.

- **Cartilage repair:** Immunocompatible Muga SF/Agarose blended hydrogels showing significantly high levels of sulphated glycosaminoglycans (sGAGs) and collagen have been prepared as an alternative biomaterial for cartilage tissue engineering [42]. In another study, gland extracted tasar SF/chitosan blended porous scaffolds with better cell attachment, proliferation and differentiation showing improved ECM deposition were developed for MSC based cartilage repair [12].

2.5.2 Wound healing applications

Non mulberry silk fibroin possesses inherent RGD motifs in protein sequence, which facilitate the binding to integrin receptors of cell which as a result provides functional advantage of mediating cell-biomaterial interaction for wound healing. PVA has been explored as one of the non-protein blend materials which can provide stability to the dressing material in rich proteolytic surroundings of chronic wounds. Bioactive nanofibrous wound dressing material has been prepared by blending *B. mori*, gland extracted *A. assama* and *P. ricini* with PVA respectively [44]. These blend materials functionalized with epidermal growth factor (EGF) or drug have shown scar less, accelerated wound healing with regulated ECM deposition.

Chapter 3 :

Rheological Studies of Tasar Silk Fibroin- PVA Blend Solutions

3.0   Overview

In this chapter, several blend ratios of *Antheraea mylitta* (Tasar) silk fibroin (ASF) and Polyvinyl alcohol (PVA) have been prepared and tested for their rheological behaviour. Different concentrations of both ASF and PVA stock solutions are prepared and blended in variable concentrations. All other concentrations except 10% w/v were found to form heterogeneous solutions, visible through naked eye. However, the 10% w/v ASF and 10% w/v PVA solutions blended at all the tried compositions presented homogeneity so are used for all the studies. The steady state and dynamic rheological tests are carried out for all these blend solutions with the stimulus to apprehend the spinnability and exploring the optimization of process parameters. The relationship between the shear viscosities and shear rates are obtained for the blend solutions. The essence of microstructural architecture of blend solutions is gained by applying the Cox-Merz rule on apparent and complex viscosities data. The impact of blending on the viscoelastic behaviour of silk fibroin and PVA solutions is also studied and the creep recovery of blend solutions is analysed.

3.1   Materials

Cocoons of *Antheraea mylitta* silkworm were bought from Central Silk Board, Son Bhadra, U.P, India. Polyvinyl alcohol (M.W.: 14000) was procured from Thermo

Fisher Scientific, India. Formic acid was bought from Loba Chemie Pvt. Ltd, India. Methanol was provided by Finar Chemicals Limited, India.

3.2 Methods & Characterization

3.2.1 Extraction of silk fibroin from tasar silk cocoons by degumming

The *Antheraea mylitta* silkworm cocoons were degummed to remove sericin using the procedure described in literature[83]. Briefly, the cocoons were cut into small pieces and heated in distilled water with 0.02 M $NaHCO_3$ at 100 °C for 30 mins twice. The fibroin so obtained was given two washes of distilled water to get rid of all the residual sericin. The degummed silk fibers were dried overnight in oven at 60°C.

3.2.2 Preparation of tasar silk fibroin-PVA blend solutions

The silk firoin was obtained via degumming the silk obtained from tasar silkworm cocoons following the methodology detailed in section 3.2 of chapter 3. Degummed silk fibers were dissolved in BMIMAc ionic liquid in temperature range 80-100°C under nitrogen atmosphere. This silk fibroin ionic liquid solution was dialyzed against miliQ water for 5 days and the water was changed at every 12-hour interval. The obtained aqueous silk fibroin solution was kept in hot air oven to evaporate the water. This dried silk powder so obtained was further dissolved in formic acid to prepare silk fibroin stock solution (10% w/v) which was used to make blends with PVA stock solution (10% w/v) in formic acid. Both the solutions were stirred separately on magnetic stirrers for one hour to achieve homogeneity. The so prepared stock solution of pure silk fibroin and pure PVA were mixed in specific ratios (100:0, 70:30, 50:50,

30:70, 0:100) to obtain the desired blend compositions (Fig. 3.1 & Table 3.1).
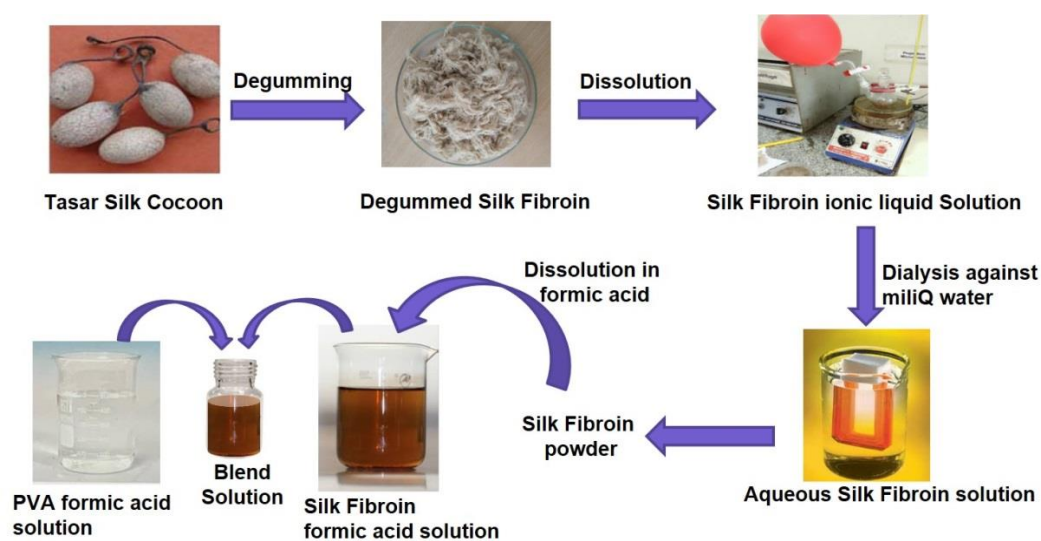
Fig. 3.1: Schematic representation of methodology adopted for preparation of tasar silk fibroin/PVA blend solutions**.**

Table 3.1: Blend compositions and abbreviations for silk fibroin/PVA blend solutions in formic acid

S.No.	PVA content (10% w/v)	Silk fibroin content (10% w/v)	Sample code
1	0	100	P0S10
2	30	70	P7S3
3	50	50	P5S5
4	70	30	P3S7
5	100	0	P10S0

3.2.3 Rheological measurements

The rheological properties of all the solutions were measured at 25°C using Modular Compact Rheometer (MCR 302) by Anton Paar. A 40 mm diameter concentric parallel plates geometry (PP40) with a 0.70 mm gap were used to carry out all the tests.

Steady shear rheology tests were performed in the shear rate range from 0.01 s^{-1} to 500 s^{-1} as well as at different constant shear rates i.e., 1, 50 and 100 s^{-1}. Dynamic shear rheological tests were performed at different strain levels for different solutions

within the linear viscoelastic region (LVER) and the respective strain value was determined by amplitude sweep test at constant 10 rad.s^{-1} angular frequency. Frequency sweep test was performed in frequency range from 0.1 to 100 rad.s^{-1}, in LVER. Creep recovery test was performed by applying a load of 5 Pa to examine the creep recovery and creep compliance. The load was applied for 500 sec and removed for next 500 sec and strain percentage were observed against the time interval.

All the tests were repeated to confirm the results and minimize the error.

3.3 Results and Discussion

3.3.1 Steady shear analysis

The viscosity profiles of silk fibroin/PVA blend solutions with variation in the shear rate were observed in the range of 0.01-500 s^{-1} and are presented in Fig. 3.2 As clearly visible from the graph, pure silk fibroin solution (P0S10) showed highest viscosity at very low shear which was found to reduce with increase in shear rate, representing typical shear thinning behaviour due to macromolecular uncoiling in the polymeric chains as a result of high shear application. Singh *et. al* have observed similar shear thinning behaviour for mulberry variety of silk fibroin [84]. On the other hand, pure PVA solution (P10S0) showed lowest viscosity at low shear rate which experienced slight shear thinning on application of high shear. Upon blending these two polymeric solutions, the viscosity of blends was observed to have shown the intermediate behavior at low shear rate. However, at high shear rates the blend solutions with higher silk content i.e., P30S70 and P50S50 showed extensive shear thinning while the viscosity profile of P70S30 remained closer to P100 solution.

26
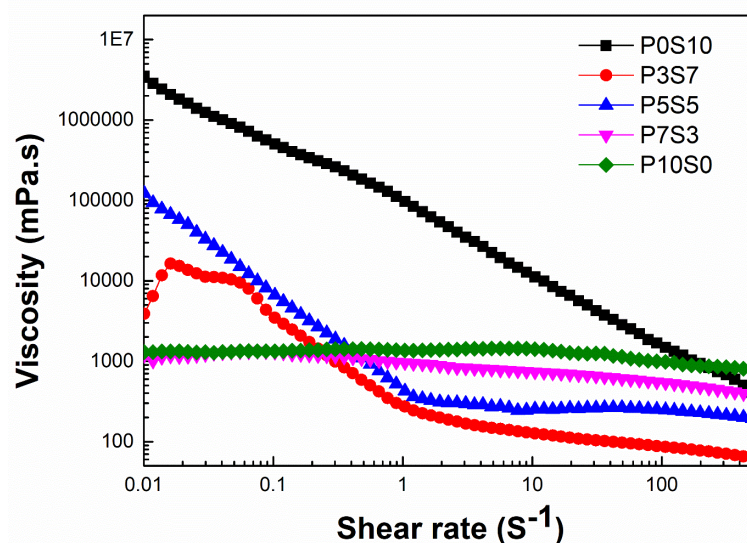
Fig. 3.2: Steady shear analysis of silk fibroin/PVA blend solutions by varying the shear rate from 0.1 to 500 s-1

3.3.2 Dynamic oscillation behavior of silk fibroin/PVA blend solutions

The dynamic behavior of blend solutions was studied through oscillatory tests including amplitude sweep and frequency sweep. The amplitude sweep study provided the linear viscoelastic region (LVER) for blend solutions which represents their respective structural integrity as shown in Fig. 3.3.

Solution with higher loss modulus than storage modulus shows the viscoelastic fluid behavior while the opposite is contemplated as viscoelastic solid. Pure PVA solution (P10S0) showed higher loss modulus than storage modulus throughout the experiment indicating viscoelastic fluid behavior with no crossover point (Fig. 3.3a) while pure silk fibroin solution (P0S10) showed the viscoelastic solid behavior as it has high storage modulus till crossover point at 44% shear strain (Fig. 3.3e).

The LVE region obtained was further used to conduct the frequency sweep analysis wherein specific strain within the limits of this region was applied for respective blend solutions as shown in Fig. 3.4.

G' and G'' were plotted against angular frequency for analysis of viscoelastic behavior of the blend solutions. It was observed that in pure silk fibroin solution (P0S10), storage modulus is dominant in the entire frequency range with no crossover point indicating viscoelastic solid analysis wherein specific strain within the limits of this region was applied for respective blend solutions as shown in Fig. 3.4.
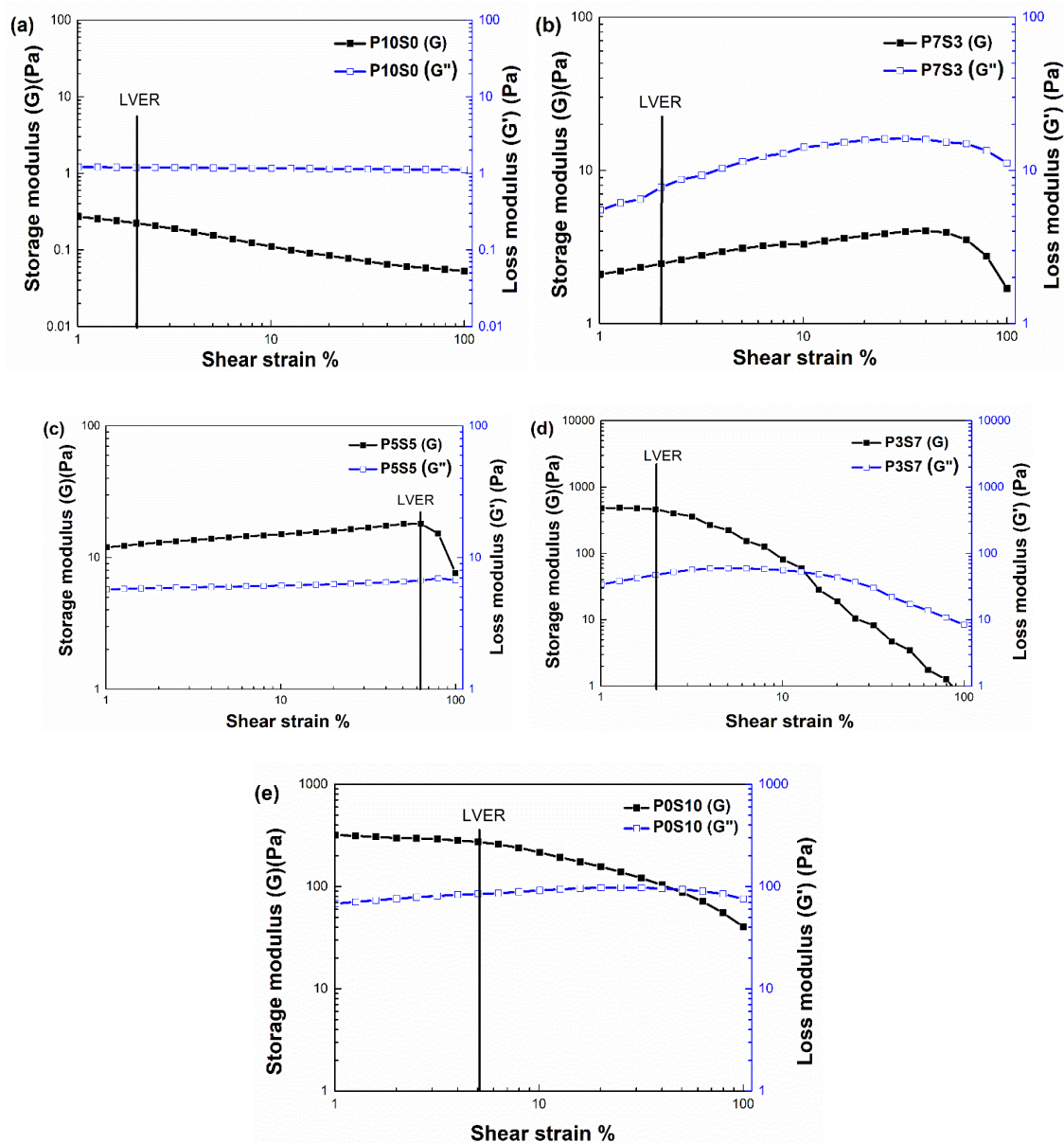
Fig. 3.3: Amplitude sweep showing linear viscoelastic (LVE) region of silk fibroin/PVA solutions (a) P10S0, (b) P7S3, (c) P5S5, (d) P3S7 and (e) P0S10
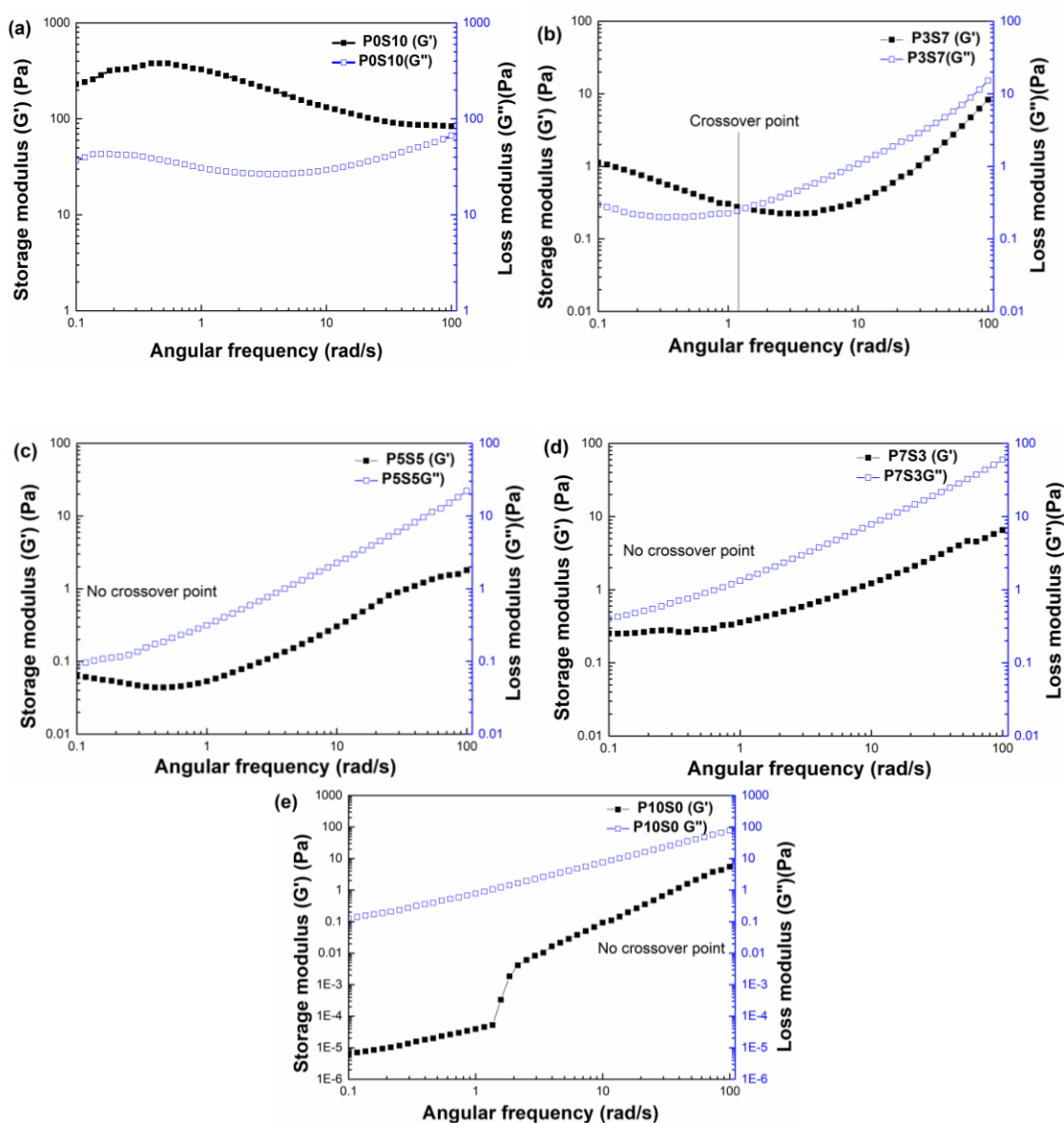
Fig. 3.4: Frequency sweep of silk fibroin/PVA solutions (a) P0S100, (b) P30S70, (c) P50S50, (d) P70S30 and (e) P100S0

G' and G" were plotted against angular frequency for analysis of viscoelastic behavior of the blend solutions. It was observed that in pure silk fibroin solution (P0S10), storage modulus is dominant in the entire frequency range with no crossover point indicating viscoelastic solid behavior however, a crossover point can be anticipated at higher angular frequency (Fig. 3.4a).

On the other hand, pure PVA solution (P10S0) showed the dominancy of loss modulus in the entire range representing the viscoelastic fluid behavior (Fig. 3.4e).

For blend solutions, it was observed that as the PVA content was increasing, loss modulus dominated the storage modulus indicating viscoelastic fluid like behaviour (Fig. 3.4). In P3S7 blend solution, particularly, change in the viscoelastic behaviour over the frequency range was observed with a crossover point at 0.4 rad/s. Below this crossover point the solution presented viscoelastic solid behaviour as indicated by higher storage modulus and above this viscoelastic fluid behaviour was dominant (Fig. 3.4b). Such behaviour of P3S7 blend solution could be attributed to intermolecular interaction of silk fibroin and PVA, however, for clear affirmation detailed study is required.

It is suggested by this study that polymer solutions can alter their behaviour through external parameters which eventually ease out their processability. In literature, viscoelastic behaviour of silk fibroin has been studied by researchers which showed dependency on the applied frequency. Mu and co-workers have applied variable frequencies to inter converted silk fibrils and gels utilizing this viscoelastic behaviour of silk [85].

Tan δ (loss factor) is another significant parameter to assess the viscoelastic properties in polymer solutions which is the ratio of loss to storage modulus. A value of Tan δ greater than one indicates viscoelastic fluid behaviour while value less than one suggests the solid like behaviour. From Fig. 3.5 it was observed that pure silk fibroin solution has loss factor value less than one while for pure PVA solution it was found to be greater than one in the entire frequency range. This data suggests dominancy of

solid like behavior in silk fibroin solution while fluid like behavior in PVA solution. As the silk fibroin content decreased in the blend ratio loss factor increased and found to be greater than one. P30S70 solution has shown the loss factor lower than one in low frequency region while greater than one at high frequency region representing its versatile viscoelastic behavior. While other two blend solution has shown the loss factor value greater than one in the entire frequency range implicate viscoelastic fluid behavior.
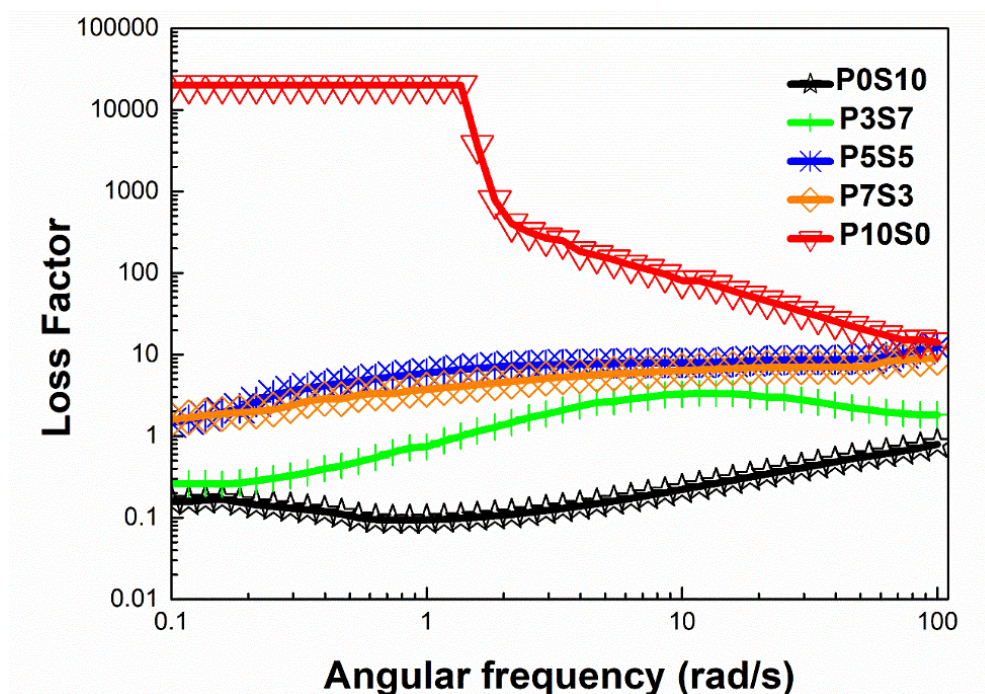
Fig. 3.5: Loss factor (Tan δ) as function of angular frequency for silk fibroin/PVA blending solutions with different blending ratios

A comparative study of the shear viscosity (η) and complex viscosity (η^*) obtained through application of steady shear ($\dot{y}$) and oscillatory shear (ω) respectively can provide an essence of the molecular architecture of polymers by applying the empirical Cox-Merz rule. According to this rule, the apparent viscosity vs shear rate curve and the complex viscosity curve as a function of angular frequency are expected

to be in very close proximity [86]. However, some deviations are observed at high shear due to molecular chain entanglements or shear fracture. As shown in Fig. 3.6, for P0S10 solution $\eta > \eta^*$ at low shear & at high shear $\eta^* > \eta$ and for P10S0 solution $\eta > \eta^*$. Deviations from this rule have previously been reported in literature for polymer solutions [87]. In general, failure of Cox-Merz rule with $\eta^* > \eta$ is attributed to the stretching of long polymeric chains in the sea of short chains or shear breakage of molecular chains and $\eta > \eta^*$ is associated with molecular chain entanglement or interchain interactions in polymers [65,88]. For blend solution P3S7 $\eta^* > \eta$ at high shear which can be attributed to the disentanglement or shear fracture in molecular chains of polymers. In case of P5S5, $\eta > \eta^*$ is observed at high shear which might be due to intermolecular chain interaction between silk fibroin and PVA. For P7S3 blend solution no such deviation was observed.
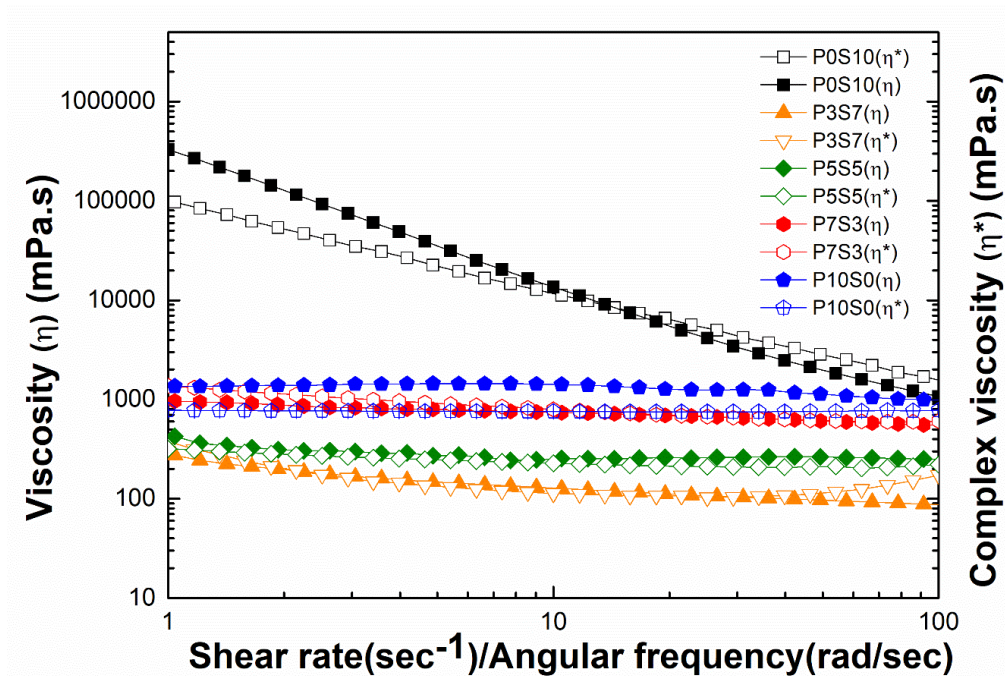
Fig. 3.6: Comparison diagram of η and η^* for silk fibroin/PVA blend solutions with different blending ratios

3.3.3 Creep recovery behavior of silk fibroin/PVA blend solutions

Creep test is used to speculate the mechanical responses of polymers as it provides their deformation behavior with respect to time [89]. The data obtained from the creep study of silk fibroin/PVA blend solutions is reported in Fig. 3.7. For pure silk fibroin solution (P0S10), it is observed that deformation occurs with around 26% strain and post release of load, it showed delayed permanent deformation at around 20% strain indicating viscoelastic solid like behavior. However, P10S0 solution showed continuous deformation upon loading and post release of load, there is no reformation observed in the solution implying ideal viscous behavior which is in agreement to our observations made through frequency sweep analysis. Upon blending silk fibroin with PVA, dramatic enhancement in the mechanical properties of blend solutions was observed. The extent of the deformation is increased significantly on increasing the proportion of PVA in blends (Table 3.2). Such observed enhancement in mechanical property gesticulates towards plausible interactions in silk fibroin and PVA in blend solutions.

Table 3.2: The enhanced % deformation observed in the blend solutions via creep analysis

S. No.	Sample	Deformation (%)
1	P10S0	323000
2	P7S3	3100000
3	P5S5	2620000
4	P3S7	480000
5	P0S10	26

3.4 Conclusions

- The blend solutions under the applied shear range showed shear thinning behaviour.

- The viscoelastic behaviour of solutions varied by altering the blend compositions. The blends with higher silk fibroin content presented viscoelastic solid like behaviour and the ones with more PVA content showed viscoelastic fluid like behaviour as observed through amplitude and frequency sweeps.

- The obtained tan δ plots complimented the amplitude and frequency sweep data.

- Upon application of Cox-Merz rule to the blend solutions, changes in the microstructural architecture were indicated as a consequence of blending as well as shear application.

- The blending of silk fibroin with PVA showed multifold enhancement in percentage deformation of blend solutions as observed in the creep recovery test.

- The blend compatibility and viscoelastic behaviour of blend solutions as assessed via rheological studies indicate that properties of these blend solutions can be varied by altering the blend compositions and rheological parameters like application of shear.

Chapter 4 :

Flexible *Antheraea Mylitta* (Tasar) Silk Fibroin & PVA Blend Films for Biomedical Applications

4.0 Overview

Structural integrity or stability at physiological conditions along with controlled biodegradability are the important factors for a successful biomaterial. Native PVA materials are known to dissolve under physiological conditions and tasar silk fibroin tends to become brittle upon regeneration during its processing. Tasar silk fibroin blended with PVA can work together to overcome the limitations associated with them in pure state. Silk fibroin can provide the stability which will solve the dissolution issue of PVA and in return PVA can impart flexibility, addressing the brittleness concern of silk fibroin. In this chapter, the preparation and analysis of regenerated *Antheraea mylitta* silk fibroin (ASF) and Polyvinyl alcohol (PVA) blend films of variable blend ratios are discussed in detail. The developed flexible blend films are found to be stable at physiological temperature. The films have shown enhanced mechanical properties along with excellent biocompatibility and their biodegradability is tailorable with variation in the blend ratio of two polymeric components. Additionally, the used methodology and processing conditions for preparation of blend films have eliminated the requirement of any additives like plasticizers and crosslinkers, reducing the possibility of any adverse health effects.

4.1 Materials

Cocoons of *Antheraea mylitta* silkworm were bought from Central Silk Board, Son Bhadra, U.P, India. Polyvinyl alcohol (M.W.: 14000) was procured from Thermo

Fisher Scientific, India. Formic acid was bought from Loba Chemie Pvt. Ltd, India. Methanol was provided by Finar Chemicals Limited, India. The L929 fibroblast cells were received from National center of cell science (NCCS), Pune, India. The ionic liquid BmimAc (1-butyl-3-methylimidazolium acetate), Fetal bovine serum (FBS) and Dulbecco's modified Eagle's medium (DMEM) were obtained from Sigma Aldrich.

4.2   Methods and Characterization

4.2.1   Extraction of silk fibroin from tasar silk cocoons by degumming

The *Antheraea mylitta* silkworm cocoons were degummed to remove sericin using the procedure described in literature[83]. Briefly, the cocoons were cut into small pieces and heated in distilled water with 0.02 M $NaHCO_3$ at 100 °C for 30 mins twice. The fibroin so obtained was given two washes of distilled water to get rid of all the residual sericin. The degummed silk fibers were dried overnight in oven at 60°C.

4.2.2   Preparation of regenerated *Antheraea mylitta* silk fibroin (ASF) and Polyvinyl alcohol (PVA) blend films

The silk fibroin stock solution was added dropwise to 10% (w/v) PVA formic acid solution in variable (100:0, 70:30, 50:50, 30:70, 0:100) blend ratios. Each blend solution was stirred continuously for 30 mins at room temperature and was then casted in polystyrene dishes. The dishes were kept overnight for drying at room temperature. The obtained blend films were then dipped in 70% methanol to regenerate crystallinity and their thickness was measured post drying. The films were found to be of thickness 0.06±0.03mm. The abbreviations used for film samples are described in Table 4.1.
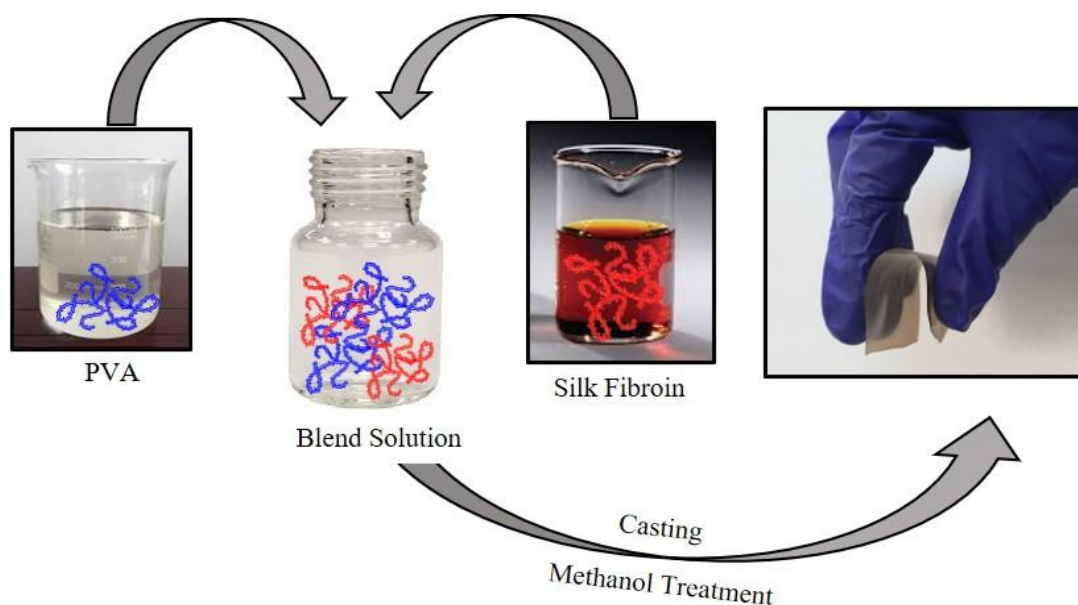
Fig. 4.1: Schematic representation of methodology of blend film preparation

Table 4.1 Abbreviations for various blend ratios used in preparation of films

S. No.	PVA 10% (w/v)	ASF 10% (w/v)	Abbreviation
1	100	0	P100
2	70	30	P70S30
3	50	50	P50S50
4	30	70	P30S70
5	0	100	S100

4.2.3 Scanning electron microscopy

The surface morphology of the samples was observed through sputter coating the samples with gold and analysed using Zeiss EVO 18 FESEM (field-emission scanning electron microscope) at a voltage of 20 kV. The cross-section images of film samples were observed. For measuring diameter of fibers in nanoweb samples, Image J software was used, considering at least 20 fibers from 5 different images of samples for measurement.

4.2.4 Fourier transform infrared spectroscopy

Fourier transform infrared (FTIR) spectroscopy was performed to access the conformational changes using Thermo Scientific Nicolet 380 spectrometer in transmission mode with wave numbers in range 4000-650 cm^{-1}. The crystalline content in the samples was analysed by applying Fourier self-deconvolution in the amide III region as described in literature using Origin Pro 9.0 software [90].

4.2.5 X-ray diffraction

X-ray diffraction intensity curves of the samples were obtained using Rigaku Ultima IV diffractometer with CuKα radiation at a λ=1.5 Å in the measurement range 2θ from 10° to 60°. Percentage crystallinity was calculated using equation 1

$$\text{Percent Crystallinity} = \frac{\text{Total area of crystalline peak}}{Total\ area\ of\ crystalline\ and\ amorphous\ region} \times 100 \qquad (1)$$

4.2.6 Thermogravimetric analysis

Thermal stability of the samples was analysed using Thermo Gravimetric Analysis (TGA) technique under nitrogen atmosphere at the rate of 10°C/min from 30° to 900°C, using Perkin Elmer pyris-4000 thermal analysis system. The derivative plots were obtained to further clearly access the thermal decomposition behaviour of samples.

4.2.7 Differential thermal analysis

Differential Scanning Calorimetry (DSC) was performed using thermal analysis instrument (TA Q200) with scanning speed of 10°C/min and 2°C/min for films and nanoweb samples respectively, under nitrogen gas flow at 20ml/min.

4.2.8 Mechanical testing

Mechanical properties of the film samples were analysed using Zwick Roell Z250 UTM in tensile mode, fitted with 50 N load cell at a test speed of 10 mm/min. The sample dimensions were kept 50×10×0.25 mm, as per ASTM D 882. The test was carried out for five sets of samples.

4.2.9 Percentage swelling

Percentage swelling capacity of the samples was determined. Briefly, pre weighed samples were immerged in miliQ water. The samples were carefully removed, pat dried with tissue paper to remove excessive fluid and weighed in the swollen state at regular intervals. This was repeated until equilibrium value of swelling was reached. Afterwards, percentage swelling of the blend films was calculated via following equation:

$$\text{Percentage Swelling} = \frac{W_t - W_0}{W_0} \times 100 \qquad (2)$$

where W_t is weight of swollen sample at time t and W_0 is the weight of dry sample initially.

4.2.10 Contact angle measurements

To measure the water contact angle, 2 ml of miliQ water was dropped on the surface the sample with a syringe using 21-gauge needle. The images of the drops were taken using a quad camera having 64-megapixel primary capturer and an f/1.8 lens, 8-megapixel secondary sensor having an f/2.2 lens, and two 5-megapixel sensors along with f/2.2 and f/2.4 lenses, within 10 seconds of dropping to avoid soaking of water

on the surface . The contact angles were measured using Image J software. The reported contact angles are mean of 10 measurements for each sample.

4.2.11 Biocompatibility tests

4.2.11.1 Cell viability through alamar blue Assay

Biocompatibility of the samples were analysed through alamar blue assay as reported in literature with slight modifications [91]. L929 fibroblast cells were used to test the cytocompatibility of blend films. The cells were maintained in Dulbecco′s modified eagle media (DMEM) with 10% fetal bovine serum (FBS) at 37°C, 5% CO_2, and 95% humidity. L929 cells, at a cell concentration of 5×10^3 cells, were seeded onto each sample of a 48 well plate. The cells were cultured for a period of 1, 3, and 5 days. On respective days, alamar blue assay was performed to assess the cell viability. In the case of film sample P100, as the scaffold was very unstable, we used an indirect cell viability study, where the 24-hour releasate from the scaffolds were used to treat the cells for the respective days.

4.2.11.2 Cell adherence and proliferation by scanning electron microscopy

The cytocompatibility of the mats were studied by checking the cell adhesion and morphology of L929 cells cultured over the samples using scanning electron microscopy (SEM). The L929 cells were cultured for 48 hours on the samples. After 48 hours, the cells were fixed with glutaraldehyde (2.5%) and then serially dehydrated using ethanol. The SEM micrographs were taken, after sputter coating these dehydrated samples with gold, by (FEI Quanta 200F SEM) microscope at 20 kV of operating voltage.

4.2.12 *In vitro* biodegradation

In vitro biodegradation of silk fibroin-PVA blend film samples was studied in simulated body fluid (SBF) according to the protocol described in literature with slight modifications [53]. The SBF was prepared following the salt compositions mentioned by Kokubo *et al.* [92]. The film samples of uniform size were cut, weighed and incubated in SBF. The temperature of incubator was maintained at 37°C. The solutions were replaced with fresh solution every two days to maintain the freshness. The weight loss data was collected at regular intervals for 6 weeks. Before weighing, samples were rinsed with miliQ water and dried in vacuum oven at 37°C. The Percentage weight loss in samples was calculated using following equation:

$$\text{Percentage weight loss} = \frac{W_f - W_i}{W_i} \times 100 \qquad (3)$$

Where, W_f is weight of sample at time t and W_i is the initial weight of sample.

4.2.13 Statistical analysis

All the tests were performed in triplicates, unless mentioned otherwise and the data is mentioned as mean±SD. Statistical significance of data at level $p<0.05$ was assessed using One-way analysis of variance (ANOVA).

4.3   Results and Discussion

In preparation of polymeric blends, the solvent used to dissolve the polymers plays a significant role. If the solvent used is incompatible with any of the polymeric component whose blend we are intending to make, it can result in phase separation and the purpose of blending the two might not get served. In our study, as we are blending PVA (which is water soluble) with non-mulberry silk fibroin, even though

water is a candidate to be used as solvent, but since ASF is unstable in water and has been found to form aggregates, as a consequence results in non-homogeneous solution when blended with PVA-water solution. Formic acid being more compatible with ASF resulted in homogenous solution and so did PVA, forming stable blend solutions at all compositions. The blend films were prepared using these solutions and were further characterized. In literature, the role of solvent has been studied by Um and co-workers on the blend miscibility of mulberry silk fibroin and PVA. They too observed formic acid to be a more suitable solvent than water for obtaining homogeneous blend solutions [93].

4.3.1   Morphological and structural analysis

The scanning electron microscopic (SEM) images of blend film cross-sections are shown in Fig. 4.2. It can be seen from the images that films show homogeneous morphology without any visible phase separation. Moreover, the surface of blend films containing silk fibroin was observed to be rough, while P100 sample showed smooth surface. The surface roughness might have appeared as a consequence of incubating the blend films in methanol to regenerate the crystallinity similar to observations made in our previous studies on non-mulberry silk fibroin materials [19,94]. Rough surface morphology is generally pragmatic to support cell attachment in biomaterials [95]. In most of the studies reported in literature, clear phase separation has been observed in silk fibroin and PVA blends, only one study reported by Um *et al* presented homogeneous morphology through SEM but the variety of silk used was mulberry [93].
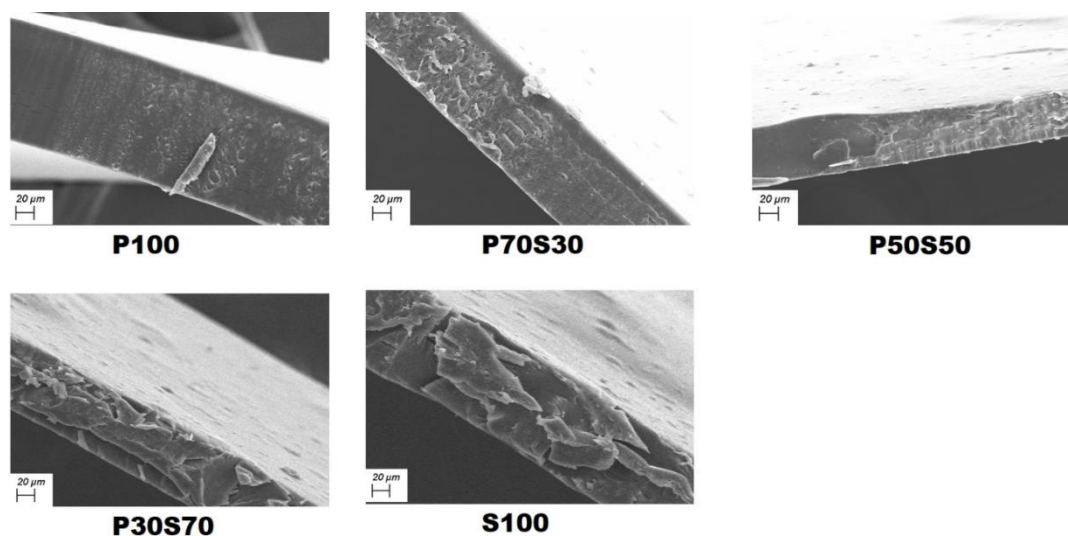
Fig. 4.2: Scanning Electron Microscopic (SEM) images of blend films

Conformational changes in materials are typically accessed by fourier-transform infrared (FTIR) spectroscopy technique. FTIR spectras of the silk-PVA film samples are shown in Fig. 4.3. The S100 sample showed a broad peak around 3413 cm^{-1} due to stretching of O-H groups. The sharp peaks in range 2921-2927 cm^{-1} corresponding to C-H stretching were observed. The amide I, II and III were observed at 1627, 1523 and 1216 cm^{-1} respectively. These amide signals represent the presence of β-sheet crystallinity in the S100 film sample[96,97].

The P100 sample showed a broad signal around 3303 cm^{-1} due to stretching of O-H groups in PVA . The signal at 2921 cm^{-1} represents the stretching of C-H groups. A sharp characteristic C=O stretching vibration was observed around 1700 cm^{-1} for pure PVA (P100) sample. This could have appeared due to presence of unhydrolyzed residual vinyl acetate in the PVA[98]. The O-H bending signal could be found at 1417 cm^{-1}.The signal at 1189 and 1183 cm^{-1} corresponds to vibrational stretching frequency of C-O-C and C-O bonds respectively. The appearance of these signals indicates towards acetal formation in some molecules of PVA while dissolved in formic acid.

The C-C stretching vibrations were observed at 830 cm^{-1}. The signals which appeared in the spectra of S100 and P100 samples individually were found to be present in all the blend samples with slight shift in frequencies and variation in their intensities depending upon the blend ratios. The hydroxyl groups in PVA and the amide groups in silk fibroin have the capacity to form intermolecular hydrogen bonds with each other which are usually suspected as broad signals in the 3200-3600 cm^{-1} region[99,100]. The broad signals for O-H bond stretching centred around 3270 cm^{-1} were observed for all three blend samples. The C-H stretching vibration signals were observed at 2927 and 2852 cm^{-1} for CH$_3$ and CH$_2$ groups respectively. The C=O stretching signal which was present in P100 was also found in blend films but with variable intensities. As expected, the reduction in PVA content, diminished the intensity of this signal from blend sample P70S30 to P30S70. The vibrational frequencies corresponding to C-O-C and C-O stretching were also observed in the blend samples. The C-C stretching frequency in blends was found to be slightly shifted towards higher wavenumber as compared to pure PVA (P100) sample.

The amide I and II signals indicating β-sheet crystallinity could clearly be detected in the blend samples as they were found in S100, but the amide III region could not be visibly resolved. In order to gain a better understanding of this region and to testify the crystallinity, fourier self-deconvolution (FSD) multi peak fit analysis was performed. A representative image of one such analysis in shown in Fig. 4.4. It was noticed that the amide II and III signals were slightly shifted as compared to the S100 sample. Shift in the FTIR signals has previously been associated with an indication of interaction amongst the polymers [33]. Luo *et al* has reported such shift in FTIR spectra of blend, due to interaction between PVA and *B. mori* silk fibroin components [101].
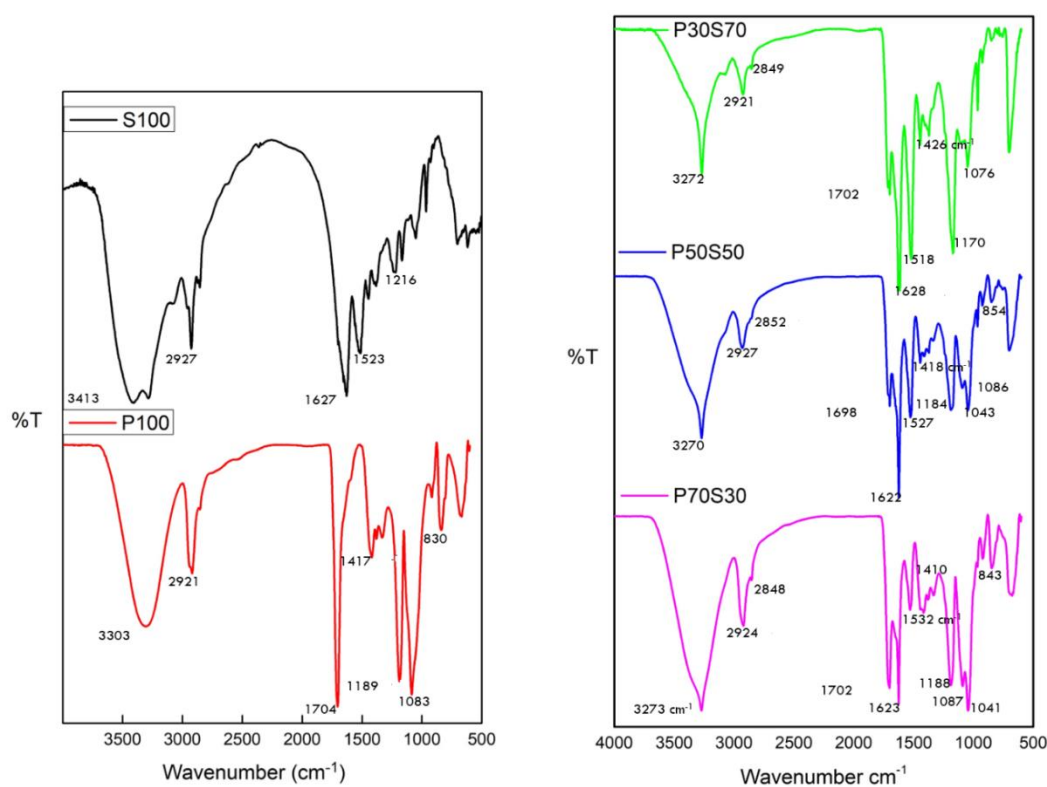
Fig. 4.3: FTIR spectras of the film samples
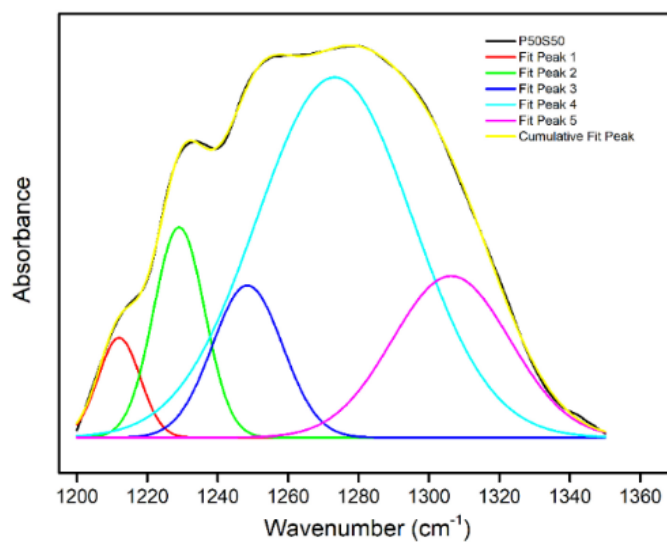
Fig. 4.4: Representative plot for Fourier self-deconvolution of P50S50 blend sample

The percentage β-sheet crystallinity index was also obtained through this analysis. The S100 film showed 42.68% β-sheet crystallinity which is in close agreement with

our previous studies and the data reported in literature for wild type regenerated silk fibroin [94,102]. P30S70, P50S50 and P70S30 showed 24.88%, 11% and 10.36% crystallinity respectively.

Furthermore, X-ray diffraction patterns were obtained in order to testify the structural analysis attained through FTIR. The XRD patterns of samples are shown in Fig. 4.5. Pure PVA has been reported to show a characteristic diffraction pattern with five signals at 2θ values of 11.5° (110), 19.5° (10⁻1), 20.1° (101), 23.0° (200) and 40.5° compound peak[103]. As observed in Fig. 5.5, P100 sample exhibited a broad diffraction pattern centred around 21.6°, which incorporates all the peak values mentioned above. In literature, the broadening of peak or enhanced amorphous characteristics of PVA dissolved in formic acid have been attributed to the acetal formation between PVA and formic acid solvent which enhances the degree of chemical crosslinking, as a result lowers crystallinity [104]. In another study reported by Um *et al.*, increased size of side groups as a consequence of partial conversion of OH groups in PVA to formate groups upon dissolution in formic acid have been made responsible for increased amorphous feature [93]. Formic acid being the solvent in our study we suspect, similar changes must have occurred in the PVA causing the peak to broaden. Upon blending silk with PVA, as expected, the crystallinity of the samples was found to decline as the content of PVA increased in blends. S100 sample presented its characteristic diffraction pattern with peaks at 17.06°, 20.08°, 24.4° and 34.1° corresponding to spacing 5.2, 4.4, 3.6 and 2.6 Å. These peaks are attributed to β-sheet crystallinity in the silk film samples Bhat and Nadiger have reported similar diffraction pattern for regenerated *Antheraea pernyi* silk fibroin, which is also a variety of wild type silk [102]. Only the peak at 2θ value around 30° was not observed in the S100 sample. The blend

film samples exhibited the diffraction pattern slightly different from both the pure components. Along with the peaks at 2θ values around 17° and 20.7° from silk and PVA components in the blend, additional new peak at 2θ value around 14° had appeared which was not found in the diffraction pattern of both P100 and S100 samples. This might have emerged as a consequence of changes in the crystal structure of polymeric blend due to interaction amongst the two polymers [105].
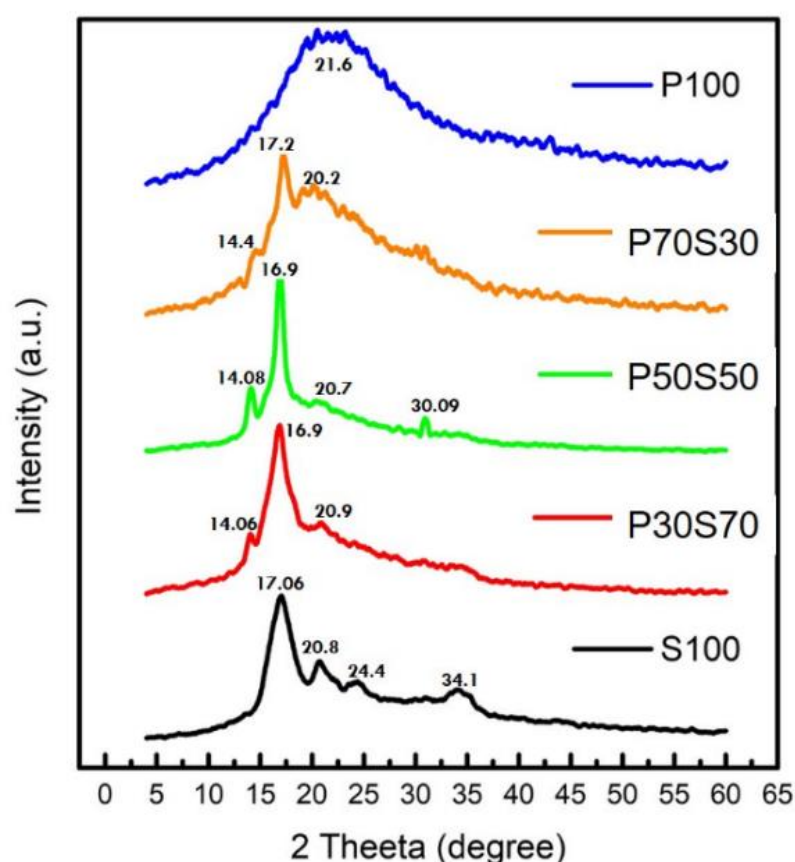
Fig. 4.5: X-ray diffraction patterns of film samples

Li *et al* has previously reported the appearance of similar diffraction peak at 2θ value around 14°, to formation of crystalline *B. mori* silk fibroin-PVA complex in the blend gel [106]. Moreover, a small peak at 2θ value 30.9° which was missing from S100 sample was found to be present in P50S50 blend.

Table 4.2: Percentage crystallinity of the film samples obtained through XRD

Sample	S100	P30S70	P50S50	P70S30
% Crystallinity	45.78±1.26	38.68±0.86	33.91±0.64	20.21±1.71

The percentage crystallinity calculated for the film samples is reported in Table 4.2. As clearly visible, the S100 sample showed high crystallinity of value 45.78% and P100 showed almost amorphous nature. Upon blending the two, the crystallinity was found to reduce with increased PVA content, which is in agreement to the pattern observed through FTIR crystallinity index. In one of the studies reported in literature on *B. mori* silk fibroin-PVA blends, role of casting solvent has been studied and it was found that in blends prepared using formic acid as solvent, silk being crystallized component, altered the overall crystallinity and blends with higher silk content presented more crystallinity [93], similar to observations made in our study.

From FTIR analysis, presence of interaction amongst the two polymeric components was suspected in the blends. Consistent with those results, the XRD patterns of blend films exhibited additional new peaks which further testifies the molecular interactions between silk fibroin and PVA in the blend films.

4.3.2   Thermal analysis

The thermal behaviour of film samples was analysed by TGA. The percentage weight loss in the films as a function of temperature is presented in Fig. 4.6a. The overall weight loss behaviour in the film samples can be divided into three distinct segments. In the first segment (Seg I), 30 to 150°C, slow weight loss with increase in temperature was observed. Majorly, due to loss of water in all the samples. In the second segment (Seg II), 150 – 400°C, S100 sample showed a major rapid weight loss

at 336°C , attributed to the breakdown of intermolecular interactions as well as the peptide backbone. The P100 sample exhibited a rapid weight loss at 300°C due to breaking of intermolecular interactions and a small weight loss in the third segment (Seg III), 400-600 at 455°C ascribed to its thermal degradation. Interestingly, the blend samples showed unique weight loss behaviour than both the pure components.
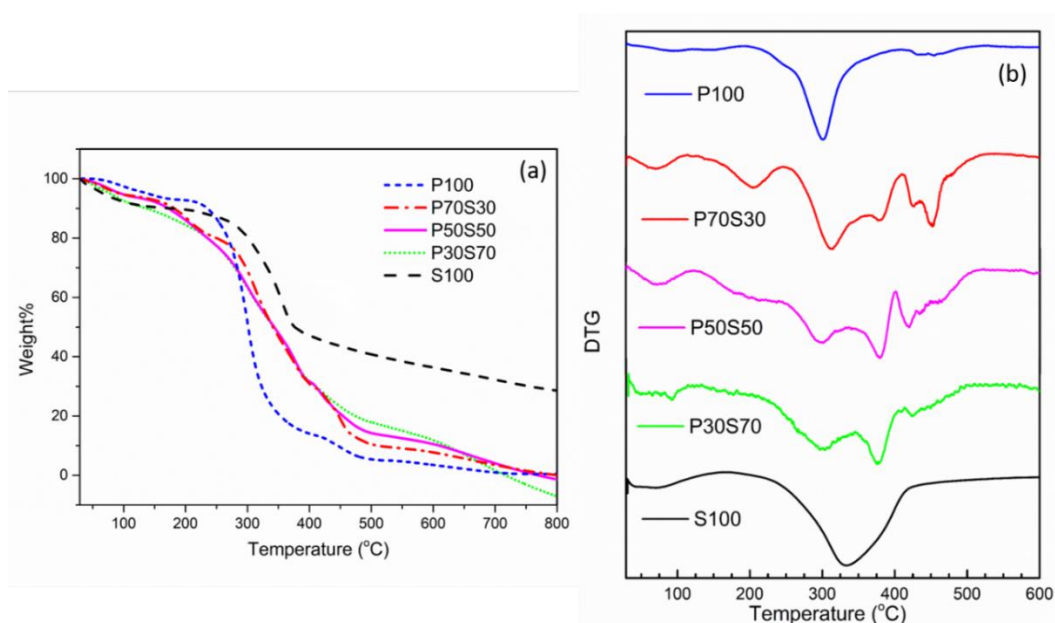
Fig. 4.6a and 4.6b: TGA and DTG curves of blend film samples

DTG (the first derivative of TGA) signals of blend film samples, as shown in Fig. 4.6b, not only differ in their position on temperature scale but also vary in their shapes as compared to the P100 and S100 film samples. The blend sample P30S70 presented two thermal degradation signals in Seg II at 300 and 375°C for the PVA and silk components. Wherein, the signal with respect to silk was found to have shifted from 336 to 375°C, this might have occurred as a result of intermolecular interaction between silk and PVA. A weak broad signal in the range 416-492°C due to thermal degradation of blend was also observed.

Upon increasing the PVA content in the blend i.e., P50S50 and P70S30, along with the appearance of signals in Seg II (like in P30S70), the signal in Seg III further refined, indicating better interaction among the two polymers .

Moreover, DSC studies were conducted for the comprehensive thermal analysis of blends. Fig. 4.7 shows the DSC curves of silk-PVA blend films with variable compositions. All the samples showed an endothermic signal around 100°C due to evaporation of bound water. The P100 sample presented one endothermic signal around 280°C responsible for degradation of PVA. The characteristic melting peak of PVA, usually observed at 223°C was found to be missing, indicating its amorphous structure which is consistent with the observations of XRD and FTIR. The glass transition temperature (T_g) of P100 sample was observed at 45.16°C. The S100 sample presented its T_g at 218°C and an endotherm at 273°C due to thermal decomposition of ordered crystalline structures was observed. Interestingly, the T_g in all three blend samples were shifted from the values observed for pure components and were found to lie in the middle of those two (45.16 and 218°C) i.e., at 148, 155.16 and 158°C for P70S30, P50S50 and P30S70 respectively. Moreover, the T_g corresponding to pure PVA and ASF were absent in blend film samples. The appearance of new single T_g in each blend sample and disappearance of T_g corresponding to pure components indicate towards formation of miscible blend between ASF and PVA. It is pertinent to note that amongst the limited work reported in literature on non-mulberry silk fibroin- PVA blends, no such observation based on T_g through differential scanning calorimetry has been reported. However, DeFrates *et al.* have reported the formation of miscible blend between thai silk and cellulose by observing single T_g in each blend along with shift in their values with varying blend

components [91]. Interestingly, Um *et al.* have reported the formation of partially miscible blend between *B. mori* silk fibroin and PVA using formic acid solvent, as they observed intermediate relaxation peaks along with the T_g of pure components in their blend samples obtained via dynamic mechanic analysis [93]. In another study described by Wang *et al.* on silk nanospheres and microspheres prepared via silk-PVA blend films have shown the appearance of T_g of both silk as well as PVA with slight shift in their position, dependent on the blend composition [32].
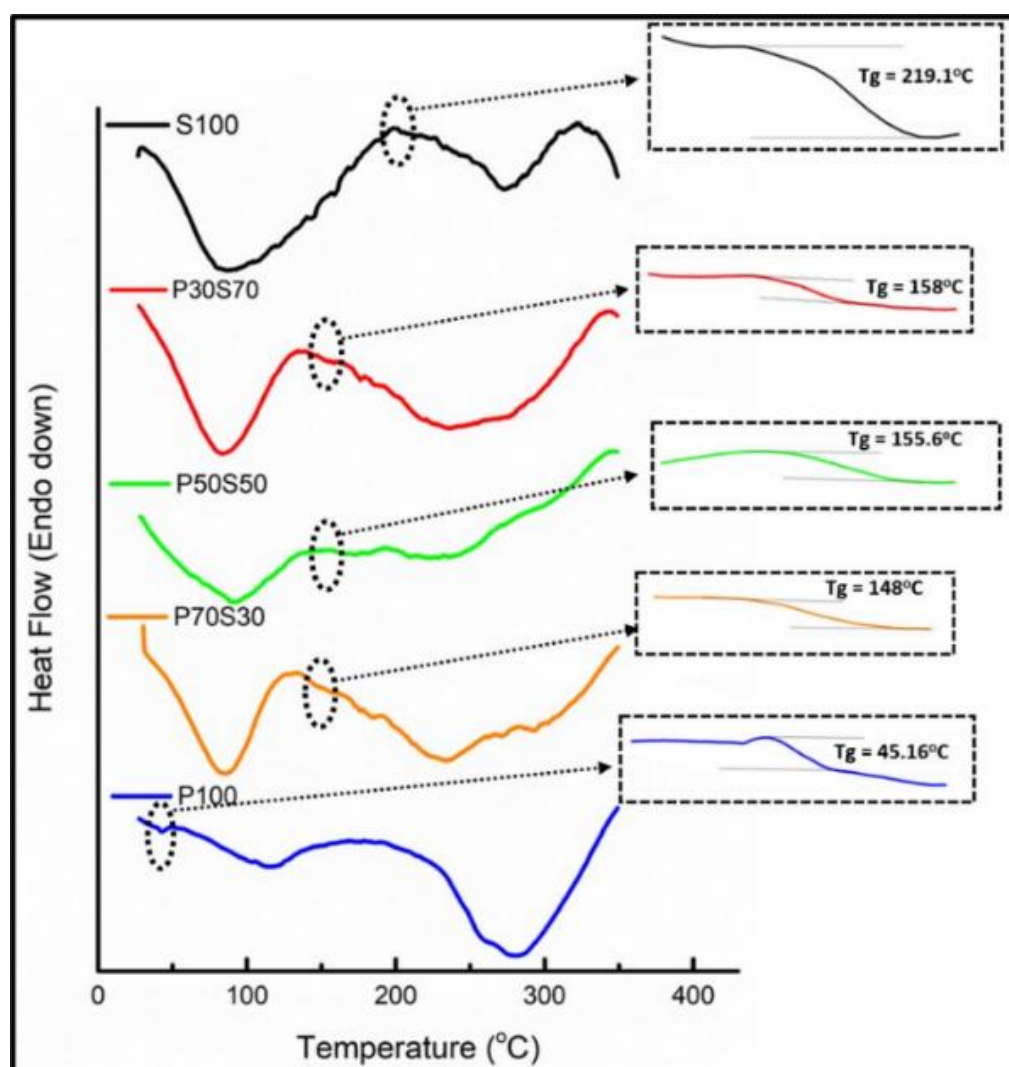
Fig. 4.7: The DSC thermogram of blend film samples

The blend film sample P70S30 showed a broad endotherm centred around 232°C with a small shoulder around 300°C corresponding to the thermal decomposition and degradation of the material respectively. Similarly, P30S70 blend film presented a broad endothermic signal where thermal decomposition (at 233°C) and the degradation signal (around 303°C) merged into each other. The P50S50 blend film showed a broad endotherm due to decomposition of blend at 229°C and a shoulder around 305°C as result of blend degradation. This broadening of signals along with the shift in peak values can be attributed to alteration in crystalline form as a result of interactions amongst the molecular chains of two polymers. Similar observations have been reported previously in literature by Luo *et al*, where broadening of endothermic signals due to addition of nanometric *B.mori* silk fibroin peptide powder to PVA was considered a consequence of change in crystal form of the blend films[101]. The change in crystalline structure of the blend films is also validated by XRD studies reported above.

The morphological, structural and thermal analysis data collectively reveals the formation of miscible blend between silk fibroin and PVA along with changes in its crystalline structure.

4.3.3 Mechanical analysis

In order to determine the performance of any material which is likely to go under any kind of stress while usage, mechanical properties are essential to be analysed. The mechanical testing of film samples was carried out in tensile mode. The obtained stress-strain curves are shown in Fig. 4.8
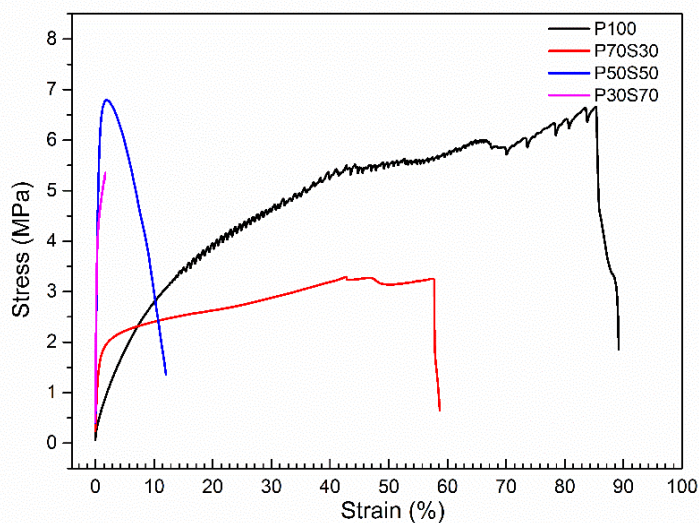
Fig. 4.8: Stress-strain curve of the film samples in tensile mode.

Table 4.3: Mechanical properties of film samples obtained through Tensile tests. The data is presented as Mean ± SD, where n=5

Sample	Ultimate Tensile Strength (MPa)	Percentage Elongation at Break	Young's Modulus (MPa)
P100	6.7 ± 0.3	85.3 ± 6.3	62±0.2
P70S30	3.2 ± 0.8	57.6± 2.6	119.9±1.2
P50S50	6.8 ± 1.2	1.8 ± 0.3	485.8±2.4
P30S70	5.3 ± 0.1	1.7 ± 0.3	475.9±0.3

The data could not be obtained for pure S100 film sample as it broke down while clamping itself, due to high brittleness. As visible in the figure, addition of PVA to silk fibroin has effectively altered the mechanical properties. Table 4.3 summarizes the mechanical properties observed for the film samples.

It was found that the P100 film was strong and tough and the toughness of blend P70S30 was also high. But the blend samples with lower proportion of PVA i.e., P50S50 and P30S70 were quite brittle. The young's modulus which provides an essence of stiffness in material was found to be lower in blend samples with higher proportion of PVA except P30S70 which presented slightly lower value than P50S50

53

despite higher PVA content. The breaking strain of the blend film samples increased with the increased proportion of PVA, indicating construction of miscible polymeric blend system. Similar enhancement of mechanical properties has been interpreted as formation of miscible multicomponent polymeric system in case of *B.mori* and tasar silk fibroin blend films by Yang and co-workers [107]. The structural changes at molecular level due to blending the two polymers in formic acid, as observed through FTIR and XRD could be ascribed to such mechanical enhancement of properties. As the amorphous content increases in blends with increasing proportion of PVA, it raises the inner free volume for the molecular chain movement, imparting flexibility which is indicated through enhancement in percentage elongation (Table 4.3). Since silk fibroin is providing the crystalline component to the blends, its higher proportion resulted in high value of ultimate tensile strength in P30S70 while P70S30 showed lower value.

4.3.4   Percentage swelling and contact angle measurements

The hydrophilicity of blend films was investigated through contact angle measurements. The more hydrophilicity indicated through smaller contact angles of biomaterials is known to enhance the adherence and proliferation of cells on its surface [108].

The S100 sample showed contact angle of 76°, representing hydrophilic surface, since it possesses high content of hydrophilic/hydrophobic amino acid as reported previously [109]. It was observed that as ASF was blended with PVA, the contact angles reduced further up to values 72°, 69° and 61° for P30S70, P50S50 and P70S30 blend film samples respectively. As clearly indicated by the reduced contact angles, the

surface of the blend films became more hydrophilic with increasing content of PVA due to its inherent hydrophilic nature.
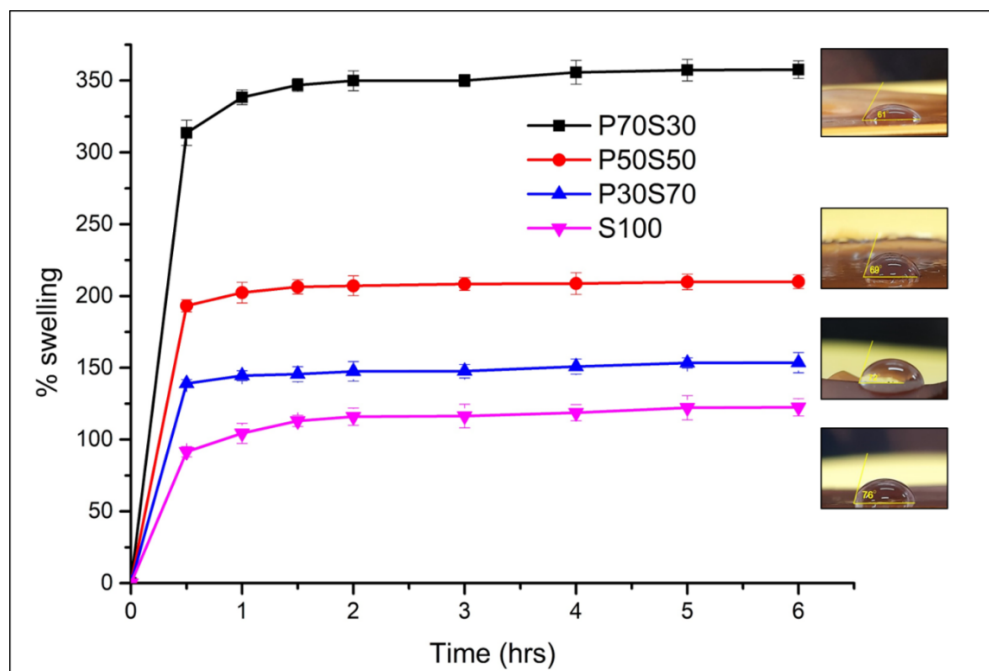
Fig. 4.9: Percentage swelling study and contact angle measurement of blend films. The error bars represent standard deviation for n=3.

The percentage swelling studies of blend films are shown in Fig. 4.9. Since PVA is hydrophilic and water soluble in nature, the P100 sample dissolved readily at physiological temperature during the study. For rest of the samples, it was observed that blending ASF with PVA tremendously enhanced the swelling which attained equilibrium after a period of four hours.

The S100 sample showed swelling of around 122% while the swelling is blend samples increased up to 154%, 210% and 358% for P30S70, P50S50 and P70S30 respectively. Enhancement of percentage swelling has also been reported in literature by Bhattacharjee and co-workers for gland extracted tasar silk fibroin/PVA blend nanofibrous matrices [41].

4.3.5 Biocompatibility

The cell viability study of L929 fibroblast cells conducted through Alamar blue assay presented all the samples with good biocompatibility as shown in Fig. 4.10. In the case of P100, the cells were treated with releasate of the films it didn't show much difference from the control values. The S100 sample showed better viability of cells in comparison to the rest of the samples on all days due to presence of RGD sequence in its protein chain, implying the processing did not alter this inherent property of ASF [110]. The cell viability index value greater than 0.7 is well supported for non-toxicity in literature [111]. The blending of ASF with PVA enhanced the viability index of fibroblast cells making the films further biocompatible.

This observed biocompatibility was well supported by SEM data shown in Fig. 4.11. Herein, we found that with increasing content of ASF in the blend, the fibroblast cells seeded on them started to spread and attain their characteristic morphology. ASF has previously been well reported in literature to support the attachment and proliferation of cells[31–34]. In one of the studies, Bharadwaj and Kundu have used AM gland extracted silk fibroin as a substrate for attachment and growth of mesenchymal stem cells in blend scaffolds with chitosan [12].

As clearly visible in Fig. 4.11b, the cells in P70S30 were observed to be spherical and not spread due to lower content of ASF, however in the case of samples P50S50 (Figure 4.11c) and P30S70 (Fig. 4.11d) the cells were found to be more spread and started attaining its characteristics morphology. These two studies in hands together suggested that blending cocoon extracted ASF with PVA favoured the adhesion and thereby growth of the cells making it a suitable candidate as a tissue engineering material.
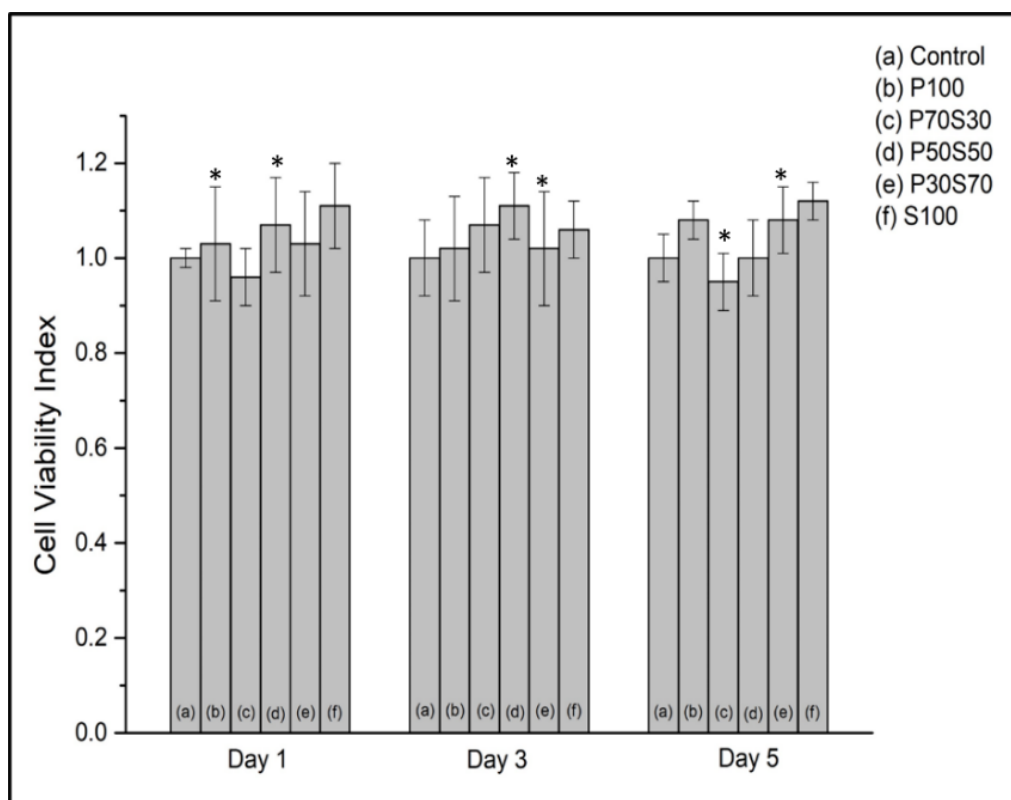
Fig. 4.10: Cytocompatibility of blend films through Alamar Blue Assay. The error bars represent the standard deviation for n =3. (*p < 0.05)

To the best of our knowledge, the efficiency of cocoon extracted ASF and PVA blend films has been reported for the very first time through this study and is well supported by the aforementioned observations. The very few studies reported on nonmulberry silk fibroin and PVA blend biomaterials have presented their efficacy in wound healing as well as tissue engineering applications but the source of extraction of silk fibroin has been from silkworm gland only. Chouhan and co-workers have investigated the wound healing capability of blends prepared by different variety of growth factors functionalized silk fibroin and PVA, the blends prepared with non-mulberry silkworm gland extracted silk fibroin were observed to be more efficient than the same prepared by mulberry variety and showed accelerated healing of chronic diabetic wounds [114] . The efficiency of silk fibroin-PVA blends has also been explored in the form of nanofibers for bone tissue scaffolding material by

Bhattacharjee *et al.* through utilization of gland extracted non-mulberry silk fibroin [41]. In this study, for the very first time, the efficiency of cocoon extracted silk fibroin and PVA blend films has been reported and is well supported by the adhesion and proliferation of L929 fibroblast cells.
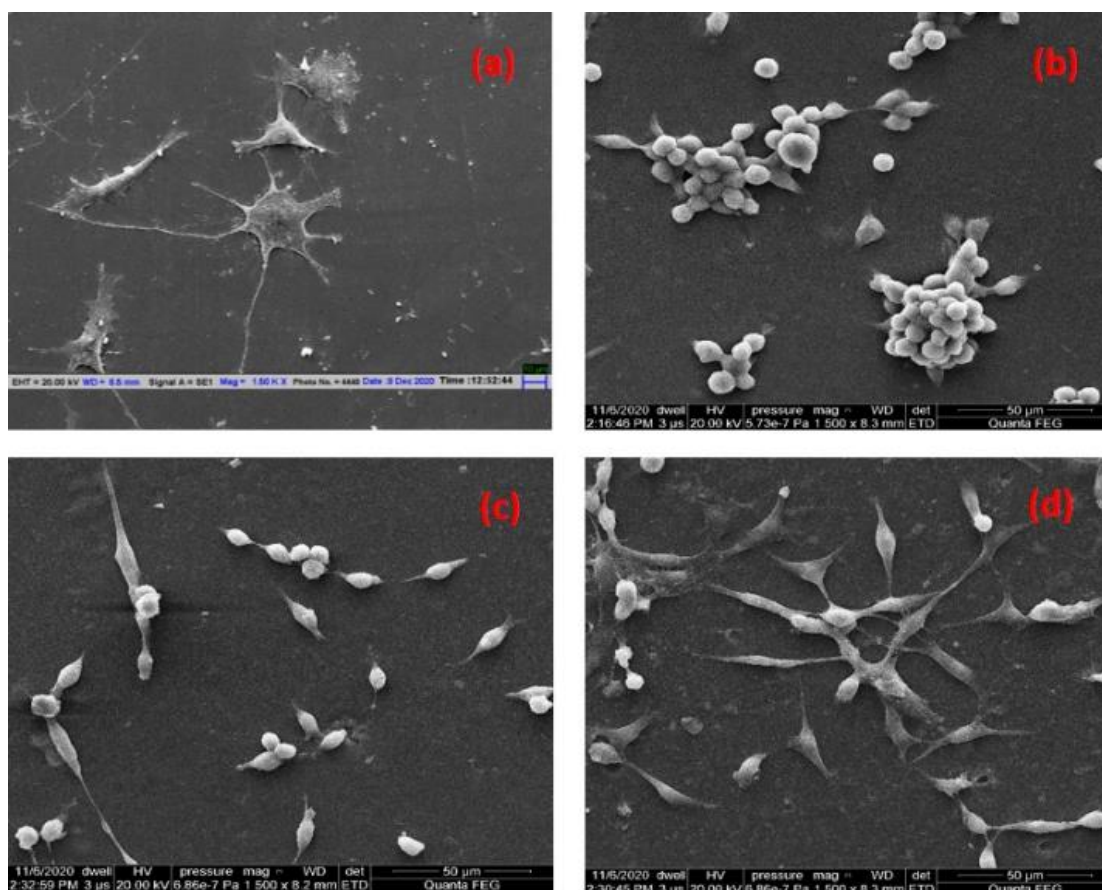
Fig. 4.11: Scanning electron micrographs of L929 fibroblast cells seeded on blend films after 48h culture (a) Control (b) P70S30 (c) P50S50 (d) P30S70

4.3.6 Biodegradation

The *in vitro* biodegradation study of all the film samples (in 5 sets) carried out in simulated body fluid(SBF) for a period of 4 weeks is presented in Fig 4.12. The P100 film sample being unstable at physiological temperature was found to readily dissolve in SBF. A relatively sharp weight loss was observed for rest of the blend film

samples for initial period of 7 days. After that, a steady weight loss was observed for all the samples, with S100 showing lowest value of weight loss (~9%) after 4 weeks.
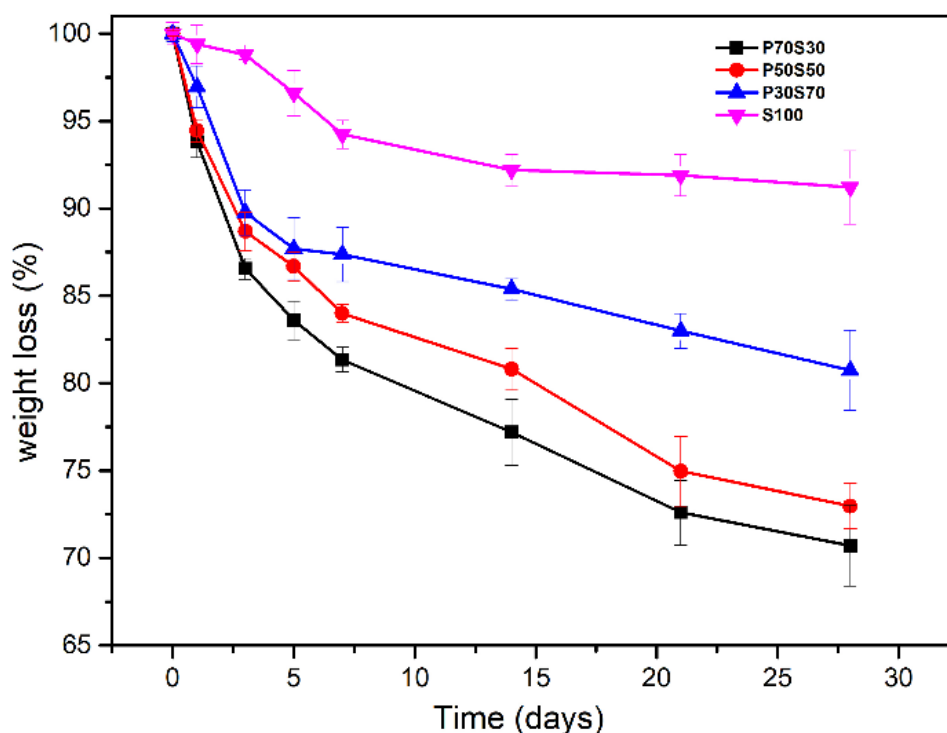
Fig. 4.12 Biodegradation of film samples with time in Simulated Body Fluid (SBF) at physiological temperature.

Low biodegradation of silk fibroin has been associated with β-sheet crystallinity in films prepared by Jin *et al* [115]. In our study, the samples with higher silk fibroin content showed slower degradation as compared to sample with high PVA content. This can be attributed to the variable crystallinity of the films at different blend ratios as confirmed by FTIR and XRD studies mentioned previously. The extent of crystallinity among polymers is known to impact their biodegradation, with amorphous regions being easily accessible for hydrolysis by enzymes and water molecules, so are more prone as compared to crystalline regions [105]. As a consequence of reduced crystallinity, the P70S30 film sample showed fastest degradation with a

weight loss of ~29% followed by P50S50 which as a result of similar crystallinity index showed ~27% weight loss. Similar impact of crystalline content was observed in one of our previous study on silk fibroin- gelatin blend films [94]. The current observed data indicates that tailored biodegradability can be achieved by varying the blend ratio in these samples as per the end use application.

4.4 Conclusions

➤ Flexible blend films of *Antheraea mylitta* silk fibroin and polyvinyl alcohol (PVA) were successfully prepared.

➤ The SEM images showed single phase morphology in the blend films.

➤ The structural studies indicated molecular interactions in the two polymeric components with variable crystallinity.

➤ The blend miscibility was further supported by thermal analysis of films. The positive impact of blending ASF and PVA was also presented by better mechanical properties.

➤ The higher swelling and hydrophilicity along with excellent cell viability index suggested biocompatibility of blend films towards growth of L929 fibroblast cells.

➤ The blending of these two polymers not only enhanced the blend properties harmonically but also eliminated the need of any chemical additives for their stability.

➤ The improved functional properties along with alterable biodegradability dependent on polymer blend ratio makes these films suitable for versatile applications in biomedical field.

➤ The results of this study have been published in **Journal of Applied Polymer Sciences.**

Chapter 5 :

CTAB Modified Montmorillonite Doped Tasar Silk Fibroin/PVA Blend 3D-Nanowebs for Tissue Engineering Applications

5.0 Overview

In this chapter, the cation exchange capacity of nanoclays is explored to modify sodium montmorillonite (MMT) clay with the quaternary ammonium ions in CTAB, which has been used as a model drug. The nanoclay is expected to enhance the mechanical properties along with acting as a drug carrier. Further, the CTAB modified nanoclay (CTAB-MT) are loaded into the blend solutions of tasar silk fibroin and PVA. The process parameters are optimized for smooth electrospinning and interestingly, novel 3D nanoweb-like architectures are observed.

This chapter summarizes the preparation, characterization and analysis of modified nanoclay. It also details the preparation, results and discussion of electrospun 3D nanowebs of *Antheraea mylitta* silk fibroin and PVA. The structural, thermal, mechanical and biological properties of the developed nanowebs is detailed in this chapter. As observed in this study the aforementioned properties can be tailored by varying the blend ratios of silk fibroin and PVA to develop materials for specific end use applications.

5.1 Materials

Cocoons of *Antheraea mylitta* silkworm were bought from Central Silk Board, Son Bhadra, U.P, India. Polyvinyl alcohol (M.W.: 14000) was procured from Thermo Fisher Scientific, India. Formic acid was bought from Loba Chemie Pvt. Ltd, India.

Methanol was provided by Finar Chemicals Limited, India. Clay nanopowder sourced from montmorillonite with 3–10 meq/100 g cation exchange capacity (CEC) and avg. particle size of 80–150 nm and cetyltrimethylammonium bromide (CTAB) were purchased from SRL Pvt. Ltd., Maharashtra, India. The L929 fibroblast cells were received from National center of cell science (NCCS), Pune, India. The ionic liquid BmimAc (1-butyl-3-methylimidazolium acetate), Fetal bovine serum (FBS) and Dulbecco's modified Eagle's medium (DMEM) were obtained from Sigma Aldrich.

5.2 Methods & Characterization

5.2.1 Extraction of silk fibroin from tasar silk cocoons by degumming

The *Antheraea mylitta* silkworm cocoons were degummed to remove sericin using the procedure described in literature[83]. Briefly, the cocoons were cut into small pieces and heated in distilled water with 0.02 M $NaHCO_3$ at 100 °C for 30 mins twice. The fibroin so obtained was given two washes of distilled water to get rid of all the residual sericin. The degummed silk fibers were dried overnight in oven at 60°C.

5.2.2 Modification of sodium montmorillonite nanoclay with CTAB

Montmorillonite (MMT) clay was modified with CTAB and the modification method is described as follows. The clay (3 g) was added to 1mM CTAB solution (30 mL) and stirred continuously at room temperature for 7 days followed by ultrasonication. To remove the excess salts, resulting solution was filtered and washed several times with miliQ water. The dispersion was then centrifuged, supernatant was discarded and clay was dried at 90°C. The dried CTAB-MT clay was stored (Fig. 5.1) and analysed for successful modification via FTIR and XRD.
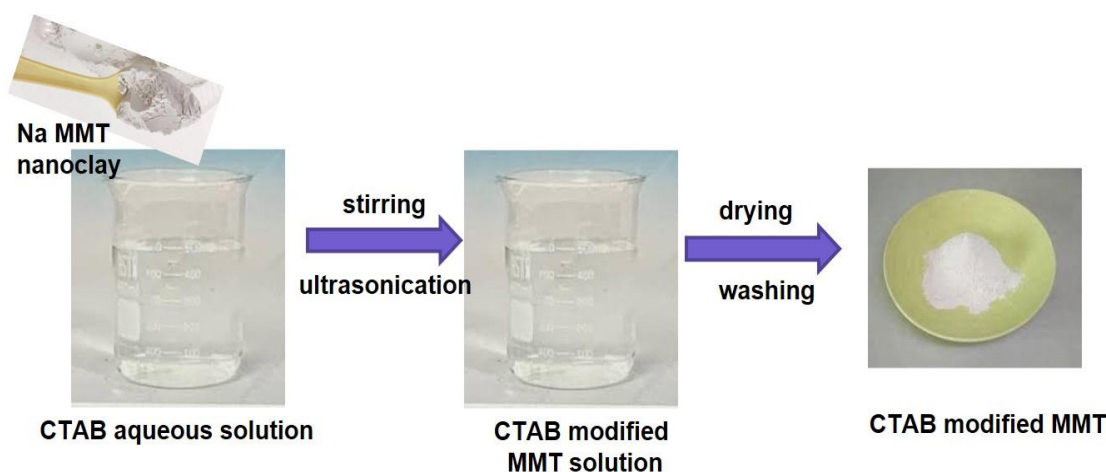
Fig. 5.1 The schematic representation of nanoclay modification process.

5.2.3 Preparation of CTAB modified montmorillonite clay doped 3D nanowebs

Silk fibroin stock solution (10% w/v) and PVA stock solution (10% w/v) were prepared using formic acid as solvent. These two solutions were mixed together in blend ratios 50:50 and 30:70 to prepare PSNF50 and PSNF70 blend solutions respectively. Further, obtained modified montmorillonite clay (CTAB-MT) (0.75% w/w) was added to PSNF70 and PSNF50 blend solutions and the solutions were sonicated for 20 mins. These blend solutions were electrospun using a 20 mm gauze needle attached to a 10 mL syringe by applying voltage in the range 17-20 kV. The flowrate and tip to collector distance were maintained at 0.5 mL/hr. and 8 cm respectively. The abbreviations used for prepared samples are presented in Table 5.1

Table 5.1: Compositions and abbreviations of prepared blend 3-D nanoweb samples

S. No.	Silk 10% (w/v)	PVA 10% (w/v)	Sample	CTAB-MT %(w/w)
1	50	50	PSNF50	0
2	30	70	PSNF70	0
3	50	50	PSNF50MC	0.75
4	30	70	PSNF70MC	0.75

5.2.4   Scanning electron microscopy

The surface morphology of the samples was observed through sputter coating the samples with gold and analysed using Zeiss EVO 18 FESEM (field-emission scanning electron microscope) at a voltage of 20 kV. The cross-section images of film samples were observed. For measuring diameter of fibers in nanoweb samples, Image J software was used, considering at least 20 fibers from 5 different images of samples for measurement.

5.2.5   Atomic force microscopy

The Asylum Research (MFP3D-BIO MNF) instrument equipped with a V shape cantilever having 40 N/m spring constant was used in tapping mode to analyse the surface morphology of samples. The scanning area of 5 × 5μm size of samples was analysed at room temperature. The roughness parameters were obtained by using Nanoscope analysis software.

5.2.6   Fourier transform infrared spectroscopy

Fourier transform infrared (FTIR) spectroscopy was performed to access the conformational changes using Thermo Scientific Nicolet 380 spectrometer in transmission mode with wave numbers in range 4000-650 cm^{-1}. The crystalline content in the samples was analysed by applying Fourier self-deconvolution in the amide III region as described in literature using Origin Pro 9.0 software [90].

5.2.7   X-ray diffraction

X-ray diffraction intensity curves of the samples were obtained using Rigaku Ultima IV diffractometer with CuKα radiation at a λ=1.5 Å in the measurement range 2θ from 10° to 60°. Percentage crystallinity was calculated using equation 1

$$\text{Percent Crystallinity} = \frac{Total\ area\ of\ crystalline\ peak}{Total\ area\ of\ crystalline\ and\ amorphous\ region} \times 100 \qquad (1)$$

5.2.8 Thermogravimetric analysis

Thermal stability of the samples was analysed using Thermo Gravimetric Analysis (TGA) technique under nitrogen atmosphere at the rate of 10°C/min from 30° to 900°C, using Perkin Elmer pyris-4000 thermal analysis system. The derivative plots were obtained to further clearly access the thermal decomposition behaviour of samples.

5.2.9 Differential thermal analysis

Differential Scanning Calorimetry (DSC) was performed using thermal analysis instrument (TA Q200) with scanning speed of 10°C/min and 2°C/min for films and nanoweb samples respectively, under nitrogen gas flow at 20ml/min.

5.2.10 Mechanical testing

Mechanical properties of the film samples were analysed using Zwick Roell Z250 UTM in tensile mode, fitted with 50 N load cell at a test speed of 10 mm/min. The sample dimensions were kept 50×10×0.25 mm, as per ASTM D 882. The test was carried out for five sets of samples.

5.2.11 Percentage swelling

Percentage swelling capacity of the samples was determined. Briefly, pre weighed samples were immerged in miliQ water. The samples were carefully removed, pat dried with tissue paper to remove excessive fluid and weighed in the swollen state at regular intervals. This was repeated until equilibrium value of swelling was reached. Afterwards, percentage swelling of the blend films was calculated via following equation:

$$\text{Percentage Swelling} = \frac{W_t - W_0}{W_0} \times 100 \qquad (2)$$

where W_t is weight of swollen sample at time t and W_0 is the weight of dry sample initially.

5.2.12 Porosity measurements

The porosity of samples was measured by liquid displacement method using hexane as it is a non-solvent for PVA and silk fibroin [18].Squared piece samples of 30×30 mm were dipped for 15 minutes in the known volume of hexane (V_i) in a graduated measuring cylinder. After 15 minutes the volume of hexane (V_f) was noted. Then the samples were removed from the cylinder and the residual hexane volume (V_r) was recorded. The porosity of nanoweb samples was calculated using the equation (3).

$$\text{Porosity (\%)} = \frac{V_i - V_r}{V_f - V_r} \times 100 \qquad (3)$$

5.2.13 Biocompatibility tests

5.2.13.1 Cell viability through alamar blue Assay

Biocompatibility of the samples were analysed through alamar blue assay as reported in literature with slight modifications [91]. L929 fibroblast cells were used to test the cytocompatibility of blend films. The cells were maintained in Dulbecco′s modified eagle media (DMEM) with 10% fetal bovine serum (FBS) at 37°C, 5% CO_2, and 95% humidity. L929 cells, at a cell concentration of 5×10^3 cells, were seeded onto each sample of a 48 well plate. The cells were cultured for a period of 1, 3, and 5 days. On respective days, alamar blue assay was performed to assess the cell viability. In the case of film sample P100, as the scaffold was very unstable, we used an indirect cell viability study, where the 24-hour releasate from the scaffolds were used to treat the cells for the respective days.

5.2.13.2 Cell adherence and proliferation by scanning electron microscopy

The cytocompatibility of the mats were studied by checking the cell adhesion and morphology of L929 cells cultured over the samples using scanning electron microscopy (SEM). The L929 cells were cultured for 48 hours on the samples. After 48 hours, the cells were fixed with glutaraldehyde (2.5%) and then serially dehydrated using ethanol. The SEM micrographs were taken, after sputter coating these dehydrated samples with gold, by (FEI Quanta 200F SEM) microscope at 20 kV of operating voltage.

5.2.14 Antimicrobial activity

The antimicrobial activity of these nanoweb samples was determined against *E. coli* (Gram negative) and *S. aureus* (Gram positive) strains using the method as described previously [116]. The samples were cut into small circular discs of 6 mm diameter and were placed on the agar plates cultured with bacteria post UV light treatment. The sealed plates were then incubated at 37°C for 24 hours. Subsequently, these incubated samples were carefully picked up from the agar plates and dipped in 10 mL of miliQ water in test tubes and were kept in an incubator shaker bath for 30 mins at 120 rpm to release the bacteria from samples. Further, serial dilution of these solutions was carried out up to 10^{-5} times. The agar plates were prepared and these serially diluted solutions (20 µL) of respective samples were spread over it. The plates were then sealed and incubated for 24 hours at 37 ^{o}C. After 24 hours, the bacterial colonies grown over plate were counted and the percentage antimicrobial activity of samples was measured using equation (4).

$$\text{Antimicrobial activity (\%)} = \frac{c-s}{c} \times 100 \qquad (4)$$

where, C and S represent the number of colonies in control and test samples respectively.

5.2.15 *In vitro* biodegradation

The silk fibroin- PVA nanoweb samples were tested for their biodegradation in enzymatic solution of Proteinase K enzymes at 37 ^{o}C respectively [19,112]. The activity of enzymatic solution was maintained by regular exchange with fresh solution. The percentage weight loss was obtained following equation 5.

$$\text{Percentage weight loss} = \frac{W_f - W_i}{W_i} \times 100 \tag{5}$$

Where, W_f is weight of sample at time t and W_i is the initial weight of sample.

5.2.16 Statistical analysis

All the tests were performed in triplicates, unless mentioned otherwise and the data is mentioned as mean±SD. Statistical significance of data at level $p < 0.05$ was assessed using One-way analysis of variance (ANOVA).

5.3 Results and Discussion

5.3.1 Fourier Transform Infrared Spectroscopy of modified clay

The FTIR of pure clay sample and the clay modified with CTAB (CTAB-MT) was obtained to verify the modification of clay. As visible in Fig. 5.2, pure clay presented its conventional signals in 950-1100 cm^{-1} region corresponding to vibrational stretching of Si-O bond and signal corresponding to stretching vibrations of structural O-H group [117]. The CTAB-MT sample showed additional signals in the range 2790-3050 cm^{-1} corresponding to CH$_2$ asymmetric stretching vibrations at 2918 cm^{-1} and CH$_2$ symmetric stretching vibrations at 2854 cm^{-1} for alkyl chains of CTAB along

with the Si-O and O-H stretching signals as present for pure clay. The presence of these additional signals indicates towards successful modification of clay with CTAB-MT [118].
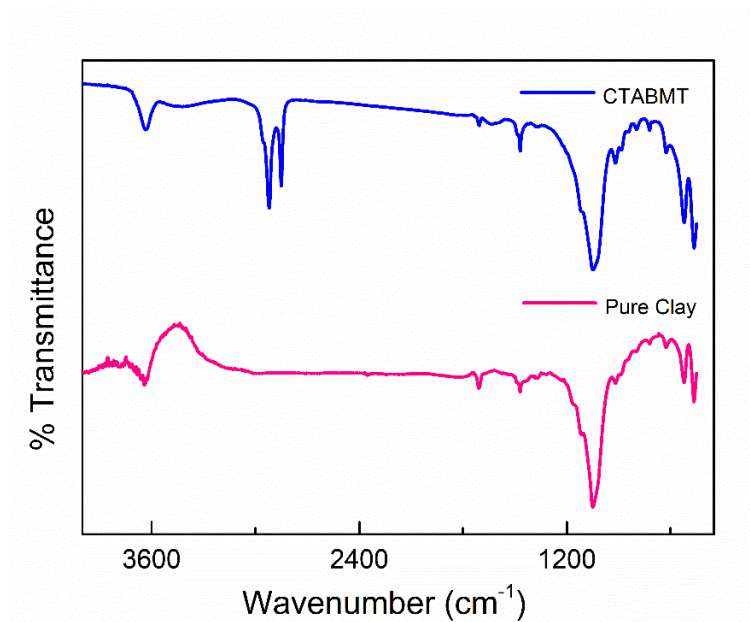
Fig. 5.2: FTIR spectra of pure and modified clay sample

5.3.2 X-Ray Diffraction of modified clay

The XRD of the clay samples was studied as shown in Fig. 5.3. The spectra of montmorillonite presented its charachterstic peaks at 2θ value 4.76° corresponding to d^{001} plane with basal spacing of 1.11 nm. While for CTAB-MT the peak was found to shift to 5.26° and the basal spacing increased to 1.57 nm due to intercalation of large CTA^+ ions in the interspace gallery of clay. Similar observations of increserd basal spacing of clay layers have been associated with clay modification in literature [117,119]. The peak corresponding to CTAB-MT in the XRD pattern of both PSNF50MC and PSNF70MC was absent indicating complete exfoliation of clay in the polymer matrix [120].
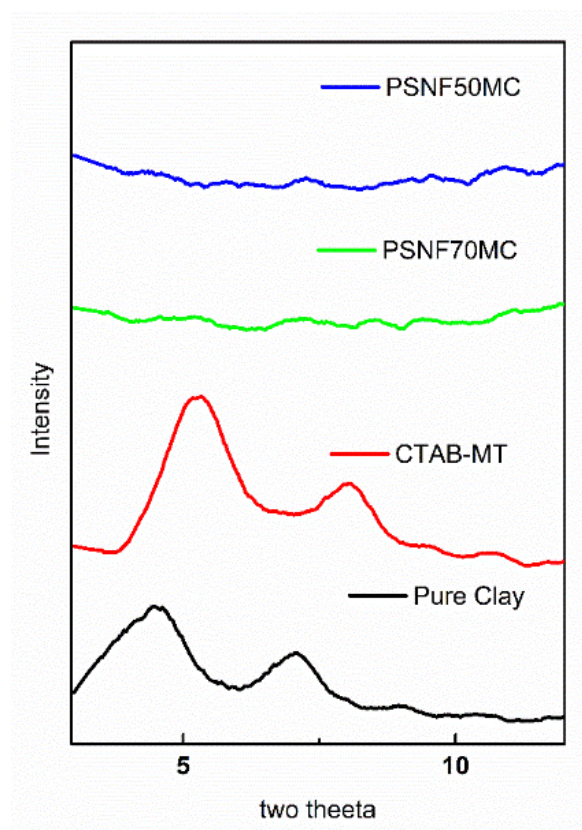
Fig. 5.3: XRD of pure clay, modified clay, PSNF70MC and PSNF50MC samples

5.3.4 Morphology of nanowebs

5.3.4.1 Scanning electron microscopy

The SEM images of pure as well as modified clay loaded nanofibers showed unique morphology with fibers being interconnected to each other forming nanowebs as shown in **Fig. 5.4** (a-f). In literature, nanofibers with similar morphology have been termed as nanonets which usually have very fine diameter (5-50 nm) and are observed to be forming nets which act like bridges between the main nanofibrous strands of higher diameters [121] .

Contrary to the general observations, the nanowebs in this study have been found to be randomly spread throughout the sample without showing any distinction between primary nanofibers and secondary nanonet bridges.
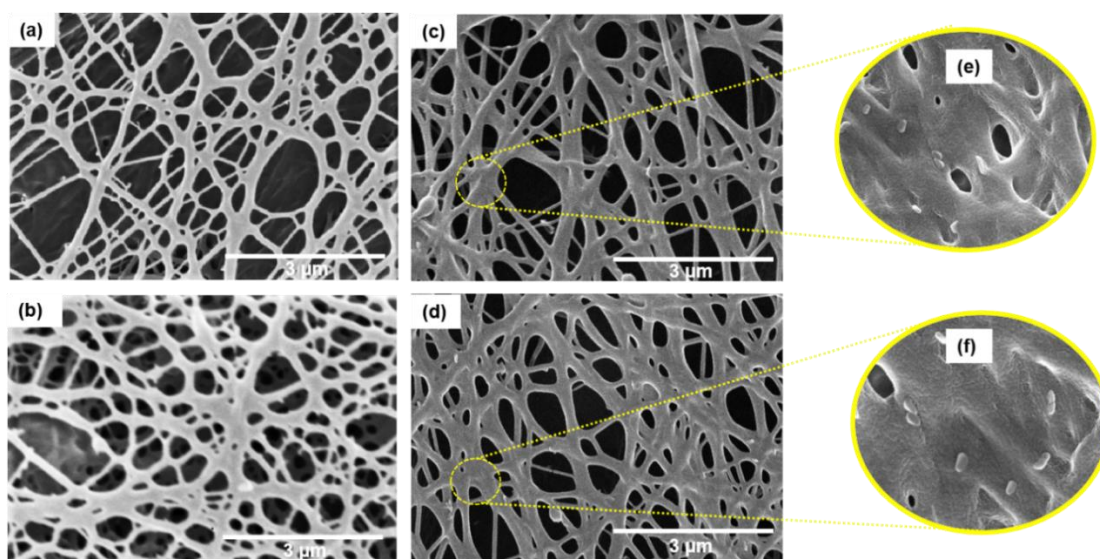
Fig. 5.4 Scanning electron micrographs of (a) PSNF50, (b) PSNF70, (c) PSNF50MC, (d) PSNF70MC at 15kX magnification, (e) and (f) show the presence of clay on the surface of nanowebs at higher magnification of 100kX.

The appearance of 3D nanoweb like morphology in current study can be attributed to the combined effect of several factors like high applied voltage, high conductivity and viscosity of the polymer solution. During electrospinning, the highly viscous charged droplet at the needle tip experiences instability under the influence of applied high voltage. Above certain threshold value, this results in deformation of the charged droplet causing ramification of jet into multiple tiny jets as the drag force and columbic repulsions overcome the viscoelastic forces and surface tension in the solution. These jets whipping individually experience bending instabilities, tend to intertwine with each other, overcoming their inherent repulsive tendencies during their very short time of interaction while flying towards the collector at high a speed. The rapid evaporation of formic acid during this flight results into formation of interconnected 3D nanowebs as depicted through Fig. 5.5. The splitting of polymer jet into multiple tiny jets has been reported by several researchers which did not always result into the formation of nanowebs. Amiraliyan *et al.* have noticed the splitting of *B.*

mori silk fibroin jet into multiple jets while electrospinning and reported the change in the morphology of nanofibers from having spherical cross-section to ribbon like, with change in temperature [122]. Abdel-Hady *et al*. reported the splitting of branching jets as the cohesive forces were overcome by the radial forces in the charged jets during electrospinning [123]. Reneker and co-workers have discussed the concept of jet splaying and bending instabilities experienced by the jet during the electrospinning process similar to our observations [124].
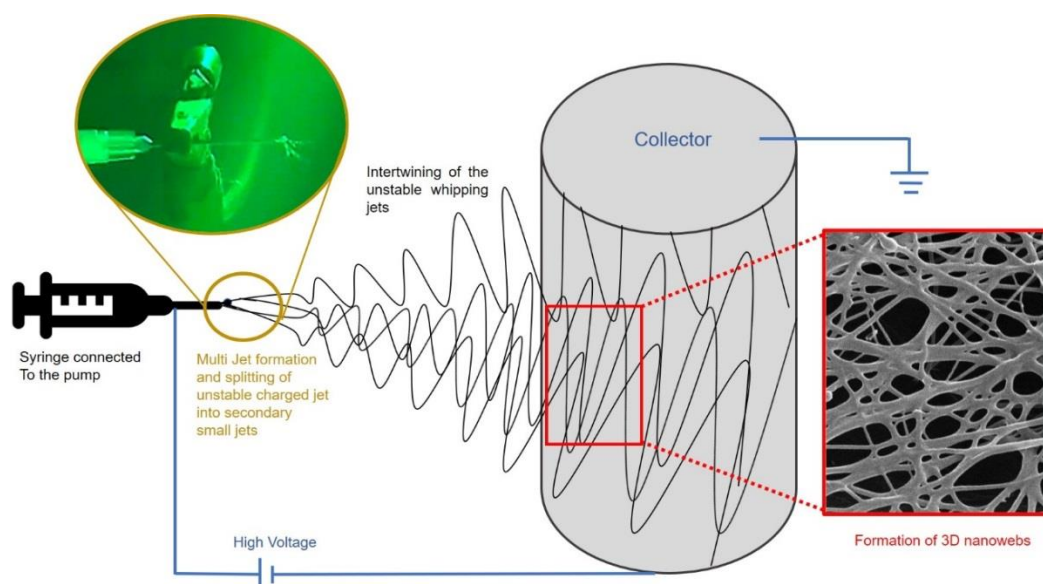
Fig. 5.5: The schematic representation of the process of 3D nanoweb formation.

The diameter of nanoweb strands was found to vary with blend composition and incorporation of modified clay into the blend solutions. The PSNF50 sample yielded nanowebs with average diameter 133±55nm and the average diameter of PSNF70 having lesser silk content reduced to 108±36nm in the range. The smaller diameter of the PSNF70 sample can be attributed to the reduced viscosity and conductivity of the polymer solution owing to lower silk fibroin content (**Table 5.2**). Due to this reduced conductivity and viscosity, the solution experiences lesser stretching under the applied

voltages resulting in higher diameter nanofibers [125]. Similar trend of reduced nanoweb strand diameter was observed in modified clay doped samples where the average diameter was smaller for PSNF70MC i.e., 138±61 as compared to PSNF50MC which presented an average diameter of 161±60 nm.

Table 5.2: The respective viscosities, conductivities and average fiber diameters of nanowebs

S. No.	Sample	Viscosity (mPaS)	Conductivity (µS/cm)	Average Diameter (nm)
1	PSNF50	1050±6	1180	133±55
2	PSNF70	995±14	1168	108±36
3	PSNF50MC	1092±8	1236	161±60
4	PSNF70MC	1060±11	1215	138±61

However, the incorporation of CTAB-MT clay has increased the average fiber diameter from their corresponding samples without modified clay, due to increase in the viscosity of the dope solution (Table 5.2). The increased viscosity of dope solution due to clay inclusion is extensively reported to increase fiber diameter in literature [126,127]. In one of our previous studies too, the clay content in polymer dope solution was found to enlarge the final average diameter of sericin/PVA/clay nanofibers due to increase in viscosity [128].

5.3.4.2 Surface roughness and porosity

The roughness of nanoweb samples was obtained in terms of Rq and Ra values by analysing the AFM images (Fig. 5.6). The Rq and Ra values denote the root mean square average of deviation in height and arithmetic average of the absolute values of the surface height deviations from the mean plane of scanned area respectively. The blended nanowebs exhibited high surface roughness as indicated though roughness

parameters in **Table 5.3**. The porosity of all the samples measured via liquid displacement method was found to lie between 68-77% with variation between the blends and nanocomposite webs (Table 5.3). The observed reduction in the porosity of PSNF50MC (68±3%) & PSNF70MC (73±6%) from their corresponding samples without modified clay i.e. PSNF50(74±2%) & PSNF70 (77±6%) respectively can be ascribed to the enhancement of fiber diameter on incorporation of CTAB-MT as observed in SEM analysis.
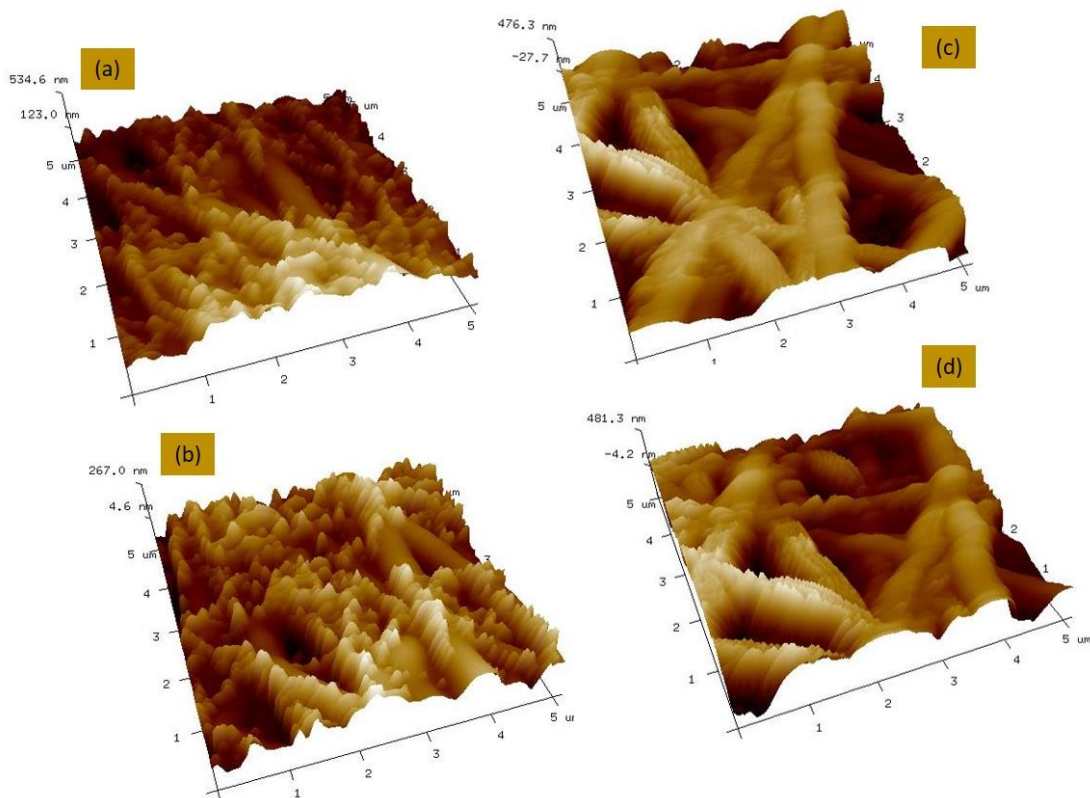
Fig. 5.6: The 3D AFM images of nanoweb samples (a) PSNF50, (b) PSNF70, (c) PSNF50MC and (d) PSNF70MC

Table 5.3: Surface roughness and depth of the 3D nanoweb mats obtained through analysis of AFM images and porosity via liquid displacement method

S. No.	Sample	Surface Roughness		Depth (nm)	Porosity (%)
		Rq (nm)	Ra (nm)		
1	PSNF50	85.1	68	346	74±2
2	PSNF70	67.7	53.8	353	77±6
3	PSNF50MC	151	126	315	68±3
4	PSNF70MC	140	114	340	73±6

The surface roughness and porosity of scaffolds has been reported to influence cell attachment, growth and its organization over the scaffolds by several researchers in literature [129,130]. Zamani *et al.* have reported the enhancement of nerve cell adherence and proliferation on the electrospun porous scaffolds of PLGA (Poly(lactide-co-glycolide)) [131]. In one of our previous studies on comparative analysis of muga silk fibroin cast film and nanofibrous mats, the high surface roughness and porosity of nanofibers were found to be advantageous for adherence and proliferation of fibroblast cells on the scaffold [18].

5.3.5 Structural analysis

The FTIR spectra of the nanoweb mats was observed and is shown in Fig. 5.7 The PSNF50 and PSNF70 blend samples presented the signals for both silk fibroin as well as PVA indicating successful blending of the two. The nanoweb samples, PSNF70 and PSNF50 showed sharp signal at 1713 cm^{-1} and 1711 cm^{-1} respectively, corresponding to C=O stretching of PVA component. The vibrational signals corresponding to amide groups of silk fibroin component were observed for PSNF70 and PSNF50 at 1620 cm^{-1} (amide I), 1530 (amide II) and 1624 cm^{-1} (amide I), 1527 cm^{-1} (amide II) respectively. These signals are known to represent β-sheet structure in

silk fibroin [96,97]. A sharp signal corresponding to C-O stretching vibration was observed at 1166 cm^{-1} and 1152 cm^{-1} for PSNF70 and PSNF50 respectively.
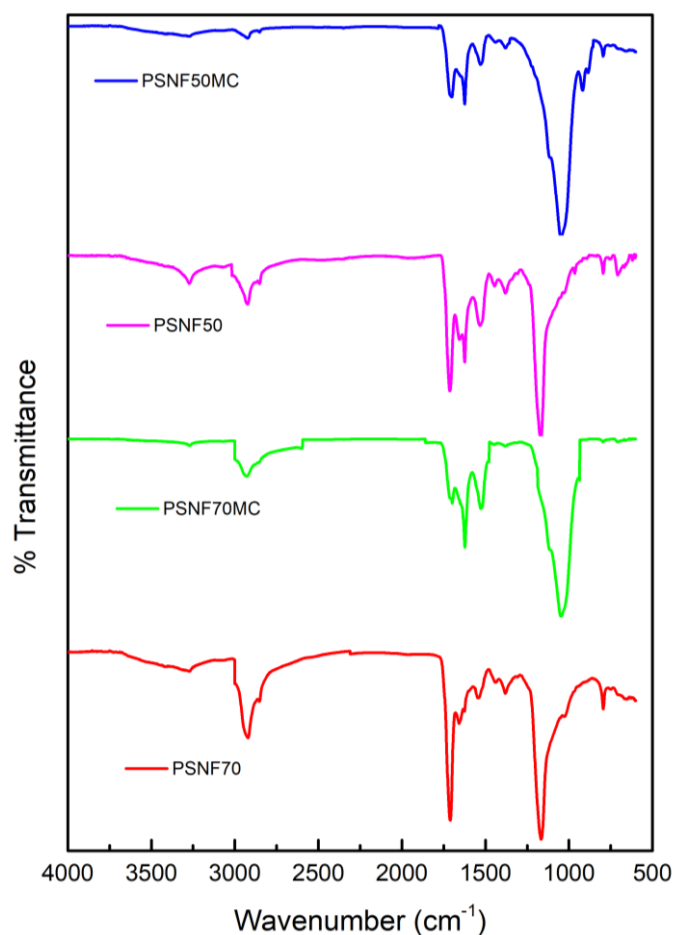
Fig. 5.7: FTIR spectra of the 3D nanoweb samples

The signals corresponding to C=O stretching of PVA component and the amide I, II of silk fibroin component representing β-sheet conformation were also observed in PSNF70MC as well as PSNF50MC. This suggests that structural conformation of polymeric blend did not deteriorate as a consequence of incorporation of CTAB-MT clay. The appearance of signals at 1030 cm^{-1} (Si-O stretch), 919 cm^{-1} (Al-Al-OH bending) and 1045 cm^{-1} (Si-O stretch), 937 cm^{-1} (Al-Al-OH bending) for PSNF70MC and PSNF50MC respectively indicated towards the presence of clay in these samples

[132]. Signals in the frequency range (3000-2840 cm^{-1}) for C-H stretching in alkyl groups and broad, weak signals (3550-3200 cm^{-1}) for O-H stretching of hydrogen bonds were observed for all the samples.

Further, X-ray diffraction was carried out to analyse the crystallinity of these nanoweb samples. In literature, PVA has been reported to present diffraction signals at 2θ 11.5°, 19.5°,20.1°, 23.0° for 110, 10$^-$1,101, 200 plane respectively and 40.5° represents the compound peak [103]. Tasar silk fibroin is generally encountered with a characteristic diffraction pattern showing peaks at 17.5°, 20.08°, 24.4°, 30.9° and 34.1° corresponding to its β-sheet crystallinity [103].

Table 5.4: β-sheet crystallinity in the nanoweb samples, calculated via Fourier self-deconvolution of their XRD patterns

S. No.	Sample	Crystallinity (%)
1	PSNF50	42.84
2	PSNF70	34.74
3	PSNF50MC	58.01
4	PSNF70MC	44.59

As visible from Fig 5.8, the diffraction patters observed for all the samples are quite broad with some peaks emerging out. Moreover, as clearly visible in Fig 5.3 section 5.3.2, no signal corresponding to CTAB-MT was observed, indicating complete exfoliation of clay into the polymer matrix [103]. Park *et al.* have reported the similar observation for PVA/clay nanofibers due to exfoliation of clay in the polymer matrix [127]. In one of our previous studies on Sericin/PVA/clay nanofibrous mats, the peaks corresponding to clay were observed to be missing as clay exfoliated completely in the samples [128]. The broadening of peaks is generally associated with high amorphous content in the polymer matrix.
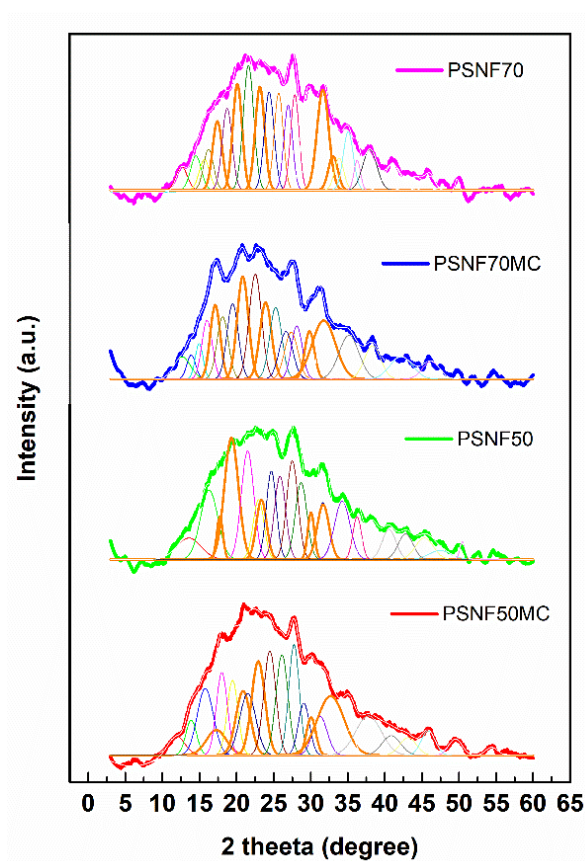
Fig. 5.8: X-ray diffraction pattern of the nanoweb samples with their fourier self-deconvolution. The peaks highlighted with orange represent diffraction signals corresponding the β-sheet crystallinity in the nanowebs.

It has been reported by Um and co-workers that dissolution of PVA in formic acid causes the size of side group in PVA to increase, as the OH groups are partially converted to formate, enhancing its overall amorphous content [93]. PVA being one of the components of our blend samples dissolved in formic acid can be suspected for such broadening of signals (also supported by FTIR data). However, the signals corresponding to β-sheet crystallites of silk fibroin component were observed in the FTIR spectra of all the samples. For more clarity, these diffraction patterns were further resolved by carrying out their Fourier self-deconvolution and subsequently, their percentage crystallinity was calculated.

From Table 5.4, it is visible that PSNF50 having higher silk fibroin content presented more crystallinity (42.84%) as compared to PSNF70 (34.74%). Moreover, the crystallinity was further increased to 58.01% and 44.59% for PSNF50MC and PSNF70MC respectively with introduction of CTAB-MT. This increase in crystallinity upon incorporation of clay can be ascribed to the increased charge density of the system which is also responsible for the complete exfoliation of clay in the polymer matrix.

Tasar Silk fibroin has been reported to contain high content of R-motifs [129] which possessing positive charge tries to locate itself around the negatively charged clay surface due to electrostatic force of attraction. In CTAB-MT modified clay containing samples, it is expected that silk fibroin will experience stearic hinderance and electrostatic repulsion from the positively charged bulky quaternary ammonium ions. These two opposing forces direct the silk fibroin chains to rearrange themselves in to β-sheet structures while adhering to the clay surface. Globular proteins in literature have been reported to form β-sheet structures at the interfaces by many researchers [133,134]. Dang and co-workers in a study have suggested the formation of surface induced antiparallel β-sheet structures of *B. mori* silk fibroin in their nanocomposite due to reorganization of silk fibroin chains at the clay surface [133].

Structural analysis through FTIR and XRD collectively suggest that introduction of CTAB-MT clay into polymeric blends further induces the β-sheet crystallinity in the

nanoweb mats and by altering the blend ratios crystallinity can be tailored according to requirement as it is dependent on the polymer content.

5.3.6 Thermal analysis

TGA of the samples was performed and their percentage change in weight with respect to time was analysed as shown in Fig. 5.9a. A small weight loss in all the samples due to evaporation of moisture was observed up to $100^{o}C$. The blending of silk fibroin with PVA and incorporation of clay resulted in the variation of weight loss profiles of samples, for further clarity their derivative plots were obtained as shown in Fig. 5.9b. As clearly visible from the figure, PSNF70 presented a sharp weight change in the temperature range 213-393°C which can be attributed to destruction of intermolecular interaction between the polymeric chains and breakdown of peptide backbone. However, PSNF50 showed a weight loss in the temperature range 266-408°C, indicating better thermal stability due to higher silk fibroin content and its higher crystallinity as established from structural analysis. The incorporation of CTAB-MT further improved the thermal stability of PSNF70MC and PSNF50MC as weight loss in the range 252-403°C and 280-394°C respectively were observed. Moreover, the percentage residual content of PSNF50 & PSNF70 at 900°C were 25.78% & 17.95% which is higher that their corresponding samples without CTAB-MT i.e., PSNF50 (3.54%) & PSNF70 (0.38%).
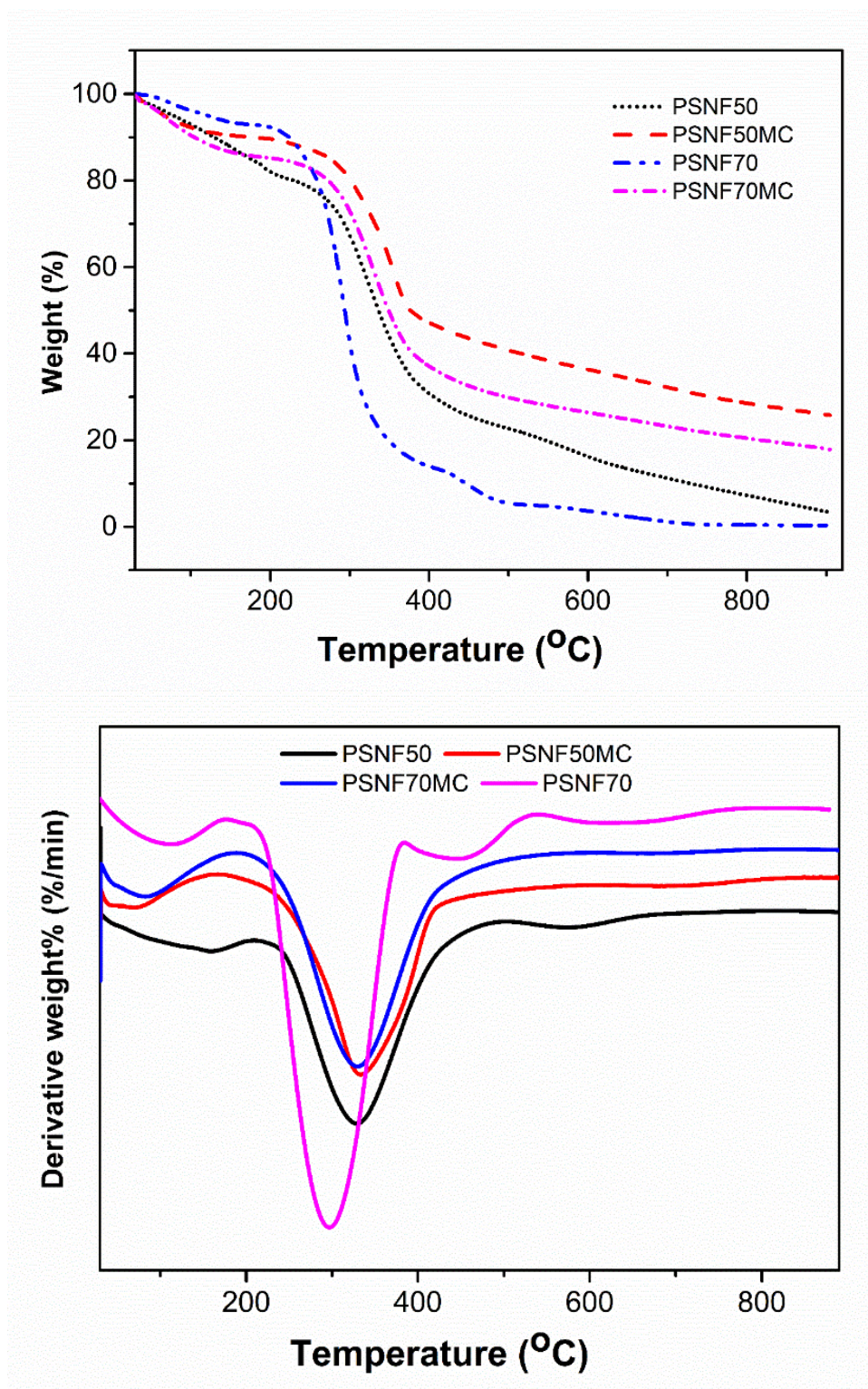
Fig. 5.9: **(a)** TGA thermograms of the nanoweb samples under nitrogen atmosphere **(b)** DTG (the first derivative of TGA) curves of nanoweb samples

In literature, incorporation of clay into polymer matrix has been reported to modify its structural properties and as a consequence their thermal stability is altered [135,136]. The aforementioned structural analysis directed that clay incorporation has enhanced the β-sheet content in the samples, which is responsible for such enhancement of thermal behavior in PSNF70MC and PSNF50MC. Further, differential scanning calorimeter was performed to study the thermal behaviour of these nanowebs as shown in Fig. 5.10. PSNF50 presented two separate endotherms at round 200°C & 260°C corresponding to the crystal melting and thermal degradation of polymer blend respectively. However, in case of PSNF70 both the melting and degradation endotherms seem to have merged with appearance of only one broad endotherm centred around 215°C. It can be said that due to difference in the blend composition and crystalline content (as established through structural analysis) of both PSNF50 and PSNF70, they are showing variation in their thermal behaviour.

Tasar silk fibroin and PVA have been reported to show their melting endotherms at 235 and 193°C respectively [137]. It is pertinent to note that the signals corresponding to the melting of these blend nanoweb samples are shifted from the melting temperature of both the pure components. With incorporation of clay, a shift in the thermal profiles was observed for both PSNF50MC and PSNF70MC. The melting endotherm and degradation of PSNF50MC was observed at higher temperatures i.e., 206 & 272°C respectively. The higher crystallinity of this sample is responsible for the increased melting temperature of PSNF50MC. The broad endotherm was observed at 226°C for PSNF70MC, 11 degrees higher than PSNF70. The broadening of

endotherms along with the shift in peak positions have been associated with change in

the crystalline structure of polymeric blends in literature. A study reported previously
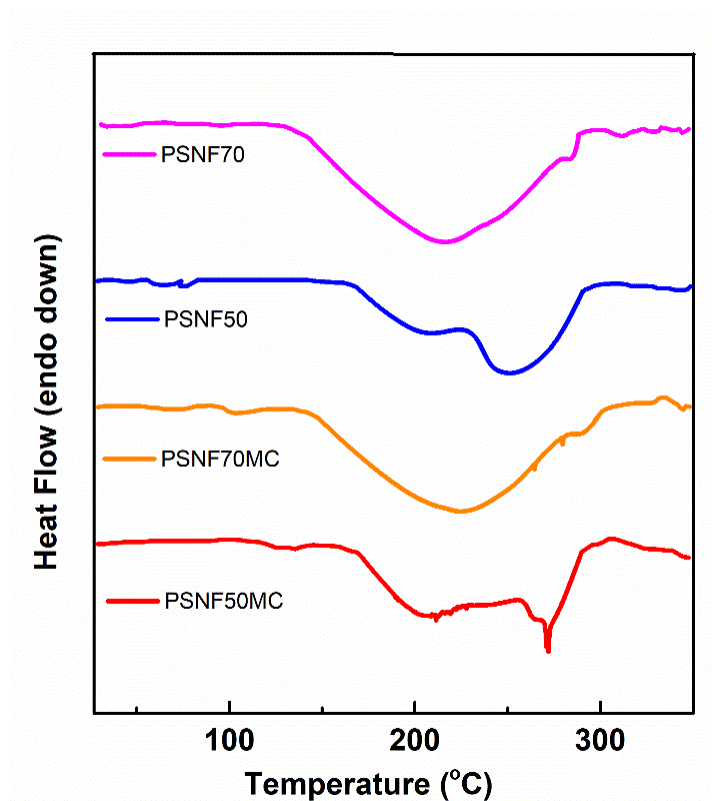
Fig. 5.10 DSC thermograms of the nanoweb samples.

by Liu and co-workers has shown similar broadening of endothermic signals, as *B.*
mori silk fibroin powder was added to PVA for blend film preparation, due to
alterations in their crystal form [103]. The increased thermal stability of nanocomposite
samples is in good correlation with the observed TGA data. The thermal analysis
jointly through TGA and DSC establishes that as a result of blending tasar silk fibroin
with PVA and reinforcing with CTAB-MT the crystalline structure of these nanowebs
has been reformed which as a consequence enhanced their thermal stability. These
observations very well support the structural analysis data.

5.3.7 Mechanical analysis

The mechanical properties of samples studied under tensile mode are shown in Fig. 5.11 and Table 5.5. PSNF50 presented with tensile strength of 5.35 MPa which was reduced to 4.8 MPa in PSNF70, however, the percentage elongation was higher in PSNF70 (8.54%) as compared to 3.26% in PSNF50. It can be related to the crystalline content with respect to silk fibroin in the polymer matrix.
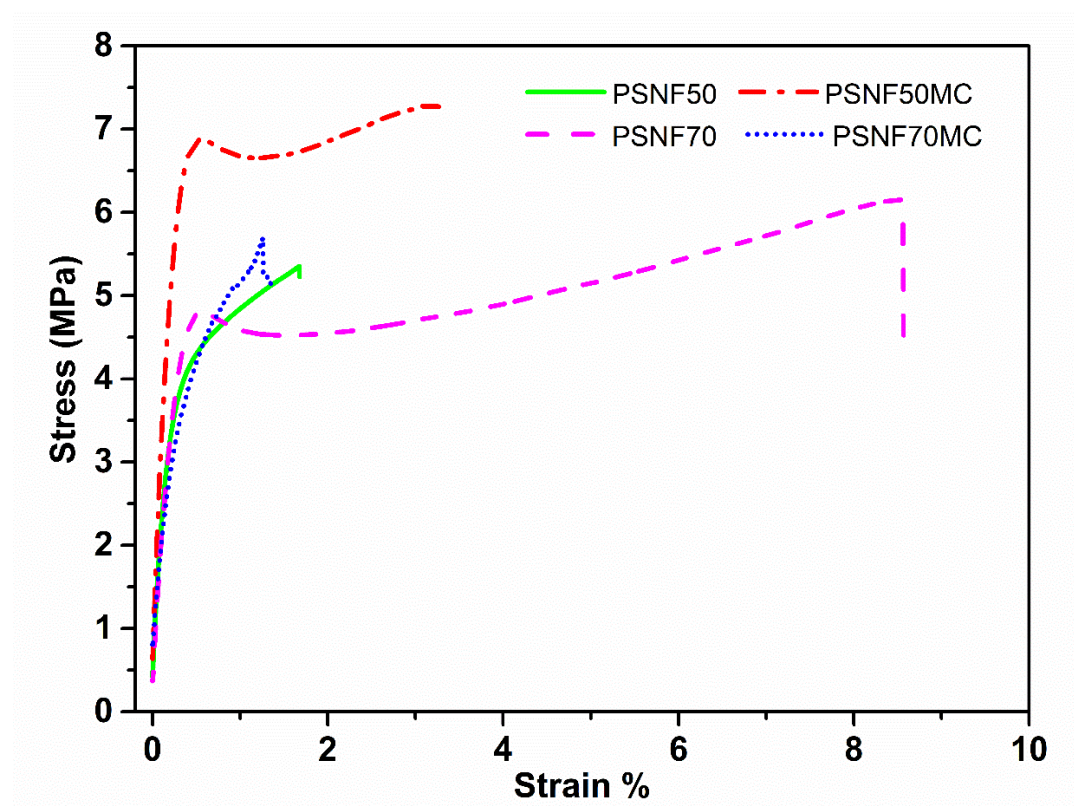
Fig. 5.11: Stress-Strain plot of the nanoweb mats in tensile mode.

Table 5.5: Mechanical properties of the nanoweb samples obtained in tensile mode (n=5).

S. No.	Sample	Tensile Strength (MPa)	Elongation at break (%)
1	PSNF50	5.35±0.82	1.67±0.22
2	PSNF70	4.80±1.3	8.54±0.61
3	PSNF50MC	6.87±1.8	3.26±0.54
4	PSNF70MC	5.70±0.54	1.26±0.39

The remarkable mechanical strength of silk fibroin is often accredited to its β-sheet crystallinity in literature [3,138]. Su *et al.* have achieved enhanced mechanical strength of silk fibroin hydrogels by conformationally transforming the random coils to β-sheets [138]. As observed through XRD, samples with higher silk fibroin content presented more crystallinity, so higher tensile strength is displayed by PSNF50 and since PSNF70 possessed more amorphous content, it demonstrated more elongation than PSNF50. In literature, incorporation of nano clays is generally reported to enhance the mechanical properties of silk and PVA individually [138,139]. Upon incorporation of CTAB-MT clay, as more β-sheet crystallinity is induced in silk fibroin, PSNF50MC showed highest value of tensile strength (6.87 MPa) among all the four samples analysed in this study. The tensile strength of 5.7 MPa was presented by PSNF70. As expected, an increase in tensile strength reduced the percentage elongation of fiber in PSNF70MC. However, it was observed that apart from increase in tensile strength, elongation property of PSNF50MC is also enhanced. This may be due to the increased diameter of nanofibers in this sample which facilitates molecular chain movement causing increased ductility in fibers. Similar observations are also reported in literature [140–142]. The observed mechanical properties of nanoweb samples are potentially suitable for skin tissue regeneration as the values are comparable to the matrices produced by fibroblast cells and native skin [18].

5.3.8   Water uptake capacity

The water uptake capacity of nanoweb samples was analysed and is shown in Fig. 5.12. The PSNF50 and PSNF70 samples showed the water uptake capacity value of 161% and 138% respectively. The higher water uptake in PSNF50 can be attributed to higher hydrophilicity of the blend due to overall increase of hydrophilic groups like -NH and -C(O) with higher composition of silk fibroin in it. It was observed that the water uptake capacity was slightly reduced with incorporation of modified clay. The

PSNF50MC and PSNF70MC samples presented with 126% and 117% water uptake capacity respectively. This could have occurred because of the reason that with introduction of modified clay, hydrophobic groups are being exposed through clay exfoliation in polymer matrix, reducing its overall hydrophilicity [143]. Moreover, due to complete exfoliation of modified clay in the polymeric blend matrix, clay molecules adhering interfacially to the polymer chains restrict their movement by creating more crosslinking points. As a consequence of this, water molecules experience tortuous path of diffusion which hinders theirs passage through the nanoweb composite, resulting in reduced water uptake capacity.
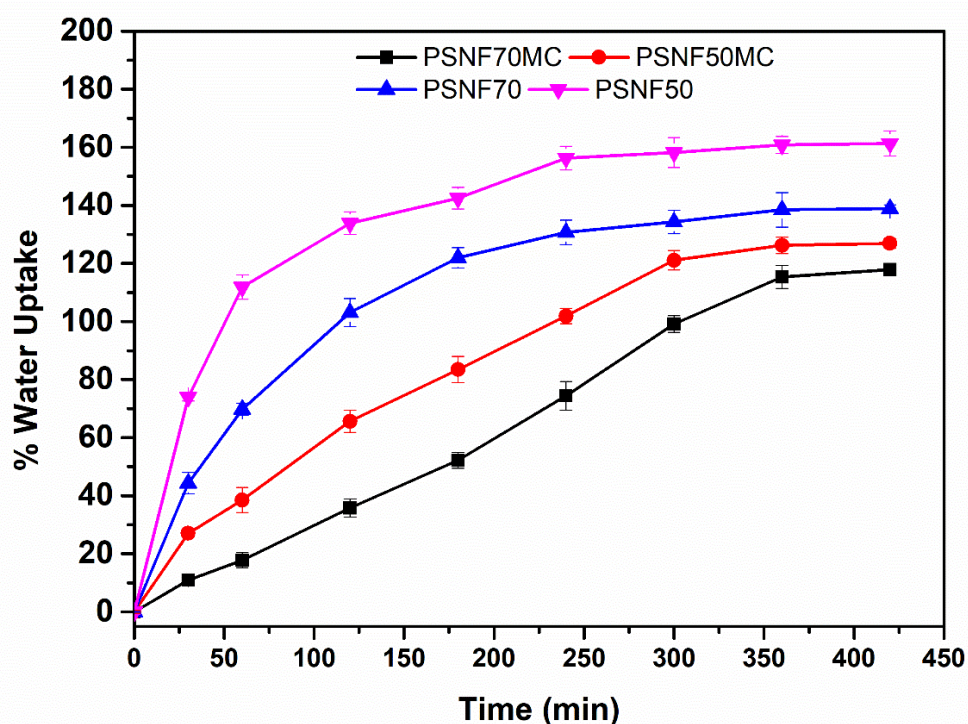
Fig. 5.12: The water uptake capacity of nanoweb samples at physiological temperature; error bars represent standard deviation for n=3.

The nanofiber diameter and porosity of nanoweb mats also plays a role in regulating the water uptake capacity. As mentioned previously, PSNF50MC & PSNF70MC samples have shown reduced porosity due to incorporation of modified clay therefore

are less accessible to water molecules as compared to their corresponding samples without clay (PSNF50 & PSNF70), resulting in reduced water uptake capacity.

5.3.9   Biodegradation

The nanoweb samples were tested for their biodegradability using PBS and proteinase K enzyme over a period of 28 days, as it is known to hydrolyse the peptide bond. All the samples yielded insignificant degradation in PBS. In case of enzyme solution, as shown in Fig. 5.13, all the samples showed faster degradation in the initial phase of 7 days with PSNF70 showing maximum degradation of 30.41% and PSNF50 showed minimum degradation of 20.70%.
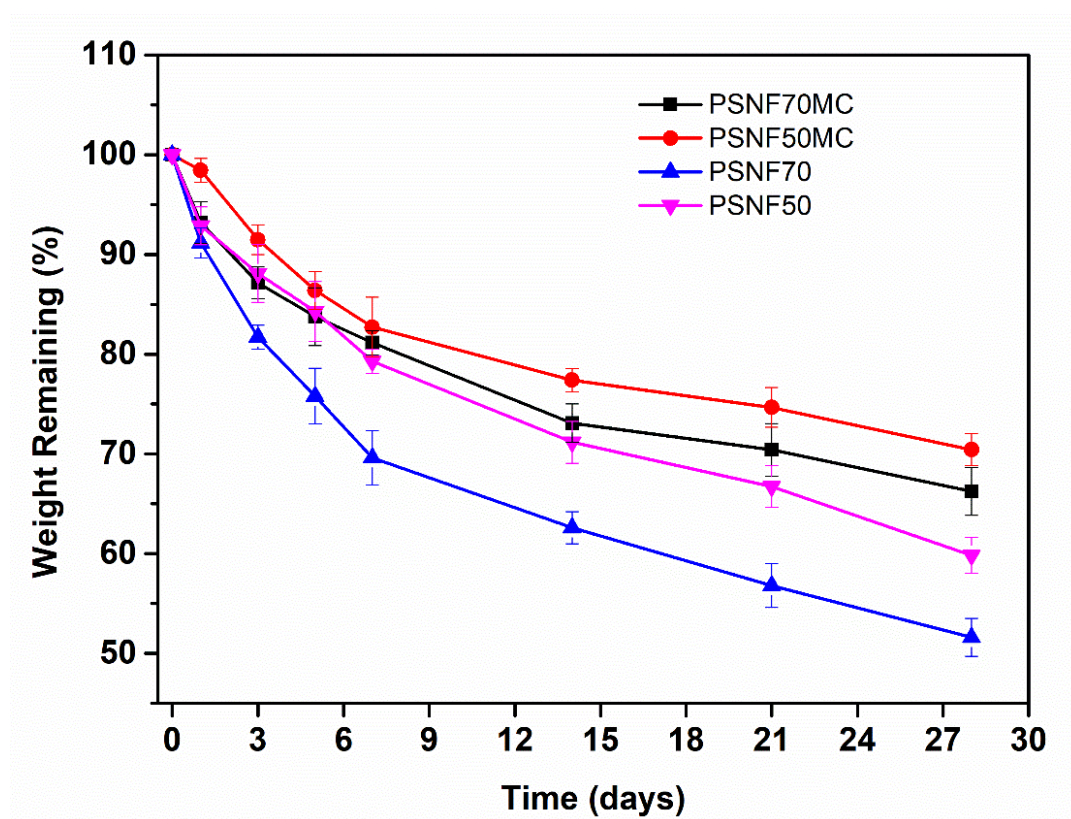
Fig. 5.13: Enzymatic degradation of nanoweb mats over a period of 28 days under physiological conditions; error bars represent standard deviation for n=3.

The degradation was found to slow down post 7 days with PSNF70 showing degradation of 48.37% and PSNF50 showing degradation of 40.16% after a period of 28 days. It can be said that as proteinase is to digest silk fibroin, the blend sample with higher silk fibroin content must present more degradation similar to the findings of Bhattacharjee *et al.* [41], but as analysed through XRD, since the crystalline content in PSNF50 is higher than PSNF70, it showed slower degradation. The percentage crystallinity in polymers has previously been observed to alter its degradation in literature. In one of our previous study on silk fibroin gelatin blend films, the enzymatic degradation was found to be varying with change in the distribution of crystallinity in the molecular structures, the blends with higher crystallinity showed slower biodegradation [94]. She *et al.* has reported similar correlation of high crystallinity and low biodegradation for *B. mori* silk fibroin films [94]. In this study, the samples incorporating CTAB-MT clay showed less degradation as compared to their corresponding blends without clay, this could be attributed to the altered hydrophilicity and reduced porosity of the material as a result of clay introduction. As observed previously, introduction of clay reduced the water uptake capacity of the samples making the polymers less accessible to the enzymatic solution. Moreover, it further induced β-sheet crystallinity in the material, so the degradability was reduced. PSNF70MC and PSNF50MC showed degradation of 33.74% and 29.57% respectively, lower degradation in PSNF50MC is due to its higher β-sheet crystallinity.

5.3.10 Biocompatibility

The viability of L929 human fibroblast cells was studied via Alamar blue assay to analyse the biocompatibility of prepared nanoweb samples. Alamar blue assay utilizes the spectrophotometric measurement of the conversion of the oxidized form of

Alamar dye to its reduced form due to reducing cellular environment maintained by the metabolizing cells.

The study showed that (Fig. 5.14) all the nanofibrous samples were cytocompatible with high cell viability index. In literature, cell viability index value greater than 0.7 has been considered to represent non-toxicity [111]. Tasar silk fibroin is well known for its biocompatibility owing to its inherent RGD sequence [110]. High cell viability index of PSNF50 and PSNF70 indicated that blending of silk fibroin with PVA enhanced the biocompatibility of the nanoweb mats. Moreover, the incorporation of CTAB-MT was not found to alter the biocompatibility of material as clearly visible from the cell viability index of PSNF50MC and PSNF70MC (Fig. 5.14).
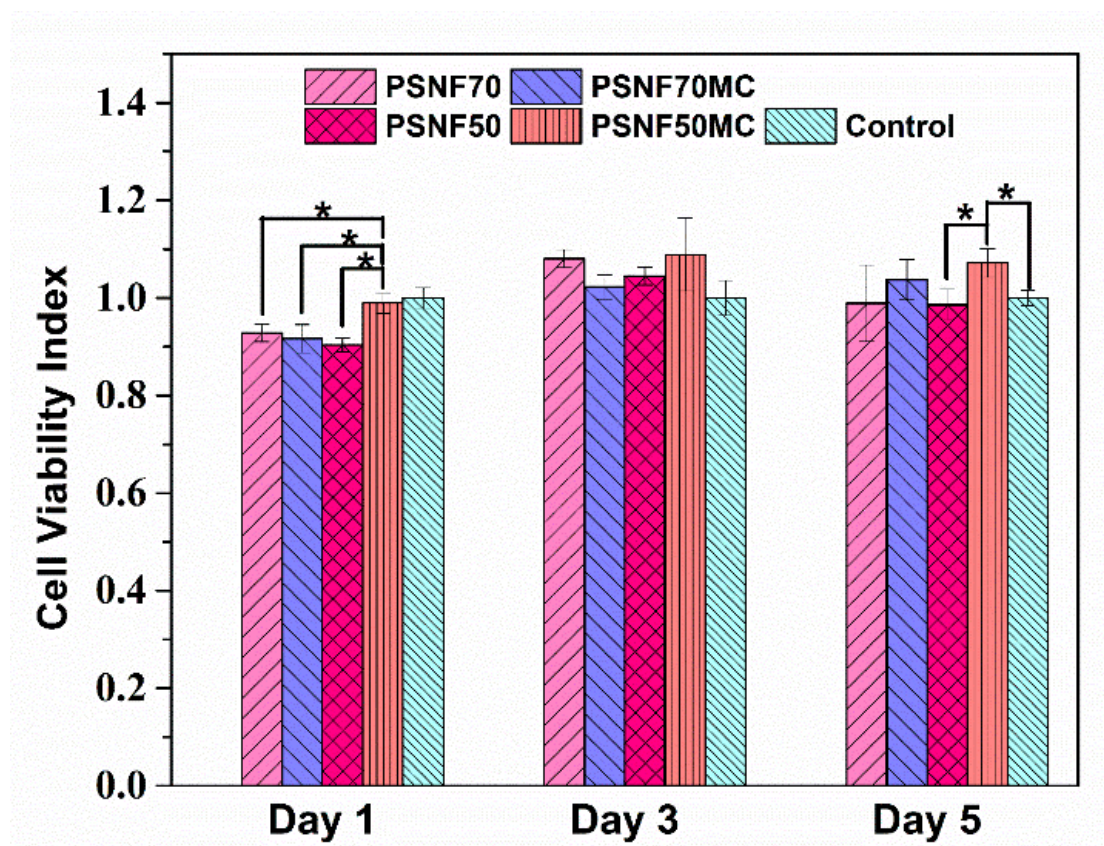
Fig. 5.14: Cytocompatibility of the nanoweb mats through Alamar Blue assay; error bars represent standard deviation for n=3. (p*≤ 0.05)

The biocompatibility of these nanoweb mats was further verified by checking the morphology of L929 cells cultured over the mats for a period of 48 hours, using SEM (Fig. 5.15). It was observed that cells readily adhered to the material surface and were found to have spread covering almost the entire area available to them in the nanoweb mats. The cells integrated with each other forming continuous layered sheets on the surface of PSNF50 and PSNF70 blend nanowebs. In the case of samples PSNF50MC and PSNF70MC, cells were spread along the surface with their characteristic morphology and also exhibited the formation of cellular matrices over the material surface. The cell spreading and matrix formation clearly indicated the cytocompatible nature of blended nanoweb mats. It was evident from the previous literature that blending of natural polymers such as silk fibroin with other artificial polymers has enhanced their cytocompatibility and cell adhesion property [12,72,75,99]. This could be attributed to the presence of cell adhesion moieties such as RGD sequence present in silk fibroin. Further, as observed in AFM studies, reinforcement of CTAB-MT has enhanced the surface roughness of the mats which might have aided in the cell adhesion and spreading. Moreover, high adherence of cells towards the material surface could also be attributed to the high surface to volume ratio of these nanowebs and non-uniform diameters of the nanofibers in the range 50-300 nm which mimics the microenvironment of natural ECM along with the inherent capacity of silk fibroin due to RGD sequence which provides cell binding sites [144].
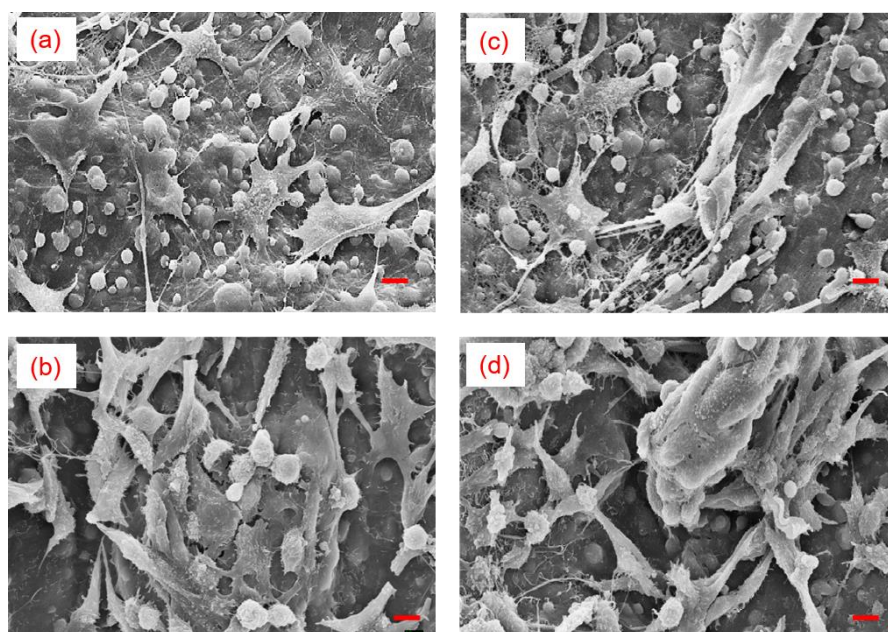
Fig. 5.15: SEM micrographs of nanoweb samples (a) PSNF50, (b) PSNF50MC, (c) PSNF70 and (d) PSNF70MC after 48 hours of seeding L929 fibroblast cells; Scale: 10 μm

5.3.11 Antimicrobial activity

The antimicrobial activity of CTAM-MT modified nanoweb mats was studied, where samples without clay were kept as control. It was observed that the zone of inhibition around the mats was not clearly visible but the surface of these mats was found to be free from any bacterial strains. Further, serial dilution method was adopted to check the antibacterial activity. The PSNF50MC sample showed excellent antimicrobial activity of 97.96% and 90.48% (Table 5.6)

Table 5.6: The antimicrobial activity presented by CTAB-MT clay modified nanoweb samples against *E. coli* and *S. aureus* bacterial strains.

S. No.	Sample	Escherichia coli (*E. coli*)		Staphylococcus aureus (*S. aureus*)	
		CFU/mL × 10^6	Antibacterial activity (%)	CFU/mL × 10^6	Antibacterial activity (%)
1.	Control	490	-	420	-
2.	PSNF50MC	10	97.96	40	90.48
3.	PSNF70MC	50	89.79	75	82.14

against *E. coli* and *S. aureus* bacteria respectively. The PSNF70MC showed slightly lower antimicrobial activity as compared to PSNF50MC. A possible explanation behind this could be the variance of electrostatic interaction in the polymer- CTAB-MT clay matrix. In PSNF50MC, higher silk fibroin content having more positively charged amino acids provides electrostatic repulsion to the quaternary ammonium ions, which results in more release of these ions causing better antimicrobial activity. The quaternary ammonium surfactants are well known for their antimicrobial action, as their positively charged head groups can interact with the bacteria membrane which is negatively charged and consequently, the long carbon chains penetrate into it, causing the cytoplasmic material to leak out, ultimately results in bacteria lysis [144]. Nakata and co-workers have reported antibacterial activity of CTAB against *E. coli*, as it induces excess superoxide generation in the bacterial cells [144].

5.4 Conclusions

❖ Novel CTAB-MT modified tasar silk fibroin and PVA blended 3D nanowebs were developed by electrospinning.

❖ The morphological analysis depicted rough morphology of these nanowebs with small diameters and good porosity.

❖ Structural, thermal and mechanical analysis collectively directed towards modification in the crystallinity of these nanowebs due to blending silk fibroin with PVA and incorporation of CTAB-MT, consequently altering their physicochemical properties.

❖ The inclusion of modified clay induced higher crystallinity in nanocomposite nanowebs as compared to their respective samples without clay, consequently their mechanical strength improved.

❖ The increased fiber diameter and reduced porosity upon addition of CTAB-MT to blend samples resulted in reduced water uptake capacity and slow biodegradation of nanoweb nanocomposites.

❖ The nanowebs were found to show high biocompatibility through Alamar blue assay, blending silk fibroin with PVA and incorporation of CTAB-MT further enhanced the attachment and growth of L929 fibroblast cells mimicking the extra cellular matrix behaviour.

❖ Addition of CTAB-MT imparted antibacterial activity to these nanowebs against *E. coli* and *S. aureus* bacterial strains.

❖ As indicated by the aforementioned studies, these materials have the capacity to tune their physicochemical properties through variation in the blend ratios and inclusion of nanofiller for utilization as biomaterials for versatile tissue engineering applications.

❖ The results of this study have been published the journal of **Macromolecular Materials and Engineering.**

Chapter 6 :

Antheraea Mylitta (Tasar) Silk Fibroin & Gelatin Blend Films for Biomedical Applications

6.0 Overview

In this chapter, tasar (*Antheraea mylitta*) silk fibroin (AMF) is attempted to blend with gelatin with the stimulus to develop tailorable flexible biomedical constructs. The blending of gelatin with silk fibroin is expected to improve the flexibility along with altering their biodegradability. Since tasar silk fibroin is not completely soluble in available conventional solvents in which most of the natural polymers are, figuring out a suitable solvent that can dissolve both silk as well as gelatin is therefore a strenuous task. Working towards this direction, in this study, two different approaches have been adopted to prepare AMF- gelatin blend films of two Types (I and II). The blends of Type I prepared by dissolving silk in ionic liquid and blending it with aqueous gelatin solution, resulted in blend films with poor flexibility. So, as an alternative, second method is adopted to make Type II blend films. In this, silk fibroin dissolved in ionic liquid is dialysed against milli q water and further obtained silk is dissolved in formic acid, which is then mixed with gelatin-formic acid solution. Upon casting, this resulted in very flexible blend films. The blend films are characterised for their structural, thermal and biological properties. The impact of two different crosslinkers glutaraldehyde (chemical) and genipin (natural) on the properties of developed films is also discussed. The specifics on the structural, thermal, morphological and biological analysis of the blend films are detailed in the chapter.

6.1 Materials

Cocoons of *Antheraea mylitta* silkworm were bought from Central Silk Board, Son Bhadra, U.P, India. Gelatin was procured from Thermo Fisher Scientific, India. Formic acid was bought from Loba Chemie Pvt. Ltd, India. Methanol was provided by Finar Chemicals Limited, India. The L929 fibroblast cells were received from National center of cell science (NCCS), Pune, India. The ionic liquid BmimAc (1-butyl-3-methylimidazolium acetate), Fetal bovine serum (FBS) and Dulbecco's modified Eagle's medium (DMEM) were obtained from Sigma Aldrich.

6.2 Methods & Characterization

6.2.1 Extraction of silk fibroin from tasar silk cocoons by degumming

The *Antheraea mylitta* silkworm cocoons were degummed to remove sericin using the procedure described in literature[83]. Briefly, the cocoons were cut into small pieces and heated in distilled water with 0.02 M $NaHCO_3$ at 100 °C for 30 mins twice. The fibroin so obtained was given two washes of distilled water to get rid of all the residual sericin. The degummed silk fibers were dried overnight in oven at 60°C.

6.2.2 Preparation of Tasar Silk Fibroin and Gelatin Blend Films

6.2.2.1 Dissolution of silk fibroin

Antheraea mylitta silk fibroin solutions were prepared by using two different solvents. Firstly, degummed fibers were dissolved in BmimAc ionic liquid in temperature range 80-100°C under nitrogen atmosphere. This AMF ionic liquid solution was used to prepare blends of Type I. To make blends of Type II the AMF ionic liquid solution was dialysed against miliQ water for 5 days and the water was changed at every 12-hour interval as shown in Fig. 6.1.
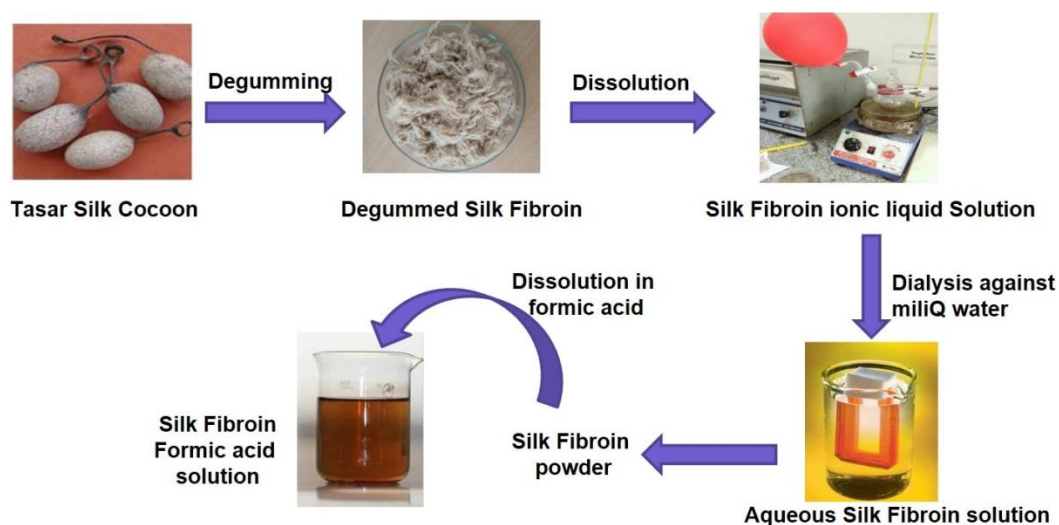
Fig. 6.1: Schematic representation for preparation of silk fibroin solutions

The obtained aqueous AMF solution was freeze dried and stored at 4 °C. This freeze-dried silk was further dissolved in 98% formic acid to obtain AMF solution, which was then used to make Type II blends with gelatin.

6.2.2.2 Preparation of blend films

Type I blend films were prepared by mixing 10% (w/v) AMF ionic liquid solution with 20% (w/v) gelatin in ratios 100:0, 70:30, 50:50, 30:70 and 100:0 and casted on polystyrene plates (Method I, Fig. 6.2). The films were dried at room temperature overnight and further coagulated in methanol bath for 3 days in order to remove ionic liquid and regenerate β-sheet crystalline structure. Among the prepared blend ratios, 30:70 silk/gelatin blend film was most stable and flexible. So, this blend ratio was further used throughout and was named S30G70. To modify the film flexibility and improve its stability, S30G70 films with 15% (w/w) dextrose and two different crosslinkers glutaraldehyde 1% (w/w) and genipin 1% (w/w) were prepared and named, S30G70GTA and S30G70GPN respectively. The overnight dried films were coagulated in methanol bath with regular exchange of methanol till removal of all of

the ionic liquid, which was confirmed by measuring the ionic conductivity of the solutions.
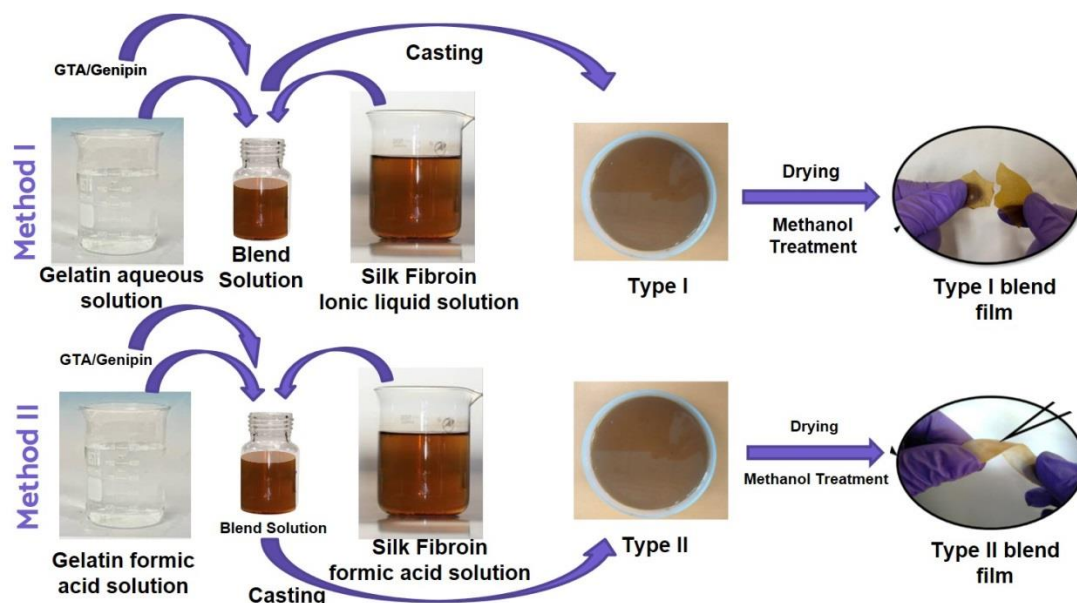
Fig. 6.2: Schematic representation of two routes followed to prepare Type I and Type II blend films

Type II blend films were prepared by mixing the 10% (w/v) AMF formic acid solution with 20% (w/v) gelatin formic acid solution in 30:70 ratio and casted on polystyrene plates. Films were modified with 15% (w/w) dextrose as plasticizer and two different crosslinkers glutaraldehyde 1% (w/w) and genipin 1% (w/w). Pure silk and pure gelatin films were prepared by casting10% (w/v) AMF formic acid solution and 20% (w/v) gelatin formic acid solution on polystyrene plates respectively. These casted films were dried overnight and coagulated in methanol bath. Same terminology was used to name the films except for asterisk used to indicate Type II blend films e.g. S30G70GTA* indicates silk-gelatin blend in 30:70 ratio crosslinked with 1% w/w glutaraldehyde. All the film samples were of thickness 0.5± 0.21 mm.

6.2.3 Fourier transform infrared spectroscopy

Fourier transform infrared (FTIR) spectroscopy was performed to access the conformational changes using Thermo Scientific Nicolet 380 spectrometer in transmission mode with wave numbers in range 4000-650 cm^{-1}. The crystalline content in the samples was analysed by applying Fourier self-deconvolution in the amide III region as described in literature using Origin Pro 9.0 software [90].

6.2.4 X-ray diffraction

X-ray diffraction intensity curves of the samples were obtained using Rigaku Ultima IV diffractometer with CuKα radiation at a λ=1.5 Å in the measurement range 2θ from 10° to 60°. Percentage crystallinity was calculated using equation 1

$$\text{Percent Crystallinity} = \frac{\text{Total area of crystalline peak}}{Total\ area\ of\ crystalline\ and\ amorphous\ region} \times 100 \qquad (1)$$

6.2.5 Thermogravimetric analysis

Thermal stability of the samples was analysed using Thermo Gravimetric Analysis (TGA) technique under nitrogen atmosphere at the rate of 10°C/min from 30° to 900°C, using Perkin Elmer pyris-4000 thermal analysis system. The derivative plots were obtained to further clearly access the thermal decomposition behaviour of samples.

6.2.6 Differential thermal analysis

Differential Scanning Calorimetry (DSC) was performed using thermal analysis instrument (TA Q200) with scanning speed of 10°C/min and 2°C/min for films and nanoweb samples respectively, under nitrogen gas flow at 20ml/min.

6.2.7 Mechanical testing

Mechanical properties of the film samples were analysed using Zwick Roell Z250 UTM in tensile mode, fitted with 50 N load cell at a test speed of 10 mm/min. The sample dimensions were kept $50 \times 10 \times 0.5$ mm, as per ASTM D 882. The test was carried out for five sets of samples.

6.2.8 Percentage swelling

Percentage swelling capacity of the samples was determined. Briefly, pre weighed samples were immerged in miliQ water. The samples were carefully removed, pat dried with tissue paper to remove excessive fluid and weighed in the swollen state at regular intervals. This was repeated until equilibrium value of swelling was reached. Afterwards, percentage swelling of the blend films was calculated via following equation:

$$\text{Percentage Swelling} = \frac{W_t - W_0}{W_0} \times 100 \qquad (2)$$

where W_t is weight of swollen sample at time t and W_0 is the weight of dry sample initially.

6.2.9 Biocompatibility tests

6.2.9.1 Cell viability by MTT assay

MTT assay was performed on different days (1, 3 and 5) with L929 skin fibroblasts to determine the cytocompatibility. The well plates containing films were seeded with cells and were introduced to 20µL aliquots of MTT solution (5mg/mL) in each well on the respective days. This was further incubated at 37 ^{o}C for 4 hrs. The medium was aspirated and formazan crystals were dissolved by adding 200 µL of DMSO to each

well followed by shaking for another 30 mins. Optical density (OD) was recorded at 570 nm with a micro plate reader (Bio-Rad) and percentage of cell viability was calculated using equation 4 as follows

$$\text{Percentage Cell viability} = \frac{\text{Mean of Test OD}}{Mean\ of\ Control\ OD} \times 100 \qquad (3)$$

6.2.9.2 Cell adherence and proliferation by phase contrast microscopy

Phase contrast microscopy was used to study the time dependant growth or proliferation of fibroblast cells on the samples. All the film samples were treated with 70% ethanol for 15 mins for sterilization. These samples were then washed with phosphate buffer saline (PBS) and dried. The dried samples were cut and placed under UV exposure in the laminar air flow for sterilization again [19]. The samples were placed in 96 well cell plate and approximately 10×10^3 cells were seeded on them per well. This was incubated at 37 ^{o}C in a 5% CO_2 humidifier. The seeded samples were washed with PBS and the cell morphology was studied under the phase contrast microscope after incubation of 1, 3 and 5 days.

6.2.10 *In vitro* biodegradation

The silk fibroin -gelatin blend films were tested for their biodegradation in enzymatic solution of 1 mg/mL protease XIV (1U/mg) and Proteinase K enzymes at 37 ^{o}C respectively [19,112]. The film samples of uniform size were cut, weighed and incubated in SBF. The temperature of incubator was maintained at 37°C. The solutions were replaced with fresh solution every two days to maintain the freshness. The weight loss data was collected at regular intervals for 6 weeks. Before weighing, samples were rinsed with miliQ water and dried in vacuum oven at 37°C. The activity of enzymatic solution was maintained by regular exchange with fresh solution. The percentage weight loss was obtained following equation 4.

Percentage weight loss $=\frac{W_f - W_i}{W_i} \times 100$ (4)

Where, W_f is weight of sample at time t and W_i is the initial weight of sample.

6.2.11 Statistical analysis

All the tests were performed in triplicates, unless mentioned otherwise and the data is mentioned as mean±SD. Statistical significance of data at level $p < 0.05$ was assessed using One-way analysis of variance (ANOVA).

6.3   Results & Discussion

6.3.1 Structural analysis

Conformational analysis of blend films was carried out by FTIR spectroscopy. FTIR spectra was obtained for both Type I and II blend films as shown in Fig. 6.3 and 6.4 respectively. The amide groups in proteins are usually distinguished by different vibrational peaks namely amide I (1700-1600 cm^{-1}) which is related to C=O stretching, amide II (1540-1520 cm^{-1}) corresponding to N-H bending and C-H stretching and amide III due to C-N stretching and C=O bending in the protein backbone. The peaks at particular vibrational frequencies are indicative of Type of conformation (e.g. α-helix, β-sheet or random coil) adapted by the protein materials. In case of Type I films, pure silk fibroin film showed strong broad bands around 1626, 1518 and 1228 cm^{-1} which are characteristic to β-sheet conformations. The pure gelatin aqueous film showed amide I band at 1641, amide II and III bands at 1532 and 1230 cm^{-1}. Upon blending silk fibroin with gelatin, as shown in Figure 6.4c the broad amide I band shifted and was centred around 1639, amide II to 1546 with a shoulder at 1510 cm^{-1} and amide III was observed at 1226 cm^{-1}. This indicates presence of

random coil conformation along with β-sheet crystallites [102]. In order to have a better understanding of the Type of secondary structure in films, Fourier self-deconvolution (FSD) was performed in the amide I region considering the bands around 1630 cm^{-1} correspond to β-sheet conformations.
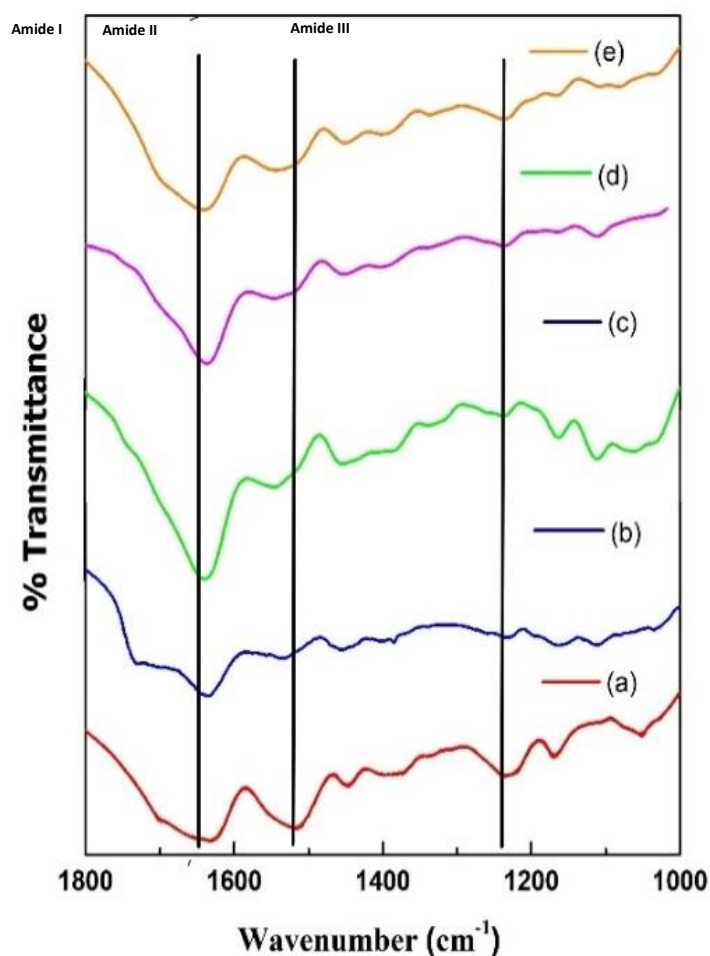
Fig. 6.3: FTIR of Type I films (a) S100, (b) G100, (c) S30G70, (d) S30G70GTA, (e) S30G70GPN

A representative graph is shown in Fig. 6.5 with FSD performed on sample S30G70GNP*. The percentage crystallinity obtained through FSD has been reported in Table 1. IR crystallinity reported in literature for wild variety of silk is in the range of 50-62% [102]. It can clearly be seen in Table 6.1, that pure silk as well as blend films

poses very low β-sheet crystallinity for Type I films. This indicates insufficient regeneration of β-sheet conformation which was lost during dissolution step. One possible explanation of this can be incompatibility of the two-polymer solution prepared in two different solvents which resulted in phase separation and hinderance to regeneration of β-sheet crystallinity.
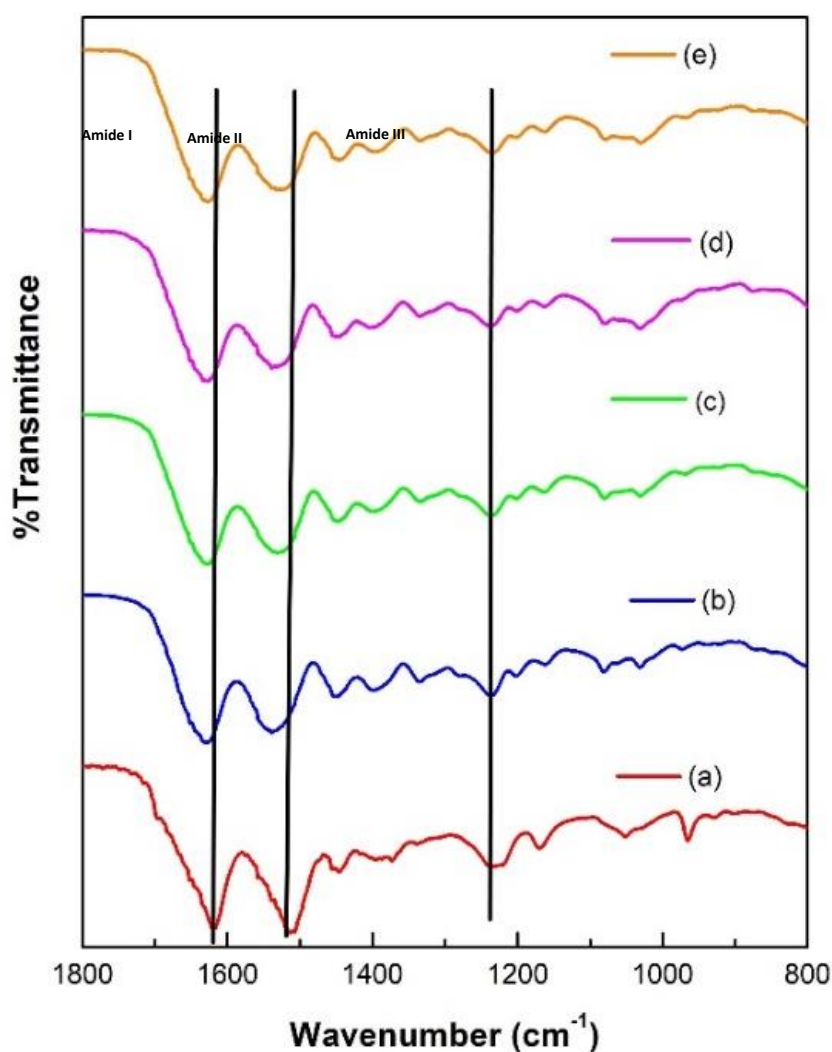
Fig. 6.4: FTIR of Type II films (a) S100*, (b) G100*, (c) S30G70*, (d) S30G70GTA*, (e) S30G70GPN*

In case of Type II films, pure silk film showed characteristic β-sheet conformation with peaks at 1620, 1510 and 1233 cm^{-1} for amide I, II and III respectively. The pure

gelatin film casted from gelatin formic acid solution showed amide I, II and III peaks at 1631, 1539 and 1235 cm^{-1} respectively. All the blend films showed amide I, II and III peaks significant of β-sheet crystallinity. Also, slight blue shift in the amide I and II peaks were observed in the blend films (Fig. 6.4 (c,d,e)) as compared to the pure silk film, which is suggestive of some interaction probably H-bonding amongst the two polymers. You and co-workers have also reported blue shift in the IR data as a consequence of interaction between egg white and *B. mori*. silk fibroin [145].
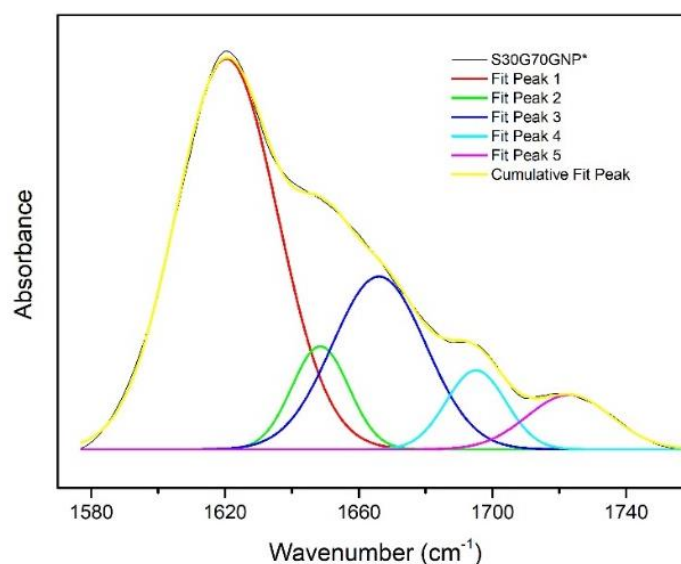
Fig. 6.5: Fourier self-deconvolution performed on Type II blend film sample S30G70GNP* (Representative graph)

Table 6.1 % β-sheet crystallinity in films obtained via FTIR and XRD calculations

			β-sheet Crystallinity through FTIR (%)	β-sheet Crystallinity through XRD (%)
Type of films	Type I	S100	30.91	
		S30G70	14.33	Almost
		S30G70GTA	14.27	Amorphous
		S30G70GNP	24.36	
	Type II	S100*	89.80	73.18
		S30G70*	41.22	54.73
		S30G70GTA*	57.30	54.56
		S30G70GNP*	57.57	52.65

The percentage crystallinity obtained through FSD is shown in Table 6.1. The blend films were found to possess β-sheet crystallinity in the range 52-58% which is comparable to the values reported in literature for wild type regenerated silk fibroin films [102]. In GTA crosslinked films, the characteristic imine C=N stretching vibration was masked by the strong amide I band and no other new bands were observed. Crosslinking with genipin did not show the characteristic band with formation of new C=C, C=N and C-N bonds since they were overlapped by the strong amide bands observed for silk and gelatin [146]. The possible crosslinking reactions in silk fibroin/gelatin blend films is shown in Figure 6.6.
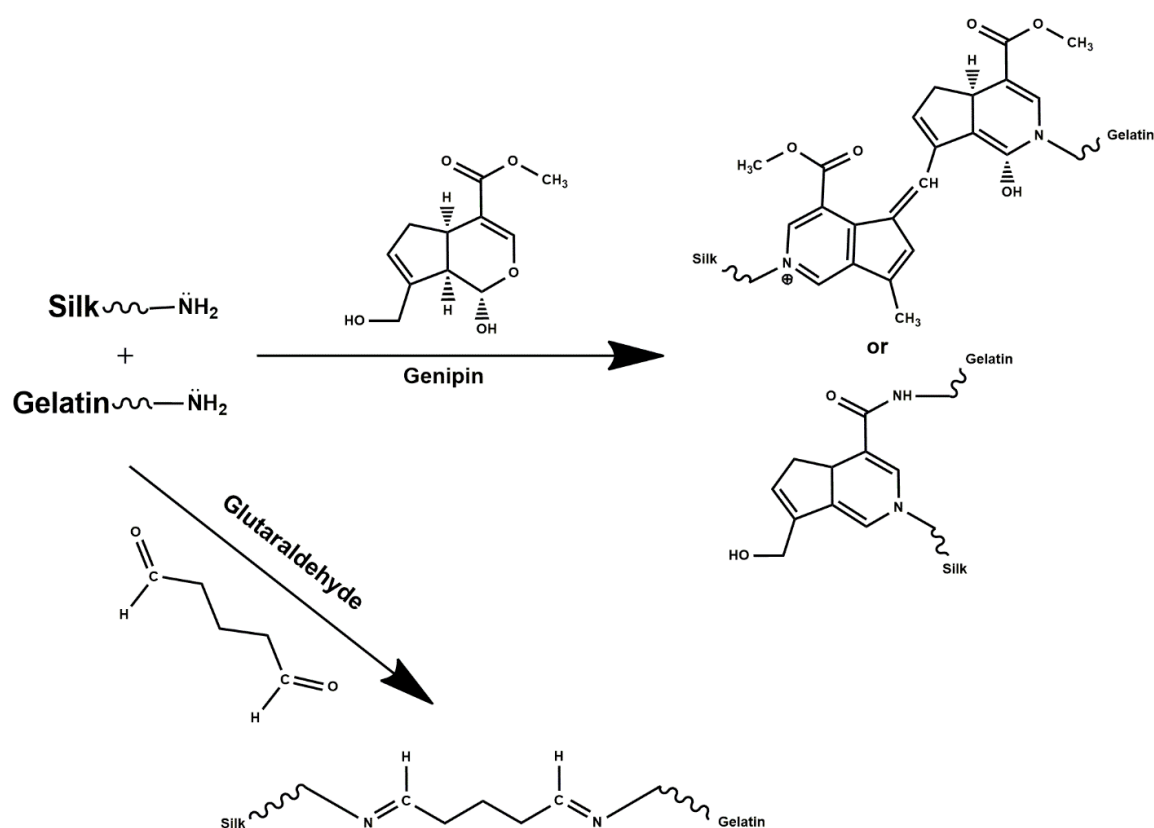
Fig. 6.6: Possible chemical crosslinking between silk and gelatin

The chemical crosslinking was further confirmed through thermogravimetric analysis (section 6.3.2)

The FTIR analysis revealed that the Type I blend films were affected conformationally after the regeneration and blending process and could not reproduce its crystallinity to a greater extent. Whereas, pure silk as well as the Type II blend films attained the β-sheet crystallinity even after regeneration and blending followed by methanol treatment. This was further verified by x-ray diffraction technique (comparative data also shown in Table 6.1).

As shown in Figure 6.7(a), regenerated pure silk film and all the blend films of Type I exhibited a broad diffraction pattern even after methanol treatment which is suggestive of very low crystallinity amongst the films. The observed amorphous structures are complimentary to the data obtained in FTIR studies. A possible explanation for this could be, the major part of polymer matrix is amorphous with presence of some small β-sheet crystals which are being revealed by FTIR [147].
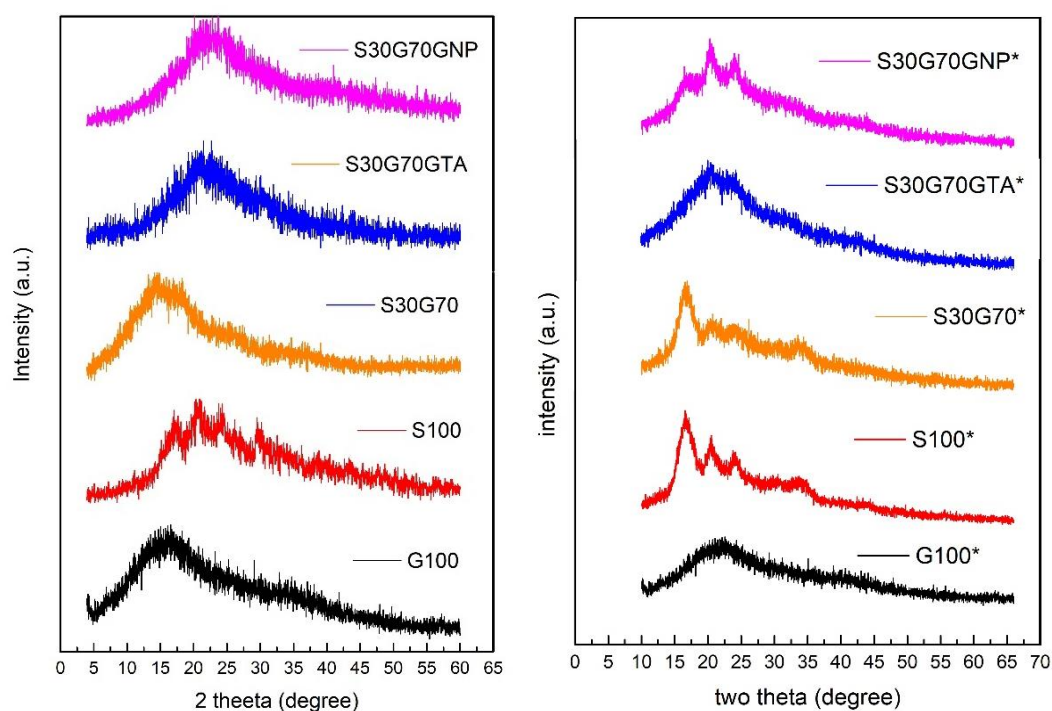
Fig. 6.7: (a) XRD patterns of Type I & **(b)** XRD patterns of Type II blend films

In case of Type II films (Figure 6.7b), pure silk film obtained by casting silk-formic acid solution showed slightly resolved crystalline pattern with three major peaks at 17.5, 20.3 and 23.4 degree along with two minor peaks at 30.2 and 33 degree corresponding to the 5.33, 4.37, 3.78, 2.91 and 2.60 Å spacing, which is indicative of β-sheet structure. Similar data has been reported by Bhat and Nadiger for regenerated *Antheraea pernyi* silk fibroin films (also a variety of non-mulberry silk), showing β-sheet crystallinity [102] . The film casted from gelatin-formic acid solution showed a broad peak around 21.4° indicating very low crystallinity. Ki *et al*. have also observed the amorphous structure of film casted by gelatin-formic acid solution [148] . S30G70* film showed a peak at 20.2 with a small shoulder at 23.6, and rest of the three peaks were absent as compared to pure silk film. Further, addition of crosslinker directed the polymeric chains to rearrange themselves into β-sheets [146]. The blend film S30G70GTA*showed one significant peak at 16.5 along with three small intensity peaks at 20.5, 23.9 and 33°. S30G70GNP* blend film exhibited a small intensity peak at 16.7 and two significant peaks at 20.3 and 24.8. respectively. It was observed that the peak which was present at 17.5 for pure silk film was shifted to 16.5 and 16.7 upon blending with gelatin for crosslinked S30G70GTA* and S30G70GNP* blend films. The peak intensity was also found to be variable as compared to pure silk film.

The XRD diffractograms reveal that, the Type II blend films showed better crystallinity as compared to Type I blend films which is majorly due to two reasons. One is the extra dialysis step while regenerating silk fibroin, which utilised water to exchange ionic liquid from silk solution, altering its conformation. Second is the solvent used to dissolve the silk fibroin powder obtained post dialysis, which is formic acid. It has been reported in literature that formic acid induces crystallisation in silk

fibroin similar to methanol treatment [149] . In Type I films, the uncoiling of silk polymeric chains was not as prominent as in Type II. Where, the combined effect of water and formic acid helped the polymeric chains to rearrange themselves into β-sheet conformation.

Upon structural analysis, it was observed that Type I blend films showed poor crystallinity along with high brittleness which is unfavourable for utilization as biomedical construct. So, the further studies were conducted for Type II blend films only, which showed good flexibility.

6.3.2   Thermogravimetric analysis

TGA thermograms of pure as well as Type II blend films are shown in Figure 6.8. The initial weight loss in all the samples at around 100°C is due to evaporation of water. The second weight loss is observed in the temperature range 230-400°C, which can be attributed to thermal decomposition of side chain groups of the amino-acids as well as the protein backbone including peptide linkages. Similar results have been reported by Andiappan *et al.* showing one weight loss at 100°C and second at 370°C for tasar silk fibroin scaffolds [150] . Also, for blend films, as observed in Figure5, there is visible shift in the weight loss curve towards lower temperature due to blending of silk fibroin with gelatin. As expected, the blend films showed lower total percentage mass loss than pure silk fibroin (79%) but higher than pure gelatin film (98%) at 900°C. Tuscado *et. al.* has also observed similar behaviour in case of *A. Pernyi/ B. Mori* SF blend films which showed intermediate thermal behaviour of the two pure components [69] .
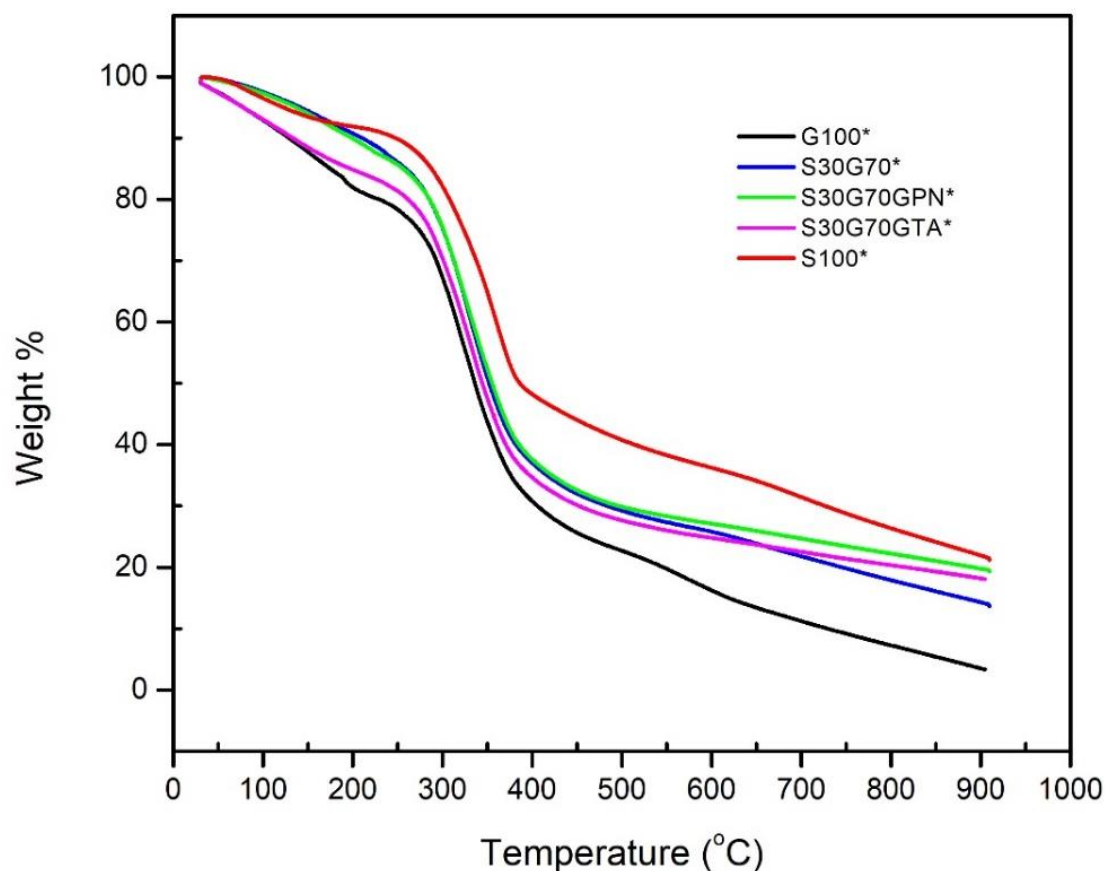
Fig. 6.8: TGA of Type II film samples.

Crosslinking in polymers is known to enhance the thermal stability [151,152] . The effect of crosslinking could also be observed in the thermograms, with uncross linked films showing 86% decomposition as compared to the blend films which showed 80 and 82% decomposition being crosslinked with glutaraldehyde and genipin respectively. Similar effect of chemical crosslinking has previously been reported for sericin/gelatin/clay blend films, where addition of glutaraldehyde reduced the percentage decomposition of films [116].

6.3.3 Differential scanning calorimetry

As shown in Fig. 6.9a, the DSC thermogram of pure gelatin film gives two major endotherms at temperatures approximately 120°C and 345°C respectively. The pure

SF film (Fig. 6.9b) shows four endotherms, bound water evaporation in the range 60-150°C, two decomposition endotherms in the temperature range of 220-280°C and one around 345°C. The endotherm at around 215°C is due to thermal decomposition of less ordered crystalline structures in silk fibroin while the ones around 265°C represents thermal disintegration of more ordered crystallites and at 345°C indicates melting of silk fibroin chains[19]. Blending of SF with gelatin has shown significant shift in the peaks as seen in the DSC thermograms. No thermal transition like T_c (crystallisation temperature) was observed due to solvent induced crystallization by methanol. Gil *et al.* have reported similar observation for *B. mori* silk fibroin/gelatin blend films where T_g and T_c disappeared from the DSC thermogram of methanol treated film samples [153] . Influence of blending *B. mori* silk fibroin and gelatin has previously been reported by Taddei and co-workers who observed significant changes in the DSC thermogram of blends with disappearance of T_g and T_c [154]. The blend film S30G70* (Fig. 6.9c) showed one major endotherm due to evaporation of water in region 70 -100°C and another one at 215°C (similar to pure silk). However, the endotherm present at 265°C for pure silk was shifted upon blending with gelatin to 257°C and merged into the degradation endotherm which also shifted by 30 degrees as compared to pure silk. In case of the blend film S30G70GTA* (Figure 6.9d) along with water evaporation endotherm, one sharp endotherm at 207°C (one present at 215°C for pure silk) and a broad endotherm in the range 230-340°C incorporating both decomposition of highly ordered crystallites along with degradation of the blend material was observed.

The significant shift in the endotherms can be associated to partial miscibility of the two components in blend films. Shift in DSC endotherms of silk-PVA blends have

previously been associated with blending amongst polymers by Lee and co-workers [155]. The endotherm present for pure silk in range 210-280°C almost disappeared upon crosslinking the blend with genipin
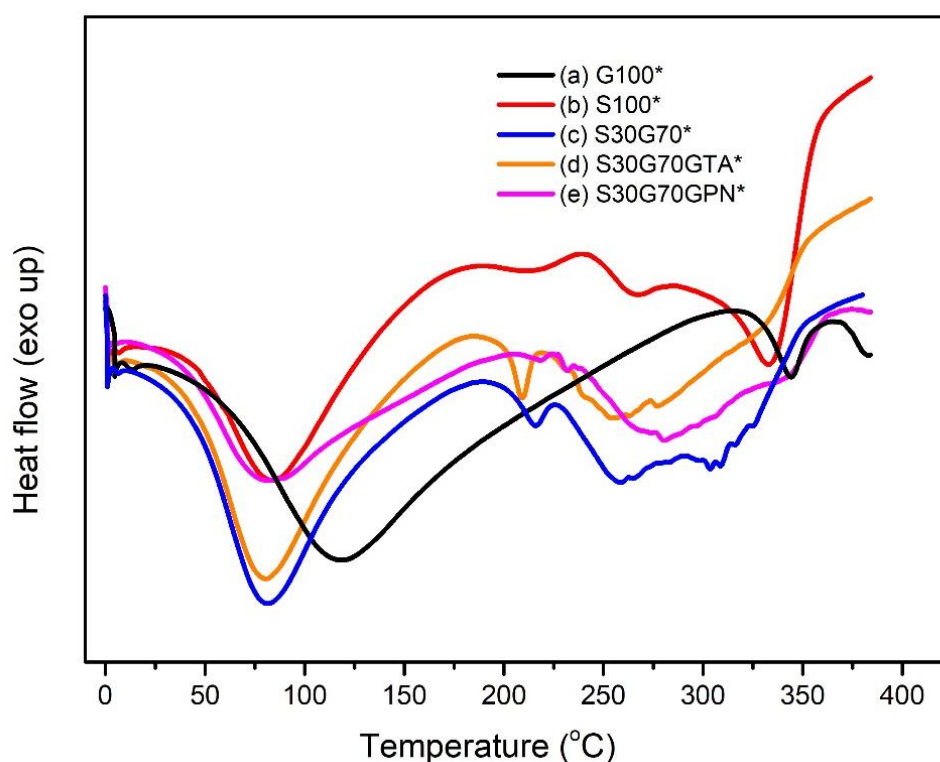
Fig. 6.9: DSC thermogram of Type II films.

(Figure 6.9e), instead one major broad endotherm appeared in the temperature range 226- 356°C with a very small shoulder around 340°C. As expected, the degradation temperature of blend films has been reduced due to incorporation of gelatin. Lee *et al.* have also reported shift in the decomposition endotherm of *B. mori* silk fibroin upon blending with S-carboxymethyl kerateine [156].

6.3.4 Water uptake capacity and *in vitro* biodegradation

The water uptake capacity of film samples with respect to time is shown in Fig. 6.10
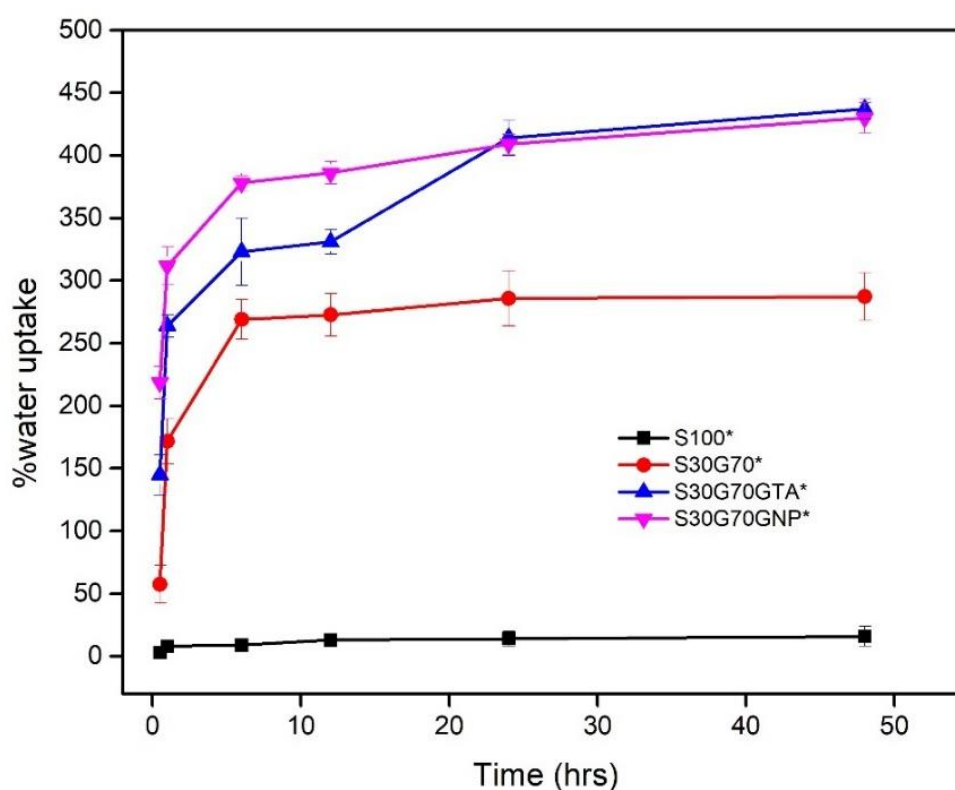
Fig. 6.10: Percentage Water Uptake Capacity of Type II films.

It is clearly visible that the water uptake capacity of the films increased with time and obtained equilibrium after a period of 48 hrs. The pure silk film showed only 16±2% water uptake capacity, similar to data reported previously [19].

The blending of silk fibroin with gelatin improved its water uptake capacity to a high value of 287±13% , which is due to the fact that gelatin itself shows a very high (around 391%) water uptake capacity [157]. Enhanced water uptake capacity of silk fibroin/gelatin blends were also reported by Kiti and co-workers. They blended B. mori silk fibroin with gelatin in various blend ratio and found that % swelling improved significantly with increase of gelatin content in the blend [158].

Apart from this fact, gelatin and silk fibroin blended together have been known to form IPNs (interpenetrating networks) during recrystallization, which increases their

water uptake capacity [159]. Upon crosslinking the blend films with glutaraldehyde and genipin, the water uptake capacity was further enhanced to 437±8 and 430±12 % respectively showing behaviour similar to hydrogel films. Silk fibroin in itself has been known to form β-sheet rich, physically crosslinked hydrogels due to formation of inter and intramolecular interactions amongst the protein chains [160]. Infact, genetically modified silk-elastin type polymers have been reported to form hydrogels with high water uptake capacity and are useful for applications like drug delivery [161].

The biodegradation of Type II film samples was studied in PBS with and without protease XIV enzyme as shown in Fig. 6.11a and 6.11b respectively. The biodegradability of the film samples was found to improve dramatically upon enzymatic exposure. Pure silk film showed negligible reduction in absence of enzyme but showed degradation of around 25±2% in enzymatic solution upon 21 days exposure. This observation is in close proximity to the data reported for enzymatic degradation of non-mulberry silk fibroin in literature [19]. The effect of blending silk fibroin with gelatin is clearly evident in the biodegradation profiles of the film samples. Addition of gelatin improved the degradation in all the three blend samples. The blend samples, S30G70*, S30G70GTA* and S30G70GNP* showed 48.8%, 45.2% and 44.1% degradation respectively in enzymatic solution over a period of 21 days.

The extent of biodegradation in polymers is influenced by distribution of crystallinity in their molecular structure. Pure silk film showed least value of enzymatic degradation, which can be attributed to its high β-sheet crystallinity, as discussed in previous sections. Gelatin being easily biodegradable, improved the biodegradation of blend films quite significantly. The extent of biodegradation observed for the blends crosslinked by glutaraldehyde and genipin is almost similar due to theirs comparable degree of crystallinity.
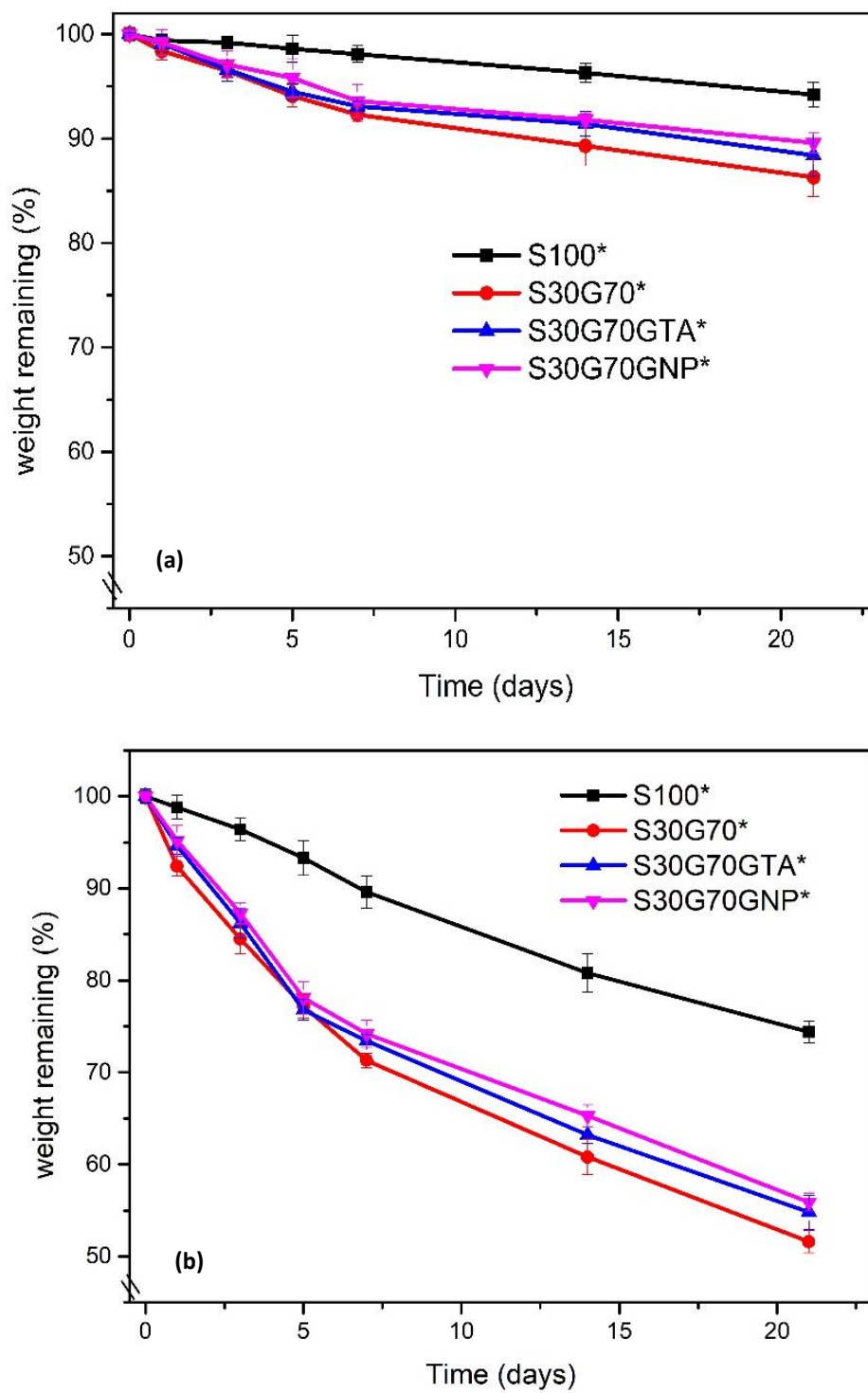
Fig. 6.11: Biodegradation of Type II films (a) in PBS solution, (b) in enzymatic solution

6.3.5   Cell adherence, proliferation and cytocompatibility

To evaluate the biocompatibility of Type II films, cell adherence and proliferation of L929 skin fibroblast cells was studied through phase contrast microscopy. As can be seen in Fig. 6.12, the cells are successfully adhered to the films and further proliferated with time. The density of cells was found to increase after 3 days of seeding. The film samples were almost covered with cells after a period of 5 days suggesting very good biocompatibility. Silk fibroin has been reported in literature to show biocompatibility due to presence of cell recognition sites in its amino acid sequence which helps in cell attachment [162] . Pure tasar silk fibroin scaffolds prepared by Srivastava and co-workers have been found to be biocompatible [113]. Taddei *et al*. have reported good biocompatibility of *B. mori* silk fibroin/gelatin blend films towards adherence and growth of cardiomyocytes [154].

Also, the surface of Type II film samples, observed in optical microscope (Fig. 6.13) before cell seeding, was found to be rough. In literature, surface roughness has been associated with providing biocompatibility due to enhanced cell adhesion and proliferation [95]. Srivastava *et al.* have also observed good biocompatibility in muga silk fibroin nanofibrous scaffold with high surface roughness [18].
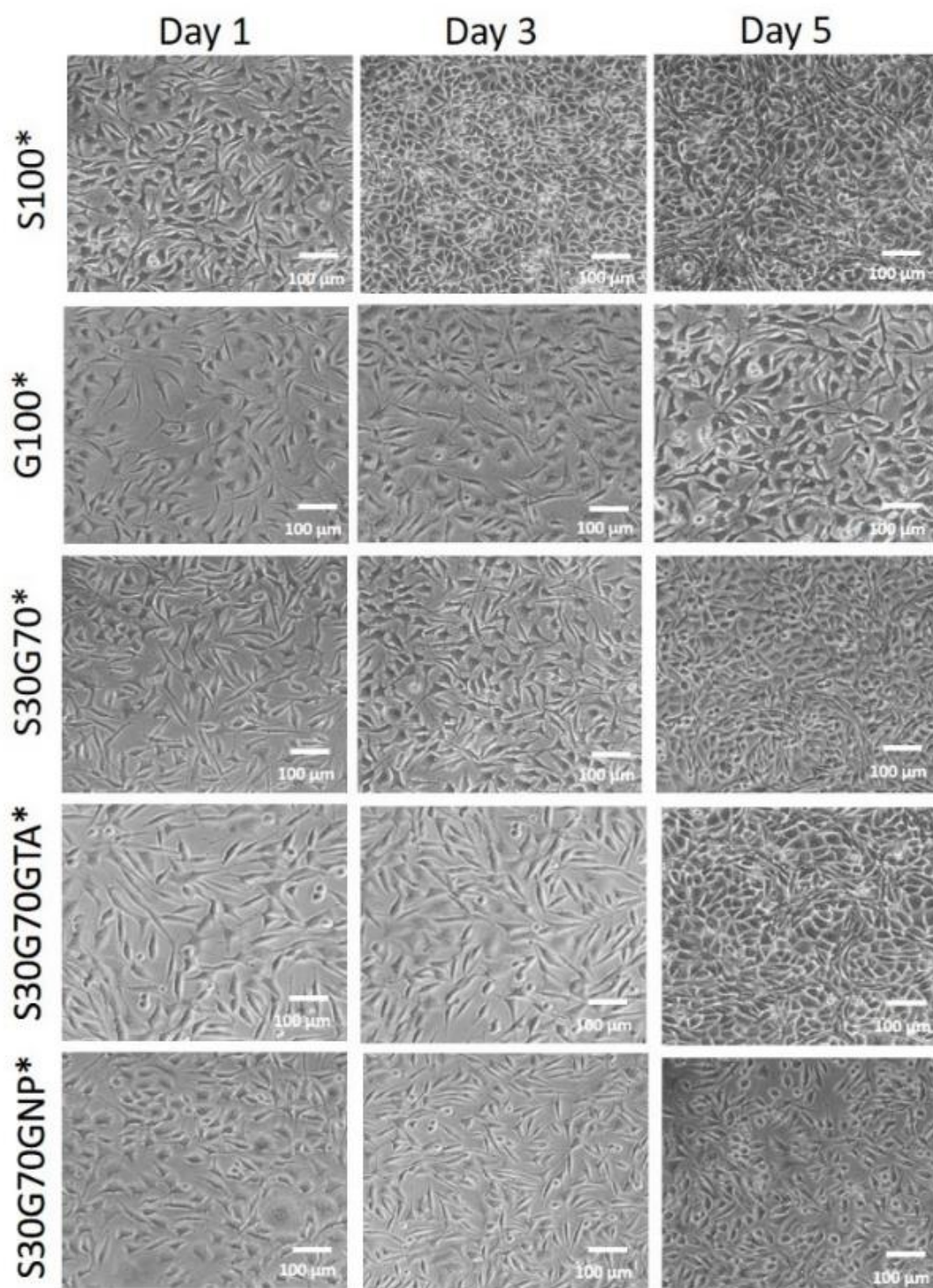
Fig. 6.12: Phase Contrast Microscopic images of fibroblast L929 cells growing on film samples
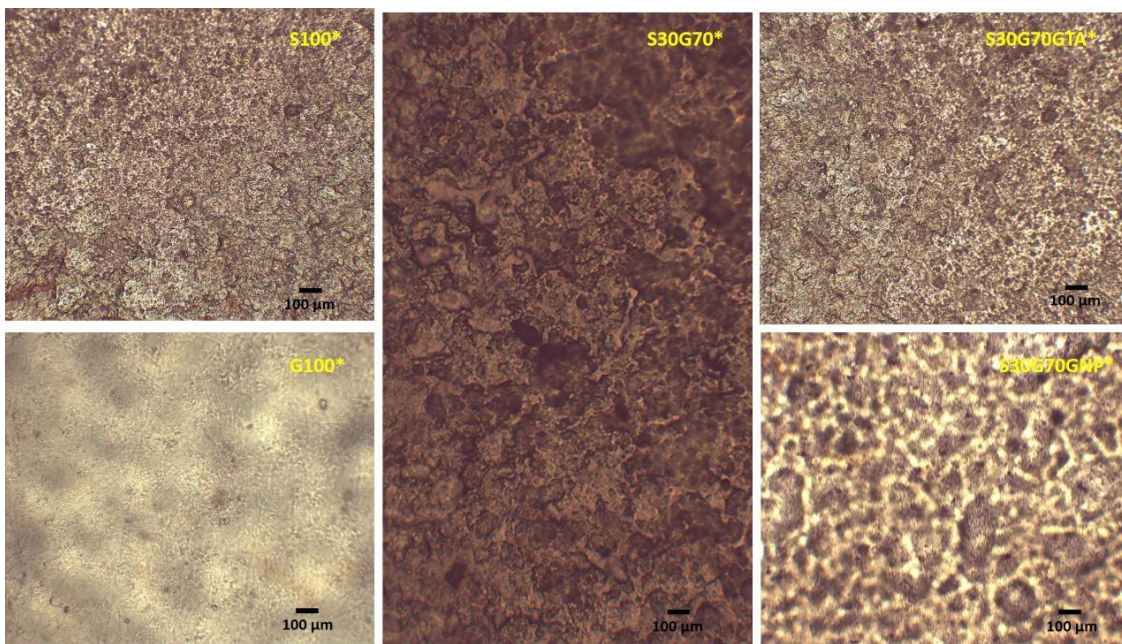
Fig. 6.13 Surface roughness of Type I films observed in optical microscope.
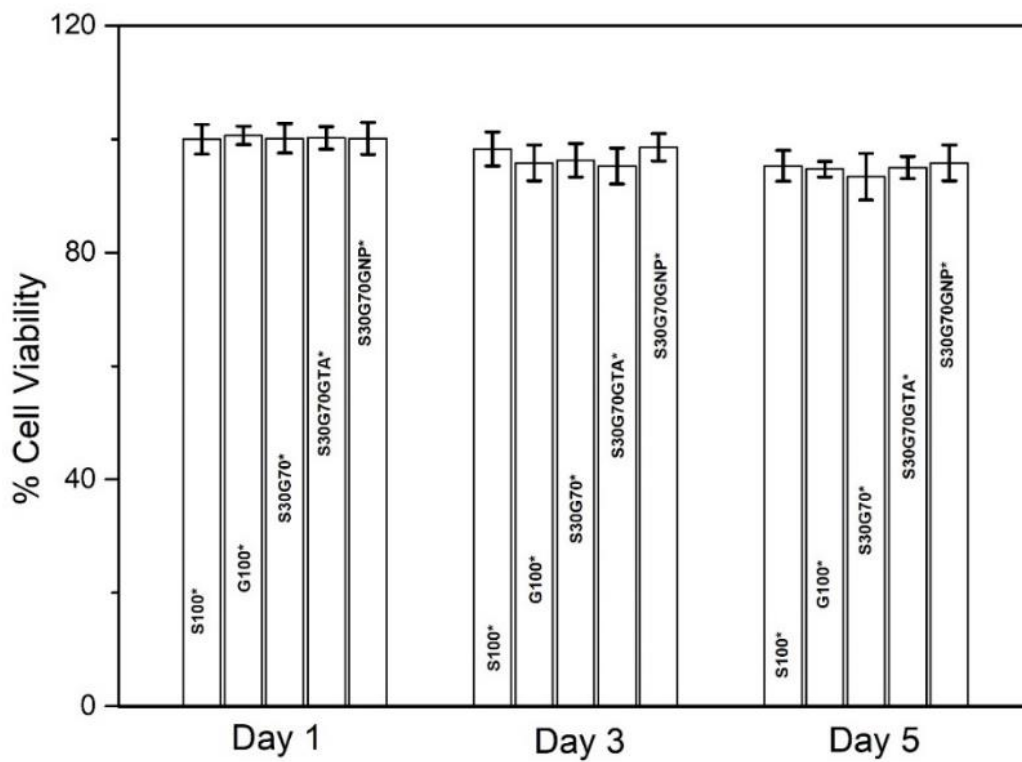
Fig. 6.14 Observed % cell viability of L929 fibroblast upon exposure to Type II films (MTT assay).

Further, MTT assay was performed in order to determine the viability of L929 fibroblast cells seeded on Type II films. This assay is an indirect manifestation of cell viability, which measures the metabolic activity of cells. In literature, the cellular metabolic activity value more than 70% has been found to signify non toxicity [111]. Fig. 6.14 shows the relative cellular metabolic activity of L929 fibroblasts on Type II films, after 1,3 and 5 days of culture. As it can be seen all the samples showed high metabolic activity (values >70%) with no toxicity.

The observed data suggests no influence of preparation or processing method as well as the additional components like crosslinkers on the biocompatibility of prepared blend films. This further directs towards the suitability of Type II films as potential candidate for applications in biomedical field.

6.4   Conclusions

➢   AMF/Gelatin blend films were prepared following two different routes. Among the two types prepared, Type II films showed superior properties than Type I.

➢   The structural studies, FTIR and XRD indicated higher percentage crystallinity in Type II films as compared to Type I.

➢   Thermal analysis of Type II films, through DSC showed partial miscibility of the pure components in blend and TGA exhibited improved thermal stability due to chemical crosslinking among the two polymers.

➢   Type II films showed impressive biocompatibility along with no toxicity towards fibroblast L929 cells.

➢ Further, high water uptake capacity and improved biodegradability suggests utilization of these Type II blend films in tissue engineering field for biomedical applications.

➢ The results of this chapters have been published in **Polymer International** journal.

Chapter 7

Conclusions and Future Scope

7.1 Conclusions

This entire research work was focused upon exploring the blending capacity of *Antheraea mylitta* (tasar) silk fibroin (ASF) with other polymers to develop biomaterials of enhanced physicochemical properties. Working in the same direction, PVA and gelatin two polymers were used to make blends with tasar silk fibroin (Fig. 7.1).
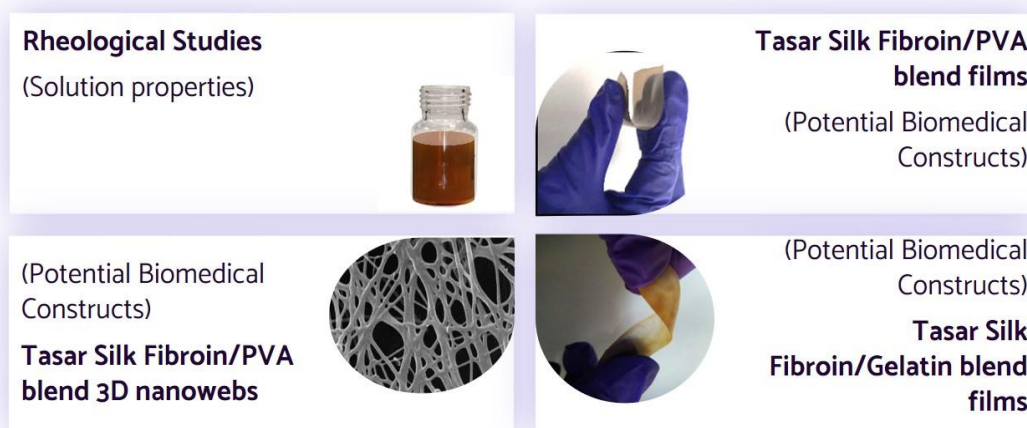
Fig. 7.1: Pictorial representation to summarise the overall research work

The silk fibroin/PVA blend solutions were first analysed for their rheological behaviour and flexible films and advanced 3D nanowebs were developed from them for utilization as biomaterials. Furthermore, tasar silk fibroin was attempted to blend with gelatin and its preparation methodology was explored to create flexible films for biomedical applications. The important discoveries of this thesis are summarised as follows:

Antheraea mylitta silk fibroin (ASF) and Polyvinyl alcohol (PVA) blend solutions were prepared and analysed for their rheological behaviour through steady and

dynamic shear tests. The viscosities of blend solutions were observed to be dependent on blend composition and applied shear. The viscoelastic behaviour of blend solutions was also altered by blend composition, blends with high silk fibroin content showed viscoelastic solid like properties and with high PVA content presented viscoelastic fluid like behaviour. The observations from frequency sweep and the tan plots complimented each other. The microstructural architecture of prepared blend solution was found to be changing upon application of shear and alterations due to blend compositions were also observed through application of Cox-Merz rule. The creep recovery data showed mechanical property enhancement in blend solutions. The percentage deformation of pure silk fibroin increased from 26% to a value as high as 3100000% upon blending with PVA in one of the blend compositions. The capacity of these blend solutions with tailorable properties, as indicated via this study, can further be used to optimize the process parameters and subsequently develop materials in different forms.

Flexible blend films of ASF and PVA were successfully prepared using formic acid as solvent. In general, the blends of silk fibroin and PVA are stabilized with crosslinkers and plasticizers, which have their own disadvantages when it comes to biocompatibility, as reported in literature. However, the methodology of blend preparation adopted in this particular study resulted in stable flexible films without any additive. The SEM images showed single phase morphology in the blend films. The structural studies indicated molecular interactions in the two polymeric components with variable crystallinity. The blend miscibility was further supported by thermal analysis of films. The positive impact of blending ASF and PVA was also presented by better mechanical properties. The higher swelling and hydrophilicity

along with excellent cell viability index suggested biocompatibility of blend films towards growth of L929 fibroblast cells. The blending of these two polymers not only enhanced the blend properties harmonically but also eliminated the need of any chemical additives for their stability. The improved functional properties along with alterable biodegradability dependent on polymer blend ratio makes these films suitable for an array of applications in biomedical field.

Novel CTAB-MT modified tasar silk fibroin and PVA blended 3D nanowebs were developed by electrospinning. The morphological analysis depicted rough morphology of these nanowebs with small diameters and good porosity. Structural, thermal and mechanical analysis collectively directed towards modification in the crystallinity of these nanowebs due to blending silk fibroin with PVA and incorporation of CTAB-MT, consequently altering their physicochemical properties. The inclusion of modified clay induced higher crystallinity in nanocomposite nanowebs as compared to their respective samples without clay, consequently their mechanical strength improved. The increased fiber diameter and reduced porosity upon addition of CTABMT to blend samples resulted in reduced water uptake capacity and slow biodegradation of nanoweb nanocomposites. The nanowebs were found to show high biocompatibility through Alamar blue assay, blending silk fibroin with PVA and incorporation of CTABMT further enhanced the attachment and growth of L929 fibroblast cells mimicking the extra cellular matrix behaviour. Addition of CTAB-MT imparted antibacterial activity to these nanowebs against *E. coli* and *S. aureus* bacterial strains. As indicated by the aforementioned studies, along with the excellent biological properties, these materials have the capacity to tune their

physio-chemical properties through variation in the blend ratios and inclusion of nanofiller for utilization as biomaterials for versatile tissue engineering applications.

ASF/Gelatin blend films were prepared following two different routes. Among the two types prepared, Type II films showed superior properties than Type I. The structural studies, FTIR and XRD indicated higher percentage crystallinity in Type II films as compared to Type I. Thermal analysis of Type II films, through DSC showed partial miscibility of the pure components in blend and TGA exhibited improved thermal stability due to chemical crosslinking among the two polymers. Type II films showed impressive biocompatibility along with no toxicity towards fibroblast L929 cells. Further, high water uptake capacity and improved biodegradability suggests utilization of these Type II blend films in tissue engineering field for biomedical applications.

7.2 Future scope

- To conduct animal based experiments for further confirming the biocompatibility of prepared *Antheraea mylitta* silk fibroin/PVA blend films & 3D nanowebs and to explore the commercialisation aspect.

- To design and develop *Antheraea mylitta* silk fibroin and gelatin blended nanowebs with tailorable properties

- Incorporation of drug/modified clay into ASF/gelatin blend nanowebs and study their drug release kinetics for utilisation in drug delivery applications.

- Expanding the scope of research in this field by exploring the other compatible polymers which can be blended with non-mulberry silk fibroin for biomedical applications.

References

1. Koh, L.-D.; Cheng, Y.; Teng, C.-P.; Khin, Y.-W.; Loh, X.-J.; Tee, S.-Y.; Low, M.; Ye, E.; Yu, H.-D.; Zhang, Y.-W.; Han, M.-Y. *Prog. Polym. Sci.* **2015**, *46*, 86.

2. Kundu, B.; Rajkhowa, R.; Kundu, S. C.; Wang, X. *Adv. Drug Deliv. Rev.* **2013**, *65*, 457.

3. Konwarh, R.; Bhunia, B. K.; Mandal, B. B. *Proc. Indian Natl. Sci. Acad.* **2017**, *83*, 85.

4. Shimura, K.; Kikuchi, A.; Ohtomo, K.; Katagata, Y.; Hyodo, A. *J. Biochem.* **1976**, *80*, 693.

5. Tanaka, K.; Inoue, S.; Mizuno, S. *Insect Biochem. Mol. Biol.* **1999**, *29*, 269.

6. Kundu, B.; Kundu, S. C. *Prog. Polym. Sci.* **2010**, *35*, 1116.

7. Sehnal, F.; Žurovec, M. *Biomacromolecules* **2004**, *5*, 666.

8. Inoue, S. I.; Tsuda, H.; Tanaka, T.; Kobayashi, M.; Magoshi, Y.; Magoshi, J. *Nano Lett.* **2003**, *3*, 1329.

9. Lucas, F.; Shaw, J. T. B.; Smith, S. G. *J. Mol. Biol.* **1960**, *2*, 339.

10. Rajkhowa, R.; Gupta, V. B.; Kothari, V. K. *J. Appl. Polym. Sci.* **2000**, *77*, 2418.

11. Li, M.; Lu, S.; Wu, Z.; Tan, K.; Minoura, N.; Kuga, S. *Int. J. Biol. Macromol.* **2002**, *30*, 89.

12. Bhardwaj, N.; Kundu, S. C. *Biomaterials* **2012**, *33*, 2848.

13. Silva, S. S.; Oliveira, M. B.; Nayak, S.; Popa, E. G.; Kundu, S. C.; Gomes, M. E.; Reis, R. L.; Mano, J. F.; Subia, B. *Acta Biomater.* **2013**, *9*, 8972.

14. Hakimi, O.; Knight, D. P.; Vollrath, F.; Vadgama, P. *Compos. Part B Eng.* **2007**, *38*, 324.

15. Mallepally, R. R.; Marin, M. A.; Surampudi, V.; Subia, B.; Rao, R. R.; Kundu, S. C.; McHugh, M. A. *Biomed. Mater.* **2015**, *10*, 1.

16. Wang, G.; Hu, X.; Lin, W.; Dong, C.; Wu, H. *Vitr. Cell. Dev. Biol. - Anim.* **2011**, *47*, 234.

17. Freddi, G.; Romano, M.; Massafra, M. R.; Tsukada, M. *J. Appl. Polym. Sci.* **1995**, *56*, 1537.

18. Srivastava, C. M.; Purwar, R. *Mater. Sci. Eng. C* **2016**, *68*, 276.

19. Srivastava, C. M.; Purwar, R.; Gupta, A.; Sharma, D. *Mater. Sci. Eng. C* **2017**, *75*, 104.

20. Sionkowska, A. Current research on the blends of natural and synthetic polymers as new biomaterials: Review. *Prog. Polym. Sci.* **2011**, *36*, 1254–1276.

21. Gil, E. S.; Frankowski, D. J.; Spontak, R. J.; Hudson, S. M. *Biomacromolecules* **2005**, *6*, 3079.

22. Gil, E. S.; Frankowski, D. J.; Bowman, M. K.; Gozen, A. O.; Hudson, S. M.; Spontak, R. J. *Biomacromolecules* **2006**, *7*, 728.

23. Marcolin, C.; Draghi, L.; Tanzi, M. C.; Faré, S. *J. Mater. Sci. Mater. Med.* **2017**, *28*, 1.

24. He, F.-L.; Deng, X.; Ye, Y.; Liu, Y.-L.; Li, D.; He, J.; Liu, Y.; Yin, D.-C. *Carbohydr. Polym.* **2017**, *178*, 69.

25. Liu, Y.; Yin, D.; Ye, Y.; Lei, X.; He, F.-L.; Li, D.; Duan, E.; Deng, X.; He, J. *Int. J. Biol. Macromol.* **2017**, *105*, 584.

26. Campana-Filho, S. P.; Ribeiro, S. J. L.; Delezuk, J. A. M.; Shimizu, F. M.; Pavinatto, A.; Rodrigues, V. C.; Oliveira, O. N.; Moraes, M. L. *Carbohydr. Polym.* **2016**, *155*, 146.

27. Rujiravanit, R.; Kruaykitanon, S.; Jamieson, A. M.; Tokura, S. *Macromol. Biosci.* **2003**, *3*, 604.

28. Zhang, Y.; Cao, C. B.; Lu, Q.; Ma, X. L.; Zhu, H. S. *Acta Polym. Sin.* **2004**, 556.

29. Tsukada, M.; Freddi, G.; Crichton, J. S. *J. Polym. Sci. Part B Polym. Phys.* **1994**, *32*, 243.

30. Tanaka, T.; Kuranuki, N.; Tanigami, T.; Yamaura, K. *Polym. Int.* **2000**, *42*, 107.

31. Li, M.; Minoura, N.; Dai, L.; Zhang, L. *Macromol. Mater. Eng.* **2001**, *286*, 529.

32. Wang, X.; Yucel, T.; Lu, Q.; Hu, X.; Kaplan, D. L. *Biomaterials* **2010**, *31*, 1025.

33. Jin, H. J.; Park, J.; Valluzzi, R.; Cebe, P.; Kaplan, D. L. *Biomacromolecules* **2004**, *5*, 711.

34. Li, C.; Vepari, C.; Jin, H. J.; Kim, H. J.; Kaplan, D. L. *Biomaterials* **2006**, *27*, 3115.

35. Yang, X.; Yu, F.; Lou, X.; Chen, M.; He, C.; Wang, H.; Fan, L.; Jiang, H.; Lin, S.; Sun, B. *Colloids Surfaces B Biointerfaces* **2015**, *139*, 156.

36. Marsano, E.; Corsini, P.; Canetti, M.; Freddi, G. *Int. J. Biol. Macromol.* **2008**, *43*, 106.

37. Shang, S.; Zhu, L.; Fan, J. *Carbohydr. Polym.* **2011**, *86*, 462.

38. Zhou, L.; Wang, Q.; Wen, J.; Chen, X.; Shao, Z. *Polymer (Guildf).* **2013**, *54*, 5035.

39. Marsano, E.; Canetti, M.; Conio, G.; Corsini, P.; Freddi, G. *J. Appl. Polym. Sci.* **2007**, *104*, 2187.

40.   Yang, G.; Zhang, L.; Cao, X.; Liu, Y. *J. Memb. Sci.* **2002**, *210*, 379.

41.   Bhattacharjee, P.; Kundu, B.; Naskar, D.; Al, E. *Biopolymers* **2015**, *103*, 271.

42.   Singh, Y. P.; Bhardwaj, N.; Mandal, B. B. *ACS Appl. Mater. Interfaces* **2016**, *8*, 21236.

43.   Bhattacharjee, P.; Naskar, D.; Kim, H.; Maiti, T. K.; Bhattacharya, D.; Kundu, S. C. *Eur. Polym. J.* **2015**, *71*, 490.

44.   Chouhan, D.; Chakraborty, B.; Nandi, S. K.; Mandal, B. B. *Acta Biomater.* **2017**, *48*, 157.

45.   Abdullah, Z. W.; Dong, Y.; Davies, I. J.; Barbhuiya, S. *Polym. - Plast. Technol. Eng.* **2017**, *56*, 1307.

46.   Musetti, A.; Paderni, K.; Fabbri, P.; Pulvirenti, A.; Al-Moghazy, M.; Fava, P. *J. Food Sci.* **2014**, *79*.

47.   Paradossi, G.; Cavalieri, F.; Chiessi, E.; Spagnoli, C.; Cowman, M. K. *J. Mater. Sci. Mater. Med.* **2003**, *14*, 687.

48.   Liu, Y.; Qian, J.; Liu, H.; Zhang, X.; Deng, J.; Yu, T. *J. Appl. Polym. Sci.* **1996**, *61*, 641.

49.   Tao, G.; Cai, R.; Wang, Y.; Song, K.; Guo, P.; Zhao, P.; Zuo, H.; He, H. *Materials (Basel).* **2017**, *10*.

50.   Wang, Y.; Hsieh, Y.-L. *J. Appl. Polym. Sci.* **2010**, *116*, 1471.

51.   Zhang, Y.; Zhu, P. C.; Edgren, D. *J. Polym. Res.* **2010**, *17*, 725.

52.   Pillai, M. M.; Gopinathan, J.; Indumathi, B.; Manjoosha, Y. R.; Santosh Sahanand, K.; Dinakar Rai, B. K.; Selvakumar, R.; Bhattacharyya, A. *J. Membr. Biol.* **2016**, *249*, 813.

53.   Pillai, M. M.; Elakkiya, V.; Lakshmipriya, H.; Gopinathan, J.; Selvakumar, R.; Bhattacharyya, A. *Biomed. Phys. Eng. Express* **2018**, *4*, 027006.

54.   Aldana, A. A.; Abraham, G. A. *Int. J. Pharm.* **2017**, *523*, 441.

55.   Xing, Q.; Yates, K.; Vogt, C.; Qian, Z.; Frost, M. C.; Zhao, F. *Sci. Rep.* **2014**, *4*, 1.

56.   Sun, K.; Li, R.; Jiang, W.; Sun, Y.; Li, H. *Biochem. Biophys. Res. Commun.* **2016**, *477*, 1085.

57.   Rujitanaroj, P. on; Pimpha, N.; Supaphol, P. *Polymer (Guildf).* **2008**, *49*, 4723.

58.   Nancy, p.; Shilpita, S.; Sen, M.; Swathi, S. *J. Tissue Eng. Regen. Med.* **2012**, *4*, 524.

59.   Cui, Z. K.; Kim, S.; Baljon, J. J.; Wu, B. M.; Aghaloo, T.; Lee, M. *Nat. Commun.* **2019**, *10*, 1.

60.   Jayrajsinh, S.; Shankar, G.; Agrawal, Y. K.; Bakre, L. *J. Drug Deliv. Sci. Technol.* **2017**, *39*, 200.

61.   Koç Demir, A.; Elçin, A. E.; Elçin, Y. M. *Mater. Sci. Eng. C* **2018**, *89*, 8.

62.   Thakur, G.; Singh, A.; Singh, I. *Sci. Pharm.* **2016**, *84*, 603.

63.   Dawson, J. I.; Oreffo, R. O. C. *Adv. Mater.* **2013**, *25*, 4069.

64.   Yao, Y.; Mukuze, K. S.; Zhang, Y.; Wang, H. *Cellulose* **2014**, *21*, 675.

65.   Zhang, X.; Pan, Z. *J. Mater. Sci.* **2020**, *55*, 15350.

66.   Das, S.; Pati, F.; Chameettachal, S.; Pahwa, S.; Ray, A. R.; Dhara, S.; Ghosh, S. *Biomacromolecules* **2013**, *14*, 311.

67.   Sheng, C.; Wenting, B.; Shijian, T.; Yuechuan, W. *Polymer (Guildf).* **2008**, *21*, 449.

68.   Goujon, N.; Rajkhowa, R.; Wang, X.; Byrne, N. *J. Appl. Polym. Sci.* **2013**, *128*, 4411.

69.   Tsukada, M.; Freddi, G.; Kasai, N. *J. Polym. Sci. Part B Polym. Phys.* **1994**, *32*, 1175.

70. Xue, Y.; Jao, D.; Hu, W.; Hu, X. *J. Therm. Anal. Calorim.* **2017**, *127*, 915.

71. Kweon, H.; Um, I. C.; Park, Y. H. *Polymer (Guildf).* **2001**, *42*, 6651.

72. Bissoyi, A.; Kumar Singh, A.; Kumar Pattanayak, S.; Bit, A.; Kumar Sinha, S.; Patel, A.; Jain, V.; Kumar Patra, P. *Biomed. Mater.* **2018**, *13*, 1.

73. Kundu, S. C.; Nandi, S. K.; Bhattacharya, D.; Maiti, T. K.; Naskar, D.; Bhattacharjee, P.; Das, P. *Colloids Surfaces B Biointerfaces* **2016**, *143*, 431.

74. Panda, N.; Bissoyi, A.; Pramanik, K.; Biswas, A. *Mater. Sci. Eng. C* **2015**, *48*, 521.

75. Wang, J.; Sun, B.; Bhutto, M. A.; Zhu, T.; Yu, K.; Bao, J.; Morsi, Y.; El-Hamshary, H.; El-Newehy, M.; Mo, X. *Front. Mater. Sci.* **2017**, *11*, 22.

76. Gao, Y.; Shao, W.; Qian, W.; He, J.; Zhou, Y.; Qi, K. *Mater. Sci. Eng. C* **2018**, *84*, 195.

77. Zhang, F.; Zuo, B. Q.; Zhang, H. X.; Bai, L. *Polymer (Guildf).* **2009**, *50*, 279.

78. Jin, H. J.; Fridrikh, S. V; Rutledge, G. C.; Kaplan, D. L. *Biomacromolecules* **2002**, *3*, 1233.

79. Shin, Y. M.; Hohman, M. M.; Brenner, M. P.; Rutledge, G. C. *Polymer (Guildf).* **2002**, *42*, 09955.

80. Deitzel, J. M.; Kleinmeyer, J.; Harris, D.; Beck Tan, N. C. *Polymer (Guildf).* **2001**, *42*, 261.

81. Kweon, H.; Ha, H. C.; Um, I. N. C.; Park, Y. H. *J. Appl. Polym. Sci.* **2001**, *80*, 928.

82. Mandal, B. B.; Kundu, S. C. *Biotechnol. Bioeng.* **2008**, *100*, 1237.

83. Srivastava, C. M.; Purwar, R. *J. Appl. Polym. Sci.* **2017**, *134*, 1.

84. Singh, B. N.; Panda, N. N.; Mund, R.; Pramanik, K. *Carbohydr. Polym.* **2016**, *151*, 335.

85. Mu, X.; Fitzpatrick, V.; Kaplan, D. L. *Adv. Healthc. Mater.* **2020**, *9*, 1901552.

86. Cox, W. P.; Merz, E. H. *J. Polym. Sci.* **1958**, *28*, 619.

87. Snijkers, F.; Vlassopoulos, D. *Rheol. Acta* **2014**, *53*, 935.

88. Yao, Y.; Xia, X.; Mukuze, K. S.; Zhang, Y.; Wang, H. *Cellulose* **2014**, *21*, 3737.

89. Chotpattananont, D.; Sirivat, A.; Jamieson, A. M. *Polymer (Guildf).* **2006**, *47*, 3568.

90. Ling, S.; Qi, Z.; Knight, D. P.; Shao, Z.; Chen, X. *Biomacromolecules* **2011**, *12*, 3344.

91. DeFrates, K.; Markiewicz, T.; Callaway, K.; Xue, Y.; Stanton, J.; Salas-de la Cruz, D.; Hu, X. *Int. J. Biol. Macromol.* **2017**, *104*, 919.

92. Kokubo, T.; Takadama, H. *Biomaterials* **2006**, *27*, 2907.

93. Um, I. C.; Park, Y.-H. *Fibers Polym.* **2007**, *8*, 579.

94. Batra, R.; Purwar, R. *Polym. Int.* **2021**, *70*, 73.

95. Mandal, B. B.; Das, S.; Choudhury, K.; Kundu, S. C. *Tissue Eng. - Part A* **2010**, *16*, 2391.

96. Miyazawa, T.; Blout, E. R. *J. Am. Chem. Soc.* **1961**, *83*, 712.

97. Bhardwaj, N.; Rajkhowa, R.; Wang, X.; Devi, D. *Int. J. Biol. Macromol.* **2015**, *81*, 31.

98. Ling, S.; Qi, Z.; Knight, D. P.; Shao, Z.; Chen, X. *Polym. Chem.* **2013**, *4*, 5401.

99. Fathi, A.; Khanmohammadi, M.; Goodarzi, A.; Foroutani, L.; Mobarakeh, Z. T.; Saremi, J.; Arabpour, Z.; Ai, J. *J. Biol. Eng.* **2020**, *14*, 1.

100. Raksa, A.; Utke, R.; Ruksakulpiwat, C.; Numpaisal, P. O.; Ruksakulpiwat, Y. *AIP Conf. Proc.* **2020**, *2279*, 4.

101. Luo, Q.; Chen, Z.; Hao, X.; Zhu, Q.; Zhou, Y. *Int. J. Biol. Macromol.* **2013**, *61*, 135.

102. Bhat, N. V.; Nadiger, G. S. *J. Appl. Polym. Sci.* **1980**, *25*, 921.

103. Liu, P.; Chen, W.; Liu, C.; Tian, M.; Liu, P. *Sci. Rep.* **2019**, *9*, 9534.

104. Wang, N.; Si, Y.; Yu, J.; Fong, H.; Ding, B. *Mater. Des.* **2017**, *120*, 135.

105. Sampieri, R. H. *Biodegradable Systems in Tissue Engineering and Regenerative Medicine*; Reis, R. L.; Román, J. S., Eds.; CRC Press, **2004**.

106. Li, M.; Lu, S.; Wu, Z.; Tan, K.; Minoura, N.; Kuga, S. *Int. J. Biol. Macromol.* **2002**, *30*, 89.

107. Yang, R.; Wu, P.; Wang, X.; Liu, Z.; Zhang, C.; Shi, Y.; Zhang, F.; Zuo, B. *RSC Adv.* **2018**, *8*, 22069.

108. Lee, K. Y. *Fibers Polym.* **2001**, *2*, 71.

109. Sen, K.; Babu K, M. *J. Appl. Polym. Sci.* **2004**, *92*, 1080.

110. Patra, C.; Talukdar, S.; Novoyatleva, T.; Velagala, S. R.; Mühlfeld, C.; Kundu, B.; Kundu, S. C.; Engel, F. B. *Biomaterials* **2012**, *33*, 2673.

111. Cannella, V.; Altomare, R.; Chiaramonte, G.; Di Bella, S.; Mira, F.; Russotto, L.; Pisano, P.; Guercio, A. *Biomed Res. Int.* **2019**, *2019*.

112. Srivastava, C. M.; Purwar, R.; Gupta, A. P. *Int. J. Biol. Macromol.* **2019**, *130*, 437.

113. Srivastava, C. M.; Purwar, R. *Macromol. Res.* **2018**, *26*, 872.

114. Chouhan, D.; Janani, G.; Chakraborty, B.; Nandi, S. K.; Mandal, B. B. *J. Tissue Eng. Regen. Med.* **2018**, *12*, e1559.

115. Jin, H. J.; Park, J.; Karageorgiou, V.; Kim, U. J.; Valluzzi, R.; Cebe, P.; Kaplan, D. L. *Adv. Funct. Mater.* **2005**, *15*, 1241.

116. Purwar, R.; Verma, A.; Batra, R. *J. Polym. Eng.* **2019**, *39*, 744.

117. Karaca, S.; Gürses, A.; Ejder Korucu, M. *J. Chem.* **2013**, *2013*.

118. Shirzad-Siboni, M.; Khataee, A.; Hassani, A.; Karaca, S. *Comptes Rendus Chim.* **2015**, *18*, 204.

119. Yu, W. H.; Zhu, T. T.; Tong, D. S.; Wang, M.; Wu, Q. Q.; Zhou, C. H. *Clays Clay Miner.* **2017**, *65*, 417.

120. Liu, S.; Yu, H.; Huang, K. *J. Mater. Sci.* **2018**, *53*, 3959.

121. Wang, X.; Ding, B.; Yu, J.; Yang, J. *Colloids Surfaces B Biointerfaces* **2011**, *86*, 345.

122. Amiraliyan, N.; Nouri, M.; Kish, M. H. *Fibers Polym.* **2009**, *10*, 167.

123. Abdel-Hady, F.; Alzahrany, A.; Hamed, M. *ISRN Nanotechnol.* **2011**, *2011*, 1.

124. Reneker, D. H.; Kataphinan, W.; Theron, A.; Zussman, E.; Yarin, A. L. *Polymer (Guildf).* **2002**, *43*, 6785.

125. Haider, A.; Haider, S.; Kang, I. K. *Arab. J. Chem.* **2018**, *11*, 1165.

126. Park, J. H.; Lee, H. W.; Chae, D. K.; Oh, W.; Yun, J. D.; Deng, Y.; Yeum, J. H. *Colloid Polym. Sci.* **2009**, *287*, 943.

127. Park, S. M.; Park, J. H.; Islam, S.; Choi, J. H.; Ghim, H. Do; Yoon, N. S.; Yeum, J. H. *Polym. Polym. Compos.* **2011**, *19*, 35.

128. Purwar, R.; Sai Goutham, K.; Srivastava, C. M. *Fibers Polym.* **2016**, *17*, 1206.

129. Ikada, Y. *Tissue engineering: fundamentals and applications.*; Elsevier, **2011**.

130. Kim, G.; Park, J.; Park, S. *J. Polym. Sci. Part B Polym. Phys.* **2007**, *45*, 2038.

131. Zamani, F.; Amani-Tehran, M.; Latifi, M.; Shokrgozar, M. A. *J. Mater. Sci. Mater. Med.* **2013**, *24*, 1551.

132. Mishra, A. K.; Allauddin, S.; Narayan, R.; Aminabhavi, T. M.; Raju, K. V. S. N. *Ceram. Int.* **2012**, *38*, 929.

133. Dang, Q.; Lu, S.; Yu, S.; Sun, P.; Yuan, Z. *Biomacromolecules* **2010**, *11*, 1796.

134. Green, R. J.; Hopkinson, I.; Jones, R. A. L. *Langmuir* **1999**, *15*, 5102.

135. Kumar, V.; Kumar, M.; Pugazhenthi, G. *Int. J. Nano Biomater.* **2014**, *5*, 27.

136. Marras, S. I.; Tsimpliaraki, A.; Zuburtikudis, I.; Panayiotou, C. *J. Phys. Conf. Ser.* **2007**, *61*, 1366.

137. Zhou, Y.; Yang, H.; Liu, X.; Mao, J.; Gu, S.; Xu, W. *Int. J. Biol. Macromol.* **2013**, *53*, 88.

138. Kaplan, D.; Adams, W. W.; Farmer, B.; Viney, C. In *Silk polymers*; Kaplan, D.; Adams, W. W.; Farmer, B.; Viney, C., Eds.; American Chemical Society Publishing, **1993**.

139. Purwar, R. *Nanotechnology in Textiles*; Joshi, M., Ed.; Jenny Stanford Publishing, **2020**.

140. Huang, Z. M.; Zhang, Y. Z.; Ramakrishna, S.; Lim, C. T. *Polymer (Guildf).* **2004**, *45*, 5361.

141. Chew, S. Y.; Hufnagel, T. C.; Lim, C. T.; Leong, K. W. *Nanotechnology* **2006**, *17*, 3880.

142. Ojha, S. *Structure-property relationship of electrospun fibers*; Afshari, M., Ed.; Elsevier Ltd., **2017**.

143. Ji, J.; Ke, Y.; Pei, Y.; Zhang, G. *J. Appl. Polym. Sci.* **2017**, *134*.

144. Liu, H.; Ding, X.; Zhou, G.; Li, P.; Wei, X.; Fan, Y. *J. Nanomater.* **2013**, *2013*.

145. You, R.; Zhang, J.; Gu, S.; Zhou, Y.; Li, X.; Ye, D.; Xu, W. *Mater. Sci. Eng. C* **2017**, *79*, 430.

146. Zhang, K.; Qian, Y.; Wang, H.; Fan, L.; Huang, C.; Yin, A.; Mo, X. *J. Biomed. Mater. Res. - Part A* **2010**, *95*, 870.

147. Vasconcelos, A.; Freddi, G.; Cavaco-Paulo, A. *Biomacromolecules* **2009**, *10*,

1019.

148. Ki, C. S.; Baek, D. H.; Gang, K. D.; Lee, K. H.; Um, I. C.; Park, Y. H. *Polymer (Guildf).* **2005**, *46*, 5094.

149. Um, I. C.; Kweon, H. Y.; Park, Y. H.; Hudson, S. *Int. J. Biol. Macromol.* **2001**, *29*, 91.

150. Andiappan, M.; Kumari, T.; Sundaramoorthy, S.; Meiyazhagan, G.; Manoharan, P.; Venkataraman, G. *Prog. Biomater.* **2016**, *5*, 81.

151. Mitra, T.; Sailakshmi, G.; Gnanamani, A.; Mandal, A. B. *Thermochim. Acta* **2011**, *525*, 50.

152. Mathew, A. P.; Packirisamy, S.; Thomas, S. *Polym. Degrad. Stab.* **2001**, *72*, 423.

153. Gil, E. S.; Frankowski, D. J.; Bowman, M. K.; Gozen, A. O.; Hudson, S. M.; Spontak, R. J. *Biomacromolecules* **2006**, *7*, 728.

154. Taddei, P.; Chiono, V.; Anghileri, A.; Vozzi, G.; Freddi, G.; Ciardelli, G. *Macromol. Biosci.* **2013**, *13*, 1492.

155. Lee, K. H.; Baek, D. H.; Ki, C. S.; Park, Y. H. *Int. J. Biol. Macromol.* **2007**, *41*, 168.

156. Lee, K. Y.; Ha, W. S. *Polymer (Guildf).* **1999**, *40*, 4131.

157. Kavoosi, G.; Dadfar, S. M. M.; Mohammadi Purfard, A.; Mehrabi, R. *J. Food Saf.* **2013**, *33*, 423.

158. Kiti, K.; Kudithalert, P.; Waratrujiwong, T.; Suwantong, O. *Polym. Bull.* **2018**, *75*, 2543.

159. Gil, E. S.; Spontak, R. J.; Hudson, S. M. *Macromol. Biosci.* **2005**, *5*, 702.

160. Wang, X.; Kluge, J. A.; Leisk, G. G.; Kaplan, D. L. *Biomaterials* **2008**, *29*, 1054.

161. Pritchard, E. M.; Kaplan, D. L. *Expert Opin. Drug Deliv.* **2011**, *8*, 797.

162. Mandal, B. B.; Kundu, S. C. *Acta Biomater.* **2010**, *6*, 360.

List of Publications

International

- **Radhika Batra**, Roli Purwar*, Deduction of a facile method to construct *Antheraea mylitta* silk fibroin/gelatin blend films for prospective biomedical applications, Polymer International, (2020) https://doi.org/10.1002/pi.6087.

- **Radhika Batra**, Roli Purwar*, Senthilguru Kulanthaivel[2], Prashant Mishra[2], Cetyl Trimethyl Ammonium Bromide Modified Montmorillonite-Doped Tasar Silk Fibroin/Polyvinyl Alcohol Blend 3D Nanowebs for Tissue Engineering Applications. Macromolecular Materials and Engineering, (2021)

  https://doi.org/10.1002/mame.202100450

- **Radhika Batra**, Roli Purwar*, Priya Bansal, Reetu Yadav, Senthilguru Kulanthaivel[2], Prashant Mishra[2], Enhancement of functional properties by blending cocoon extracted *Antheraea mylitta* silk fibroin with Polyvinyl alcohol (PVA) for applications in biomedical field. Journal of Applied Polymer Science, (2021)

  https://doi.org/10.1002/app.51913

Conference Publications

- **Radhika Batra**, Roli Purwar Poster presentation, Structural and thermal analysis of Antheraea mylitta silk fibroin/gelatin blend films, SPSI MACRO 2018, International conference on Polymer Science and Technology, held on 19th-22nd Dec 2018, at IISER Pune.

- **Radhika Batra**, Roli Purwar Poster presentation, Modified clay doped flexible gelatin/sericin blend films for food packaging applications, APA International conference on Advances in Polymer Science and Technology, held on 23rd-25th Nov

2017, at Radisson Blu Hotel, Dwarka New Delhi.

- **Radhika Batra**, Roli Purwar Poster presentation, Structure-property relationship of Tasar silk fibroin PVA blend films. CAMNP2019, International conference on Atomic, Molecular, Optical & Nano Physics with applications, held on 18th -20th Dec. 2019, at Department of Applied Physics, Delhi Technological University, Delhi.

Radhika Batra

radhikabatra92@gmail.com
+919873884201
Delhi, India

Summary

Results-driven, adaptable, experienced research professional with a highly analytical mindset and passion for innovation. Experienced in the diverse areas of Applied Chemistry & Materials with training in several experimental research techniques and hands-on practice of myriad research instruments. A quick learner who thrives on imagination, perseverance and excellence.

Education

St. Stephen's College, University of Delhi
B.Sc. Chemistry Hons. • Delhi, Delhi   06/2013

Indian Institute of Technology, Delhi (IITD)
M.Sc. Chemistry • Delhi, Delhi   06/2015

Delhi Technological University
Ph.D. Applied Chemistry • Delhi, Delhi   Present

Skills

- Research
- Scientific project management
- Scientific writing
- Troubleshooting

Areas of Interest

- Polymeric Material Research
- Fabrication of Biomaterials, Nanocomposites
- Electrospinning

Research Experience

Delhi Technological University
Senior Research Fellow • Delhi   Present
Project Title – Studies on regenerated Non mulberry silk fibroin and its blends.

- Formulation of different blend materials like flexible films and 3D nanocomposite nanofibers.
- Curation of data and analysis
- Study the structure-property relationship of developed materials Training
- B.Tech and M.Tech students
- Instruments Used: Electrospinning, FTIR, Optical microscope, UTM, TGA, DSC, Rheometer, Particle Size analyzer
- Data Analysis through FESEM with EDS, XRD, AFM, cell viability studies etc.

Drafted manuscripts and published in reputed SCI-Indexed journals.

Delhi Technological University

Research Associate • Delhi   09/2016 - 06/2017

Project Title – Development of Biodegradable polymeric films from gelatin and Silk sericin for packaging applications.

- Project Lead
- Training M.Tech student
- Data analysis and report generation Reviewing
- and Editing research manuscript

Published research article in a reputed SCI-indexed journal

Indian Institute of Technology, Delhi

Post Graduate Student • Delhi   06/2014 - 07/2015

Project Title: Studies on aggregation and disaggregation of aggregation-prone proteins using naturally occurring compounds.

- Collection of data and analysis
- Instruments used: UV-Vis Spectrophotometer, Fluorescence spectrophotometer, SDS-PAGE

Published a research article in an International SCI-indexed journal.

Indian Institute of Technology, Bombay

Summer Intern • Mumbai, Maharashtra   05/2012 - 07/2012

- Synthesis of chelating ligands for carboxylic acid
- Data curation and analysis
- Instruments/Techniques used: Column chromatography, TLC, Rotavapour, NMR, GC-MS
- Report generation

Publications

Research Articles

1. **Radhika Batra**, Roli Purwar*, Senthilguru Kulanthaivel[2], Prashant Mishra[2], Cetyl trimethyl ammonium bromide modified clay doped tasar silk fibroin/polyvinyl alcohol blend-based 3D nanowebs for tissue engineering applications, *Macromolecular Materials & Engineering*, 2021. https://doi.org/10.1002/mame.202100450
2. **Radhika Batra**, Roli Purwar*, Senthilguru Kulanthaivel[2], Prashant Mishra[2], Enhancement of functional properties by blending cocoon extracted *Antheraea mylitta* silk fibroin with polyvinyl alcohol for applications in biomedical field, *Journal of Applied Polymer Science*, 2021. https://doi.org/10.1002/app.51913
3. Reetu Yadav, **Radhika Batra**, Priya Bansal, Roli Purwar*, n-type silk fibroin/TiO2 nanocomposite transparent films: electrical and optical properties, *Polymer International*, 2021. https://doi.org/10.1002/pi.6285
4. **Radhika Batra**, Roli Purwar*, Deduction of a facile method to construct *Antheraea mylitta* silk fibroin/gelatin blend films for prospective biomedical applications, *Polymer International*, 2021. https://doi.org/10.1002/pi.6087.
5. Priya Bansal, **Radhika Batra**, Reetu Yadav, Roli Purwar*, Electrospun polyacrylonitrile nanofibrous membranes supported with montmorillonite for efficient PM2.5 filtration and adsorption of Cu (II) ions. *Journal of Applied Polymer Science*, 2021. https://doi.org/10.1002/app.51582
6. Roli Purwar*, Anjali Verma, **Radhika Batra**, Antimicrobial Gelatin/sericin/clay films for packaging of hygiene products, *Journal of Polymer Engineering*, 2019. https://doi.org/10.1515/polyeng20180406
7. Saurabh Gautam, Sandip Karmakar, **Radhika Batra** et al. Polyphenols in combination with β-cyclodextrin can inhibit and disaggregate α-synuclein amyloids under cell mimicking conditions: A promising therapeutic alternative, *Biochimica et Biophysica Acta (BBA) - Proteins and Proteomics*, 2017. http://dx.doi.org/10.1016/j.bbapap.2017.02.014

8. Priti Dwivedi, **Radhika Batra**, Roli Purwar, Multifunctional properties of nonmulberry silk fibroin and gelatin blend solutions: rheological study, Conference Proceeding for book entitled "Advances in Functional Materials" by Springer Nature (accepted, 2021)

Book Chapters

Roli Purwar and **Radhika Batra**, Chapter titled "Production of Electrospun Nanofibers: An Investigation on Governing Parameters" (In press with Cambridge Scholar Publications)

Conferences

1. **Radhika Batra**, Roli Purwar Poster presentation, Structural and thermal analysis of Antheraea mylitta silk fibroin/gelatin blend films, SPSI MACRO 2018, International conference on Polymer Science and Technology, held on 19th -22nd Dec 2018, at IISER Pune
2. **Radhika Batra**, Roli Purwar Poster presentation, Modified clay doped flexible gelatin/sericin blend films for food packaging applications, APA International conference on Advances in Polymer Science and Technology, held on 23rd -25th Nov 2017, at Radisson Blu Hotel, Dwarka New Delhi.
3. **Radhika Batra**, Roli Purwar Poster presentation, Structure -property relationship of Tasar silk fibroin PVA blend films. CAMNP 2019, International conference on Atomic, Molecular, Optical & Nano Physics with applications, held on 18th -20th Dec. 2019, at Department of Applied Physics, Delhi Technological University, Delhi.
4. Priti Dwivedi, **Radhika Batra**, Roli Purwar Paper presentation, Multifunctional properties of non mulberry silk fibroin and gelatin blend solutions: rheological study, International conference on Advanced Functional materials and Devices (AFMD 2021), held virtually on 3rd -5th March 2021.

Positions of Responsibility

Department of Applied Chemistry, Delhi Technological University

- Volunteered for the TEQIP– III sponsored One–week Faculty Development Program on Polymer analysis and Applications: Current Scenario, June 2018: Handled the inaugural ceremony event, helped organize daily expert presentations.
- Anchored for the inaugural event of Environment Day Celebrations, 2020

IPR Cell, Delhi Technological University

- Anchored for a one-day workshop on Indian Patent Filling Procedure jointly organized by RGNIIP Nagpur and DTU on 28th May,2018

Chemistry Society, Volunteer, 2010-11; St. Stephen's College

- Handled the publicity, helped organize paper presentation.
- Volunteered in the event 'Inauguration of the International Year of Chemistry 2011' by C.N.R. Rao at St. Stephen's College.

Student's Union Society, Deputy Secretary 2011-12; St. Stephen's College

- Efficiently organized events in 'Capriccio–2011' and 'Harmony' the annual college fests and helped in organization of the term dinner.
- Team member for Coordination of National Science Fest

Social Service League, Executive council member, 2010-11; St. Stephen's College

- Core team member of the Blood Donation Camp of 2010, and worked extensively to make it a remarkable success, 327 units of bloodwere donated

- Volunteered to teach underprivileged students, an hour, 6 days a week

Personal Details

Nationality: Indian

Marital Status: Unmarried

Languages

- English
- Hindi

Declaration

I hereby declare that above given information is true to the best of my knowledge and belief.

Name: Radhika Batra

Date: 07.12.2021

Place: Delhi